

NASA TECHNICAL  
MEMORANDUM

NASA TM X-53810

1968

NASA TM X-53810

COMMUNICATION AND TRACKING RESEARCH AT MSFC

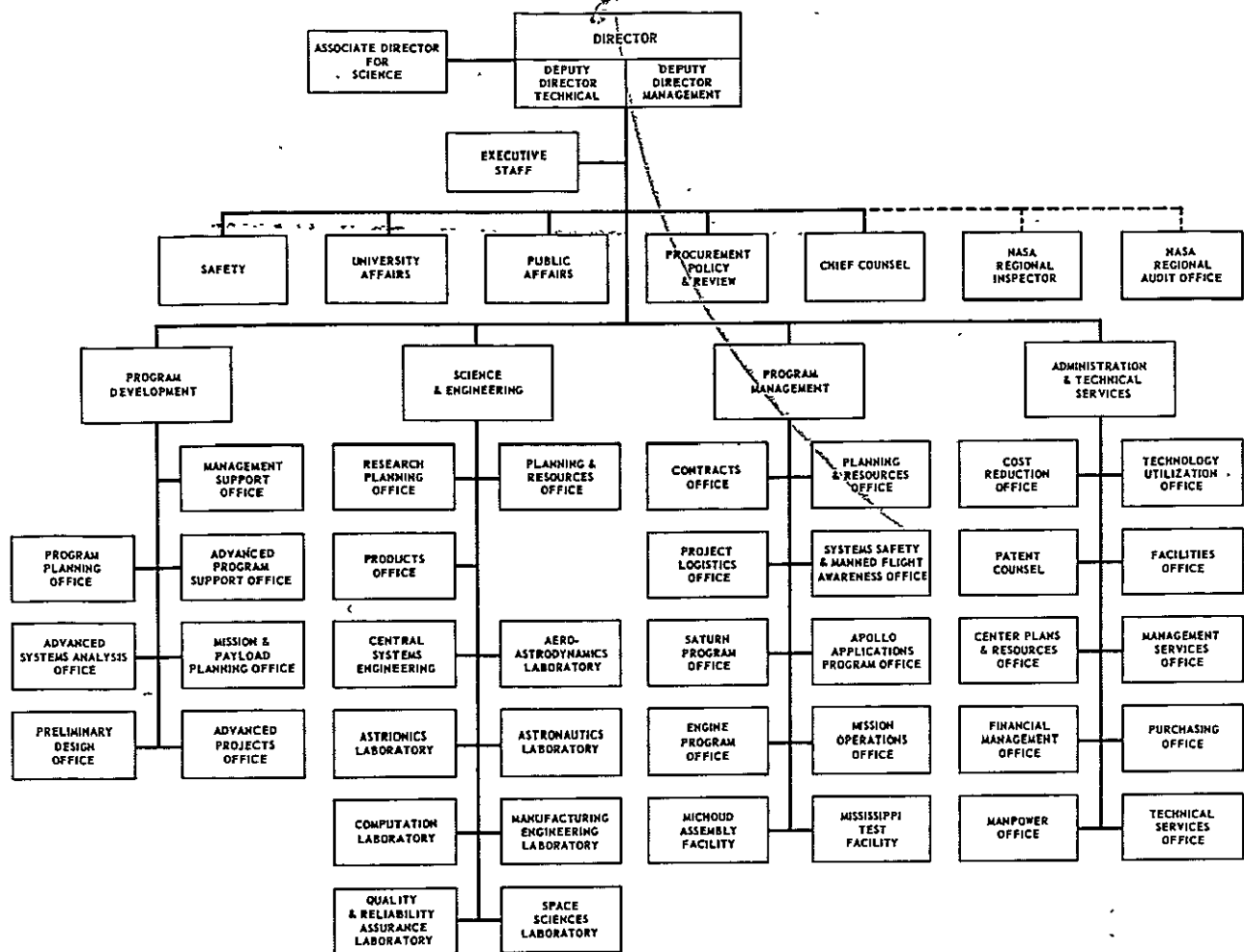
RESEARCH ACHIEVEMENTS REVIEW  
VOLUME III REPORT NO. 5

SCIENCE AND ENGINEERING DIRECTORATE  
GEORGE C. MARSHALL SPACE FLIGHT CENTER  
MARSHALL SPACE FLIGHT CENTER, ALABAMA

Reproduced by the  
CLEARINGHOUSE  
for Federal Scientific & Technical  
Information Springfield Va. 22151

N 69 - 36577 - N 69 - 36582	
(ACCESSION NUMBER)	(THRU)
83	1
(PAGES)	(CODE)
TMX-53810	01
(NASA CR OR TMX OR AD NUMBER)	(CATEGORY)

# GEORGE C. MARSHALL SPACE FLIGHT CENTER



## RESEARCH ACHIEVEMENTS REVIEWS COVER THE FOLLOWING FIELDS OF RESEARCH

- Radiation Physics
- Thermophysics
- Chemical Propulsion
- Cryogenic Technology
- Electronics
- Control Systems
- Materials
- Manufacturing
- Ground Testing
- Quality Assurance and Checkout
- Terrestrial and Space Environment
- Aerodynamics
- Instrumentation
- Power Systems
- Guidance Concepts
- Astrodynamics
- Advanced Tracking Systems
- Communication Systems
- Structures
- Mathematics and Computation
- Advanced Propulsion
- Lunar and Meteoroid Physics

NATIONAL AERONAUTICS AND SPACE ADMINISTRATION  
WASHINGTON, D.C

# **RESEARCH ACHIEVEMENTS REVIEW**

## **VOLUME III                      REPORT NO. 5**

COMMUNICATION AND TRACKING RESEARCH AT MSFC

SCIENCE AND ENGINEERING DIRECTORATE  
GEORGE C. MARSHALL SPACE FLIGHT CENTER  
MARSHALL SPACE FLIGHT CENTER, ALABAMA

1968

PRECEDING PAGE BLANK NOT FILMED.

## PREFACE

In February, 1965, Dr. Ernst Stuhlinger, Director, Research Projects Laboratory ( now Space Sciences Laboratory ), initiated a series of Research Achievements Reviews which set forth those achievements accomplished by the laboratories of the Marshall Space Flight Center. Each review covered one or two fields of research in a form readily usable by specialists, systems engineers and program managers. The review of February 24, 1966, completed this series. Each review was documented in the "Research Achievements Review Series."

In March, 1966, a second series of Research Achievements Reviews was initiated. This second series emphasized research areas of greatest concentration of effort, of most rapid progress, or of most pertinent interest and was published as "Research Achievements Review Reports, Volume II." Volume II covered the reviews from March, 1966, through February, 1968.

This third series of Research Achievements Reviews was begun in March, 1968, and continues the concept introduced in the second series. Reviews of the third series are designated Volume III and will span the period from March, 1968, through February, 1970.

*The papers in this report were presented November 21, 1968*

William G. Johnson  
Director  
Research Planning Office

PRECEDING PAGE BLANK NOT FILMED.

CONTENTS. . .

RECENT ADVANCES IN LASER COMMUNICATIONS ✓

Page

by Joseph L. Randall

INTRODUCTION . . . . .	1
RECENT ADVANCES IN POINTING AND TRACKING INSTRUMENTATION . . . . .	1
DATA RATES ATTAINABLE WITH OPTICAL AND IR COMMUNICATIONS . . . . .	5
CONCLUSIONS AND RECOMMENDATIONS . . . . .	8

LIST OF ILLUSTRATIONS

Figure	Title	Page
1.	Laser Communication System Diagram . . . . .	2
2.	Laser Communication System . . . . .	4
3.	Optical Layout of Laser Telescope . . . . .	4
4.	Laser Communication System Tracking a Simulated Earth Beacon . . . . .	5
5.	Two Ended 10.6- $\mu$ Optical Communications System . . . . .	6
6.	Heterodyne Signal-to-Noise Ratio Versus Signal Power . . . . .	7
7.	Pulse Code Modulated Optical Communication System . . . . .	7
8.	Measured System Performance, Binary Detection . . . . .	7
9.	Bit Error Rate Versus Receiving Aperture . . . . .	8

LASER POINTING, TRACKING, AND RANGING ✓

Page

by John M. Gould

SUMMARY . . . . .	9
INTRODUCTION. . . . .	9
TARGET DYNAMICS ESTIMATOR AND EXTRAPOLATOR. . . . .	9
RANGE SERVO . . . . .	10
ANGULAR CONTROL SYSTEM. . . . .	12
CONCLUSIONS. . . . .	19
REFERENCE. . . . .	19

# CONTENTS (Continued) . . .

## LIST OF TABLES

Table	Title	Page
I.	Estimator Performance as a Function of Measurement and Noise Parameters for Full Tracking Period . . . . .	11

## LIST OF ILLUSTRATIONS

Figure	Title	Page
1.	Range Servo Block Diagram . . . . .	12
2.	Range Servo Detailed Diagram . . . . .	13
3.	Range Servo Response to "Worst-Case" Tracking of Saturn V Launch . . . . .	14
4.	Angular Control System Configuration in Track Mode . . . . .	15
5.	Angular Control System Configuration in Reacquire Mode . . . . .	15
6.	Angular Control System Configuration in Acquire Mode . . . . .	15
7.	Simplified Block Diagram of the Angle Servo with Integral Compensations Removed . . . . .	16
8.	Small Signal Step Response . . . . .	17
9.	Response to Step Change in Angular Command, Resulting in Torque Command Saturations . . . . .	17
10.	Response to Step Change in Angular Command, Resulting in Both Torque and Velocity Command Saturations . . . . .	17
11.	Response to Step Change in Angular Velocity Command, Resulting in Saturations of Both Torque and Velocity Commands . . . . .	17
12.	Tracking a Slowly Moving Target. Velocity Range of 0.002 Degrees/Second through Zero . . . . .	18
13.	Simulation of the Hour Angle Servo During "Worst-Case" Tracking of a Saturn V Launch with No Rate Feedforward Used . . . . .	18
14.	Simulation of the Hour Angle Servo During "Worst-Case" Tracking of a Saturn V Launch with 85 Percent of Rate Feedforward Applied . . . . .	19
15.	Simulation of the Hour Angle Servo During "Worst-Case" Tracking of a Saturn V Launch With 100 Percent of Rate Feedforward Applied . . . . .	19

CONTENTS (Continued) . . .

LUNAR ROCKET RESCUE BEACON ✓

by Lee B. Malone, Jr.

SUMMARY . . . . .	21
DEFINITIONS . . . . .	21
INTRODUCTION . . . . .	21
INVESTIGATION OF METHODS OF COMMUNICATION . . . . .	22
RELAY TRAJECTORY INVESTIGATION . . . . .	26
RANGE AND AZIMUTH MEASURING SYSTEMS . . . . .	29
ROCKET CONFIGURATION AND PERFORMANCE CHARACTERISTICS . . . . .	38
INVESTIGATION OF PURCHASED FINISHED COMPONENTS . . . . .	39
CONCLUSIONS . . . . .	40
REFERENCES . . . . .	41
BIBLIOGRAPHY . . . . .	41

LIST OF TABLES

Table	Title	Page
I.	Transceiver Parameters . . . . .	23
II.	Transmission Parameters . . . . .	23
III.	Calculated Values of Slant Range and Azimuth . . . . .	37
IV.	Communications Relay Transceiver Requirements . . . . .	38
V.	System Capabilities . . . . .	41

CONTENTS (Continued) . . .

LIST OF ILLUSTRATIONS

Figure	Title	Page
1.	Launch Tube . . . . .	21
2.	Transceiver Block Diagram . . . . .	22
3.	Transceiver Baseband Response . . . . .	23
4.	Transmission Paths . . . . .	23
5.	CW Beacon Transmitter . . . . .	23
6.	LM Equipment for CW Beacon System . . . . .	24
7.	Coded Beacon . . . . .	24
8.	LM Equipment for Coded Beacon . . . . .	24
9.	Alternate Coded Beacon . . . . .	25
10.	LM Equipment for Alternate Coded Beacon . . . . .	25
11.	Antenna Pattern for Transceiver . . . . .	25
12.	Time of Flight of Communications Relay . . . . .	26
13.	Masking Effect of Lunar Surface . . . . .	26
14.	Determination of Blind Spot in Trajectory . . . . .	27
15.	Effect of Mask on Transmission Time . . . . .	29
16.	Range Measuring System . . . . .	30
17.	Antenna System for Azimuth Measurement . . . . .	33
18.	Azimuth Measuring System . . . . .	33
19.	Phase Angle Outputs of Phase Detectors . . . . .	34
20.	Error in Horizontal Range Caused by Launch Angle . . . . .	35
21.	Maximum Error in Extrapolated Position of EVA . . . . .	36
22.	LM to Rocket Elevation Angle . . . . .	37
23.	Lunar Rocket Rescue Beacon . . . . .	39



CONTENTS (Continued) . . .

BUFFER FULLNESS CONTROLS FOR A DATA COMPRESSOR  
USING SATURN VEHICLE DATA ✓

by Gabriel R. Wallace

Page

SUMMARY . . . . .	43
INTRODUCTION . . . . .	43
SATURN PCM/FM TELEMETRY SYSTEM . . . . .	45
ZFN DATA COMPRESSION UNIT . . . . .	45
NOTED INPUT DATA VARIATIONS OF SEVERAL SATURN FLIGHTS . . . . .	48
BUFFER LENGTH CONTROL PARAMETER EXPERIMENTS . . . . .	49
CONCLUSIONS . . . . .	53
REFERENCES . . . . .	54

LIST OF TABLES

Table	Title	Page
I.	Flight Parameter Occurrences . . . . .	48
II.	Data Input Rates to Buffer . . . . .	49
III.	Lift-Off Period Data Compression Ratios . . . . .	49
IV.	Measurement Tolerance Assignments . . . . .	50
V.	Summary of Open-Loop Plot Characteristics . . . . .	53
VI.	Tolerance Assignments . . . . .	53

# CONTENTS (Continued) . . .

## LIST OF ILLUSTRATIONS

Figure	Title	Page
1.	ZFN Airborne Data Compressor . . . . .	44
2.	Block Diagram of Buffer Fullness Experiment . . . . .	44
3.	Block Diagram of Saturn PCM/FM Telemetry . . . . .	45
4.	Saturn Flight Profiles (AS-202, AS-204, and AS-501) . . . . .	46
5.	Functional Block Diagram of the Telemetry Data Compressor . . . . .	47
6.	ZFN Algorithm (Zero Order, Fixed Corridor, Nonredundant Sample) . . . . .	47
7.	AS-202 Open-Loop Plot for Lift-Off Period ( #1) . . . . .	51
8.	AS-202 Open-Loop Plot for Lift-Off Period ( #2) . . . . .	51
9.	AS-204 Open-Loop Plot for Lift-Off Period ( #3) . . . . .	51
10.	AS-203 Open-Loop Plot for Low Activity Period . . . . .	51
11.	Possible Data Distribution of Saturn PCM Data . . . . .	52
12.	AS-202 Tolerance Control Plot ( #1) . . . . .	52
13.	AS-203 Tolerance Control Plot ( #2) . . . . .	52
14.	AS-204 Tolerance Control Plot ( #3) . . . . .	52
15.	AS-202 Priority Control Plot ( #1) . . . . .	54
16.	AS-202 Priority Control Plot ( #2) . . . . .	54

## RADIATION EFFECTS TESTING OF SATURN TELEMETRY HARDWARE

by T. C. Lawson

INTRODUCTION . . . . .	55
TEST METHODS . . . . .	55
TEST CONFIGURATIONS . . . . .	56
TEST RESULTS . . . . .	60
CONCLUSIONS . . . . .	61

CONTENTS (Continued) . . .

LIST OF TABLES

Table	Title	Page
I.	Methods of Irradiation Testing . . . . .	55

LIST OF ILLUSTRATIONS

Figure	Title	Page
1.	Test Facilities . . . . .	56
2.	Typical Saturn Telemetry System . . . . .	57
3.	Typical Test . . . . .	57
4.	Block Diagram of Test Item . . . . .	58
5.	Sideview of Test Configuration . . . . .	59
6.	Test Panel . . . . .	59
7.	Carrier Supply Output . . . . .	60
8.	Carrier Circuit . . . . .	61
9.	Power Supply Performance . . . . .	61

# RECENT ADVANCES IN LASER COMMUNICATIONS

By

Joseph L. Randall

N 69 - 36578

## INTRODUCTION

Considerable research and development (R&D) has been performed on electro-optical techniques that use a laser for optical communication and tracking. Several NASA Centers have been very active in this technology. This discussion deals primarily with the R&D program at the Marshall Space Flight Center with the aim of giving our philosophy of approach and identifying the problems and what might be done to solve them.

The basic reason that optical and infrared (IR) wavelengths have potential in the field of communication and tracking is our ability to use their high beam directivity or antenna gain. This allows high power densities for communication and accurate angle information for tracking. Several studies have been performed to determine the capabilities of optical/IR communication systems. These studies indicate that very high data rates such as 1 to 100 megabits per second (Mbps) should be attainable if the technology is developed. Such missions for optical communications may be data relay satellites where data rates of 100 Mbps are desired or a deep space communication link with 1 to 10 Mbps. Of course, there are those who say that these requirements can be met with RF communication systems, and therein lies the basis for disagreement in the communication community. The arguments of optical versus RF frequencies will not be presented here, but rather a review is given of today's optical and IR communication technology.

Several years ago, it was thought that the most basic problem associated with optical communication was that of pointing narrow laser beams. Accordingly, a theoretical and experimental program was initiated to solve this problem. At that time, it was known that the best laser for transmitting information was not yet perfected, but the techniques of pointing could

be developed with the lasers that were available; these lasers were the HeNe laser operating at 6328Å and the Argon laser operating at 4880Å.

Other problems to be attacked included (a) acquisition, (b) atmospheric effects on an optical channel and what modulation format should be used to combat these effects, (c) low electrical efficiency of the lasers and modulators which in turn means a high power consumption of the spacecraft, and (d) maintaining diffraction limited optics in space.

These problems have been systematically approached by NASA and the results of some of these programs are given to indicate the present state of the technology. One appropriate question that can be asked is this: How close to the theoretically calculated data rates can realistic, practical hardware be made to operate at this time?

## RECENT ADVANCES IN POINTING AND TRACKING INSTRUMENTATION

As was mentioned earlier, NASA began developing a precision pointing and tracking laser communication system. This work was performed for MSFC by Perkin-Elmer under Contract NAS8-20115; the program has proceeded for about four years. This work was done to meet the requirements for a deep space optical communication system in which the pointing requirements were exceedingly exacting. The basic difference in an optical communication system and an astronomical optical system is the following. An astronomical telescope must track a star so that the desired radiation falls on the film or appropriate sensor without angular motion, whereas the optical communication system must point a very narrow laser beam with information on it in the direction of the receiver. For instance, a 1-m

telescope or antenna of an optical communication system operating at visible wavelengths will have a beamwidth of only a few tenths of an arc second. At a range of 160 million km, this would cover a spot on the earth of only about 160 km; and since the beam must be pointed to within a fraction of the beamwidth to assure hitting the earth receiver, the pointing system must be very accurate and precise. Obviously, if a system operating to these specifications could feasibly be built, systems with less stringent mission requirements could be made also. This was the philosophy inherent in Perkin-Elmer's design.

Figure 1 shows how this technique functions. The basic concept of the two-way optical communication link is for both the ground station and the spacecraft to have a laser beacon and a precise tracking system so that each will track the laser beacon of the other. The optical beamwidths will be arc seconds or less; therefore, the beam must be

pointed to a fraction of this beamwidth if it is to communicate with another station. Common optics are used rather than a separate tracking telescope and transmitting telescope because of size reduction and the difficulty of boresighting and maintaining the boresight of two large independent telescopes. Both the ground station and the satellite would have such telescope systems.

After an initial acquisition phase, the received light from the ground station is reflected by the primary/secondary combination onto a coarse tracking sensor which subtends a one-degree field of view. The coarse tracking sensor is a four quadrant photomultiplier with a prism lens combination dividing the image into the four quadrants. The derived error signal is used to move the telescope so that the received light falls through an approximately 2-arc-minute field-of-view hole onto the fine sensor. Because the mass of the telescope is so large, the fine

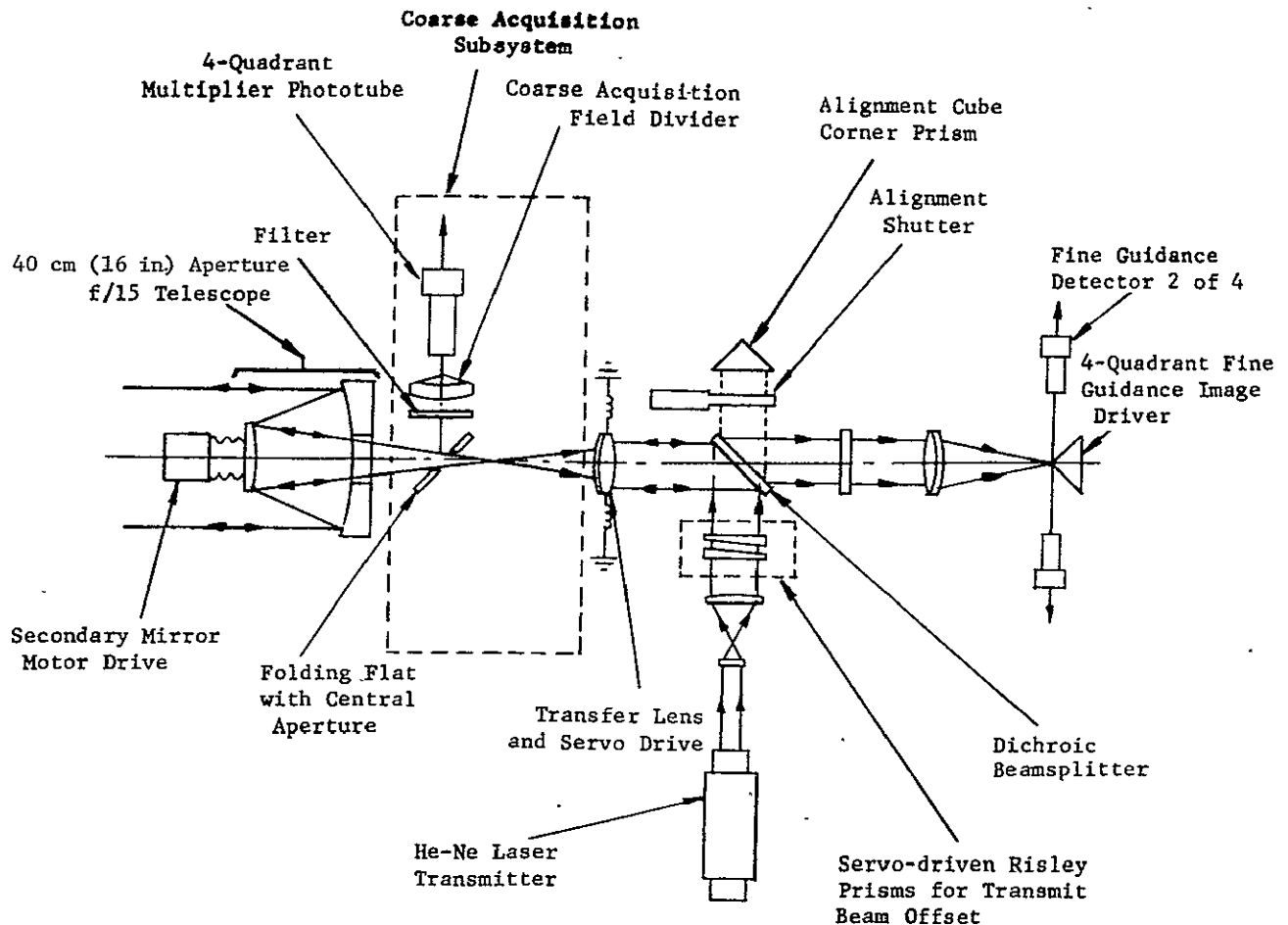


FIGURE 1. LASER COMMUNICATION SYSTEM DIAGRAM

tracking is done by a transfer lens. As the image moves off the apex of the beam-splitting prism, the error signals generated are fed to the transfer lens to bring the image back to the apex of the prism. At the same time, this motion of the transfer lens corrects the pointing of the transmitter laser; that is, small motions of the telescope are corrected by the transfer lens, and the transmitted beam with the information always goes back in the direction of the tracked beacon. An optical modulator is used to place information on the transmitted beam. The required point-ahead function of the system is shown implemented by means of a pair of Risley prisms. Relative and joint rotations of the Risley prisms accomplish two coordinate angular offsets of the transmitted laser beam from the line of sight of the receive channel. A lateral translation of either laser lens would have an identical effect.

An experimental breadboard of the fine tracking and laser reporting system with a 40 cm (16 in.) primary was systematically developed and studied to demonstrate the feasibility of the technique. The results of that study showed the following.

1. The fine guidance tracking detector and transfer lens servosystem operated satisfactorily. The system demonstrated that the transmit laser beam is pointing to an accuracy of 0.1 arc second with respect to the receive channel. This has been achieved with telescope motion that simulates a spacecraft motion.
2. Intensity fluctuations of the laser in the far field are not a problem.
3. The transmitter beam has been isolated from the tracking detector by using two wavelengths, 6328 Å and 4800 Å. Isolation of one part in  $10^{10}$  has been achieved.
4. The coarse acquisition system and the Risley prisms subsystem have been developed and are operating satisfactorily.

The transfer lens servosystem will take out motion of the telescope only within reasonable limits; therefore, the spacecraft carrying the telescope and communication system must be stabilized. Studies have shown that the required telescope stabilization should be about  $\pm 1/4$  arc minute. If the telescope is mounted directly to the spacecraft, the spacecraft must then be stabilized to the same accuracy. If a man is present in the spacecraft, disturbance torques must be isolated from the telescope. If the telescope

is mounted to the spacecraft through an active gimbaling system, then the spacecraft should be stabilized to  $\pm 1/2$  degree to perform acquisition. The Orbiting Astronomical Observatory (OAO) and the Apollo Telescope Mount (ATM) have more severe requirements.

Figure 2 shows the equipment in the breadboard stage as it was used to demonstrate feasibility. With the feasibility demonstrated, the next phase was the development of a prototype of the system in that all the hardware was combined into a telescope package that could be used in space. Several new additions, however, were incorporated into the new prototype (Fig. 3). First, the optical system was made all reflective in the transmit channel for the system to operate at any wavelength from the visible to the IR. This will allow operation with a 10.6- $\mu$  CO<sub>2</sub> laser. This was done by changing the "transfer lens" to a "transfer mirror" for image motion compensation. The transfer mirror is suspended by four piezoelectric bimorph beam benders to give the required rotation about two axes. The frequency response of the mirror is about 50 Hz. In this package, dichroic beam splitters are designed to allow the system to operate in either the visible or IR spectrum. Since the Risley prisms use refracting optics, they are now placed in the receive channel which operates at 4880 Å. This can be done because the channel in which the prisms are located is immaterial.

The second major change in the system is that the entire package is now placed in a four-axes gimbal to simulate spacecraft motion. The two inner gimbals represent the pitch and yaw gimbals that would be used to mount the telescope to a spacecraft. The outer two gimbals will give roll and a rotation about the vertical axis. These two rotations represent the spacecraft motion. Thus with the four-axes gimbal system, a simulated spacecraft motion can be performed and an analysis of the communication system performance can be evaluated while tracking on an earth beacon simulated by a 50-cm collimator (Fig. 4). In addition, the simulated earth beacon can be amplitude modulated to simulate atmospheric scintillation on the up-going beam. Laboratory experiments to study these problems are now being performed. At the present time, only a visible laser has been installed in the system, but plans call for the addition of a coherent 10.6- $\mu$  CO<sub>2</sub> laser communication system into the prototype package.

In addition to the hardware development, MSFC has also awarded a contract to IBM to perform a



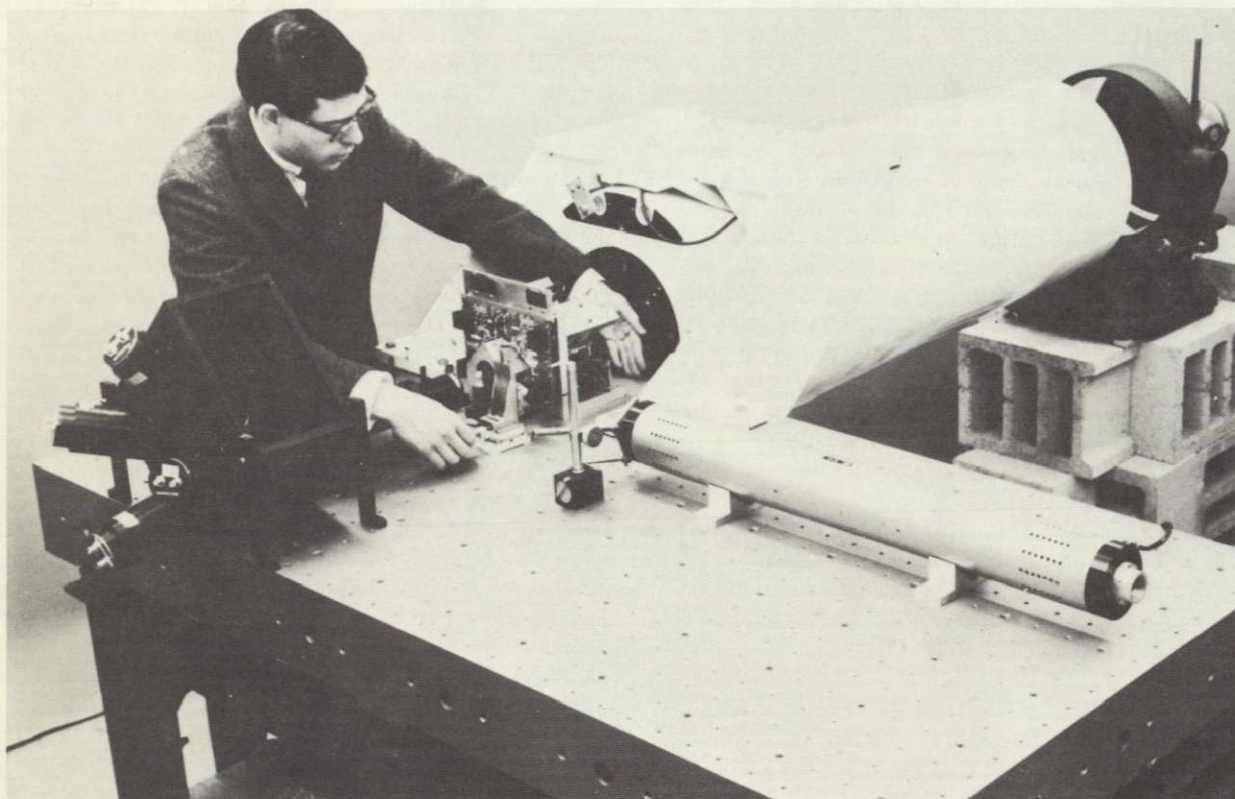


FIGURE 2. LASER COMMUNICATION SYSTEM

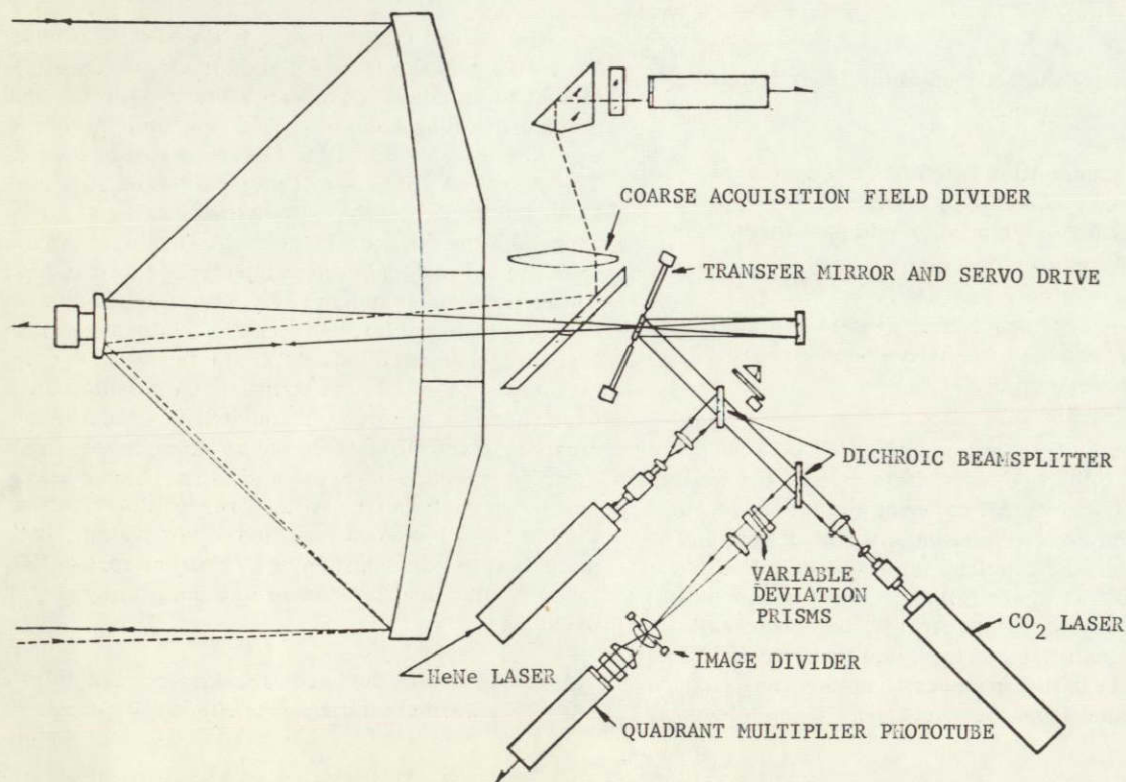


FIGURE 3. OPTICAL LAYOUT OF LASER TELESCOPE



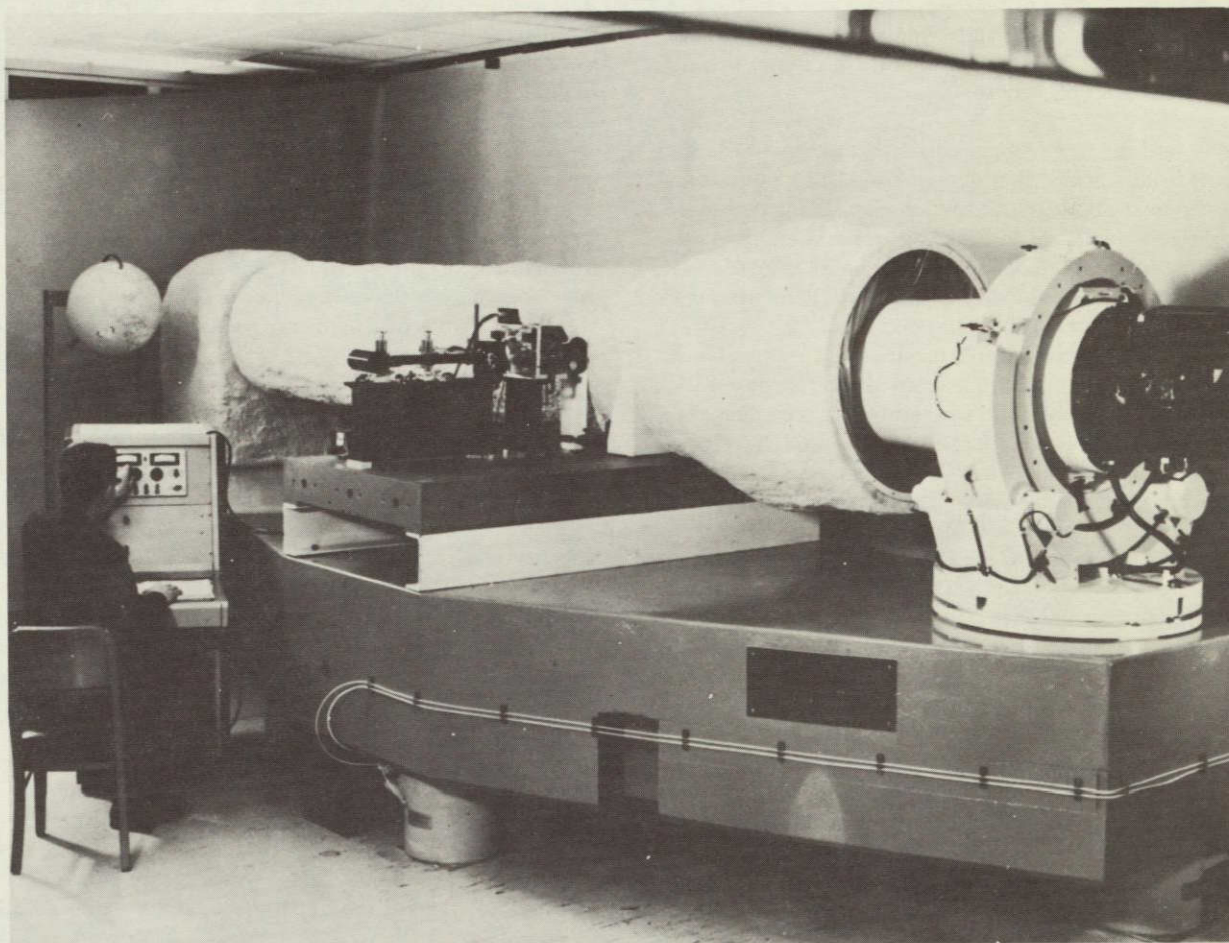


FIGURE 4. LASER COMMUNICATION SYSTEM TRACKING A SIMULATED EARTH BEACON

complete computer simulation of the spacecraft optical communication system. In this simulation an ATM spacecraft and attitude control system was used. For the communication hardware, the Perkin-Elmer system was used. This simulation will allow an analysis and evaluation of the acquisition and pointing of the complete communication system including the spacecraft. This program has been written and indicates that satisfactory operation can be achieved with existing hardware. Further studies are now being performed with this simulation to determine where improvements can be made in overall system performance.

### DATA RATES ATTAINABLE WITH OPTICAL AND IR COMMUNICATIONS

Assuming that it is possible to point laser beams with the systems discussed previously, it is now appropriate to discuss the data rates that can be achieved using optical and IR wavelengths. At the present time it appears that the two best candidates for laser communication are the frequency-doubled YAG:Nd laser that operates at  $5300 \text{ \AA}$  and the  $10.6\text{-}\mu$   $\text{CO}_2$  laser. Powers of several watts at efficiencies of about one percent should be available in the near



future with the 5300 Å frequency-doubled YAG laser. This represents by far the optimum laser in the visible wavelength region. The high power and high efficiency of the 10.6- $\mu$  CO<sub>2</sub> laser also make it a very promising candidate.

In building a communication system at these two wavelengths, analysis and experimental results show that the best approach is to use incoherent detection (or photon counting) in the visible wavelengths and a coherent (or heterodyne) detection at the 10.6- $\mu$  wavelength. This places certain requirements on each of the two systems. For instance, the 10.6- $\mu$  CO<sub>2</sub> system uses a local-oscillator laser at the receiver which heterodynes with the transmitter laser. This means that they both must be stable in frequency so that the beat signal can fall in the IF amplifier frequency range. In addition, large Doppler frequency shifts must be considered. Perhaps the most severe requirement is that a completely automated CO<sub>2</sub> laser in space must be constructed to operate at the proper frequency anytime it is turned on so that a beat signal with the local oscillator may be achieved during initial acquisition when a search in frequency and space must be made. Even though the problems exist, research at solving them is progressing and the next section will discuss some results.

#### 10- $\mu$ COHERENT COMMUNICATION SYSTEM

Two coherent 10.6- $\mu$  communication systems have been built. Hughes Aircraft built one that

transmits television bandwidths and utilizes a modulator internal to the laser cavity. The other one, built by Honeywell on contract to NASA-MSFC, uses piezoelectric pushers to modulate the laser cavity length, thereby frequency modulating the laser output. Figure 5 shows a block diagram of the Honeywell system, which is capable of transmitting two voice channels. Evaluation of the system performance has shown that it experimentally operates to within a factor of two of the theoretically calculated performance. Figure 6 shows this graphically. Thus it has been shown that coherent 10.6- $\mu$  systems can be designed and built to operate very close to the theoretical limits.

#### INCOHERENT VISIBLE COMMUNICATION SYSTEMS

Incoherent detection is superior in the visible region for several reasons. First, the atmosphere is very effective at destroying spatial coherence at visible wavelengths. This then places an upper limit on the receiver aperture size in the order of several centimeters for coherent detection. Since incoherent detection is almost as efficient as coherent detection if background noise radiation can be eliminated, it is advantageous to use incoherent detection and count photons. In that case, there is no atmospheric limitation on receiver aperture size and the receiver can be made as large as is practical to collect more energy. Analysis has shown that with small receiver fields of view and very narrow spectra bandpass filters, the background radiation can be made small

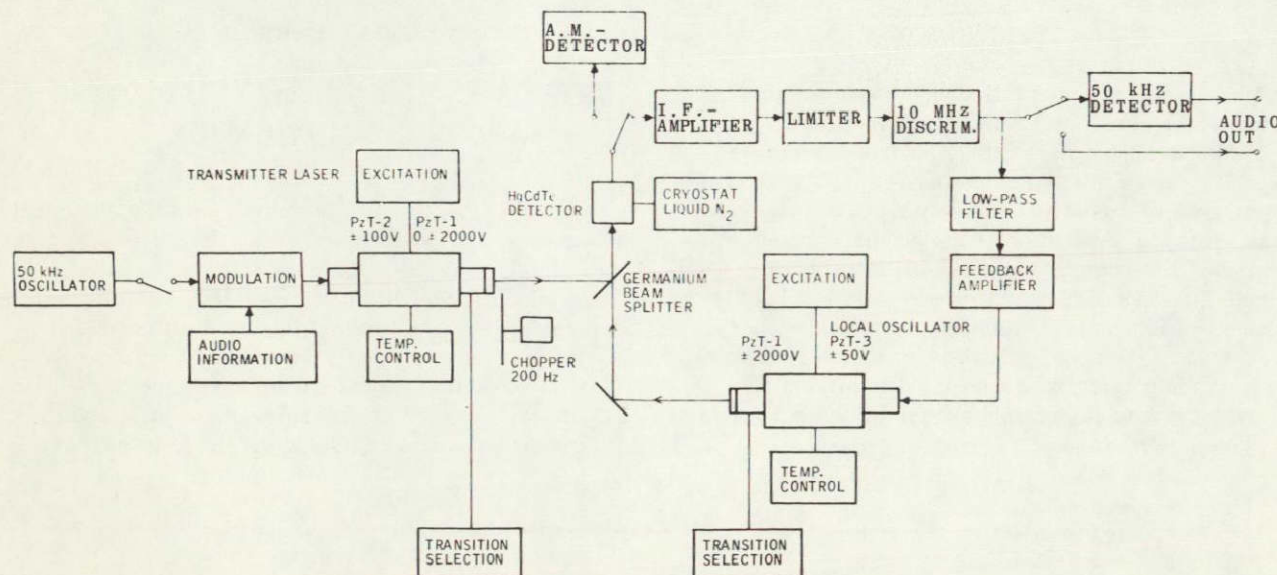


FIGURE 5. TWO ENDED 10.6- $\mu$  OPTICAL COMMUNICATIONS SYSTEM

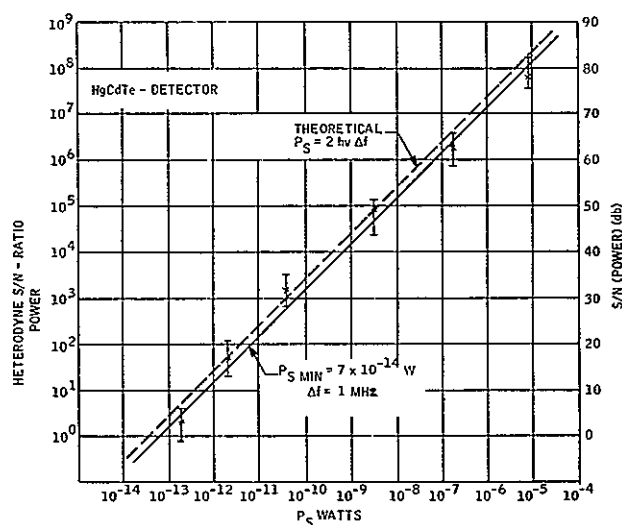


FIGURE 6. HETERODYNE SIGNAL-TO-NOISE RATIO VERSUS SIGNAL POWER

with respect to the signal radiation. Thus one can achieve signal-to-noise ratio time-bandwidth products that are equivalent to coherent detection without all the inherent disadvantages of coherent detection. The main disadvantages of the coherent visible system are that the laser efficiency is low and the quantum efficiency of detectors in the visible is low.

Experimental systems have been built to test the feasibility of high data rate incoherent systems. Analog modulation of the intensity is not practical because of the amplitude scintillation induced by the atmosphere. Pulsed modulation with threshold detection is a much better approach. Several such pulse code modulated (PCM) systems have been built and results of the performance of one built by ITT under contract to NASA are now discussed. Figure 7 shows a block diagram of the ITT system.

The ITT communication system operates at 6328 Å and is modulated at a 30 MBps rate. It is a binary coded PCM system that can operate in an "on-off" mode or it can transmit right- and left-handed circularly polarized light to mark the "ones" and "zeros" of the binary code. This system is unique in that the error rate per bit can be measured. This then allows the comparison of experimentally measured error rates and the theoretically calculated values based on Poisson statistics. The results of one such run, depicted in Figure 8, show that the

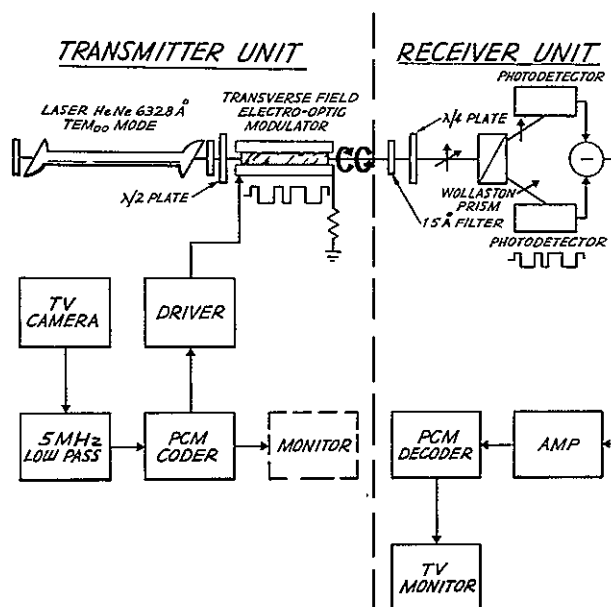


FIGURE 7. PULSE CODE MODULATED OPTICAL COMMUNICATION SYSTEM

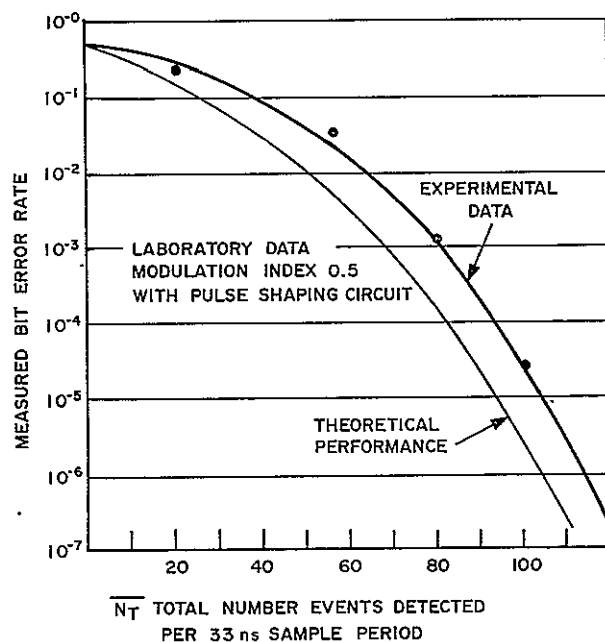


FIGURE 8. MEASURED SYSTEM PERFORMANCE, BINARY DETECTION

system is operating very close to the theoretical limit. These results are based on a 50 percent modulation depth and need to be verified for 100 percent modulation depth. Many tests of this system over an 8-km range have been performed under varying atmospheric conditions. An interesting result, shown in Figure 9, is the reduction of error rate per bit with increasing receiver aperture diameter. This curve is normalized to constant input power. These results are predicted from theory and indicate the advantage of using a large receiver aperture average and thus decrease scintillation-induced error rates.

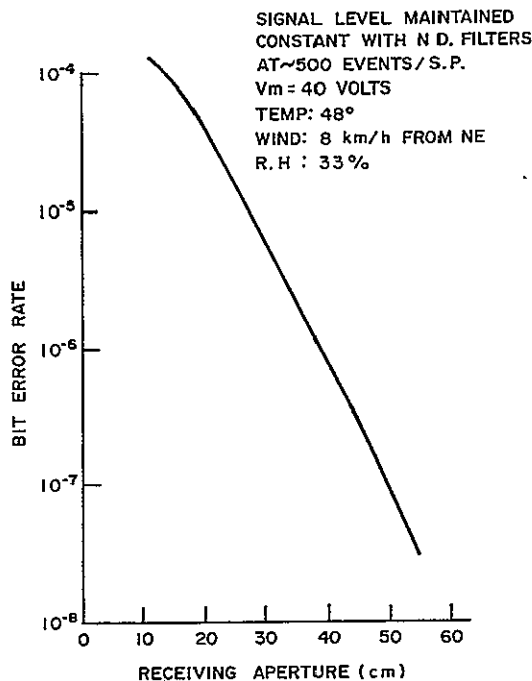


FIGURE 9. BIT ERROR RATE VERSUS RECEIVING APERTURE

## CONCLUSIONS AND RECOMMENDATIONS

From the preceding remarks it can be seen that much has been done in the past several years to develop optical and IR communication systems. Yet, we still do not have enough information to reach a decision as to what system or technique should be used in the various applications of the laser for space

communications. For instance, further R&D is required to determine whether the visible or the IR system should be used. Both wavelength regions have possibilities for considerable improvement. Some of the more obvious areas where improvements could be made are the following.

1. Laser sources. In both the visible and IR systems, a more efficient laser would mean reducing the power required as well as the requirement to eliminate the excess heat generated.

2. Modulators. In the IR system, modulators now require fairly high power. New techniques are required to reduce these power requirements.

3. Detectors. The quantum efficiency of detectors in the visible spectrum has potential for significant improvement. IR detectors have quantum efficiencies of about 50 percent now and significant improvement will be difficult.

4. Frequency shifters to accommodate Doppler frequency shifts. For coherent detection, some type of practical technique will be required to accommodate Doppler shifts in frequency. It may be that a tunable injection laser can be made to act as a local oscillator such as mixing of a PbSnTe injection laser and a CO<sub>2</sub> laser. This technique as well as others will require research to solve this problem.

5. Determination of the optimum modulation format is required for both visible and IR wavelengths to combat the degradation of the communication channel by the atmospheric effect.

In addition to solving these problems, one other task must be performed before optical communication will ever get out of the laboratory and into actual use. That task is the successful experiments that simulate mission requirements. Only when this is done will a NASA program manager give serious consideration to using an optical communication system in an actual flight mission.

NASA is now planning experiments in space which will be required to demonstrate the feasibility of optical communications and to obtain as much data as possible to allow achieving the final design of communication systems for flight missions. Definition of these experiments is being carried out primarily under the Optical Technology Extension System (OTES) program of the Office of Advanced Research and Technology (OART).

# LASER POINTING, TRACKING, AND RANGING

By

John M. Gould

N69-36579

## SUMMARY

The use of a programed digital computer to control an early-launch laser pointing, tracking, and ranging system is investigated. The three elements of the system are presented separately.

The target dynamics estimator and extrapolator describe the most likely target motion in the presence of noise. It was decided to perform a polynomial fit for each short data span (nominally, 90 data points with a 1/64 second spacing for a total period of 1.4 seconds) and to overlap these fitting polynomials. The estimator performance was simulated by processing measurements obtained from nominal tracking data and simulated measurement noise. The results are presented.

The range servo derives nonambiguous range information from a three-speed phase-modulated signal. The response of the servo during "worst case" tracking of a Saturn V launch vehicle is presented.

The angular control system must acquire, reacquire, and track the target in a stable manner in spite of the nonlinearities created by the saturation of motors, sensors, and amplifiers. The flexibility of programing has been used with advantage to implement torque and rate limits and to solve the control equations for optimum performance during operations when these limits are applied. Simulations of the complete angle servo indicate unusually quick and stable responses in both linear and saturated conditions.

## INTRODUCTION

A laser pointing, tracking, and ranging system requires a target dynamics estimator and extrapolator to describe the most likely target motion in the presence of noise; a range servo to derive nonambiguous range information from the modulated return

light signal; and an angular control system to acquire, reacquire, and track the target in a stable manner in spite of the nonlinearities created by the saturation of motors, sensors, and amplifiers.

The versatility and efficiency of a programed on-line digital computer when applied to the laser pointing, tracking, and ranging problems are demonstrated in the design, implementation, and testing of a program for the control of an early launch system.

The control computer is to accept angular pointing error information from a star tracker tube, phase error information from a laser ranging system, and mode control from a reacquisition system. During the tracking mode, the computer will provide drive signals for the tracking telescope to null angular pointing errors; it will also provide phase shift commands to the digital oscillator in the ranging system to null the phase and, hence, range error. In the reacquisition mode, the control computer supplies commands to the telescope drive and the range system oscillator, based on extrapolated target motion, and thus minimizes initial errors when the track mode is reentered after target reacquisition. In addition to its control functions, the program computes target position, velocity, and acceleration in a launch-site-centered coordinate system.

## TARGET DYNAMICS ESTIMATOR AND EXTRAPOLATOR

Before proceeding to a discussion of the basic operating principles of the target dynamics estimator and extrapolator that is basic to the system, a few remarks should be made about other estimators which were studied, and the reasons why they were found unsuitable. The most general linear least-squares estimator is the Kalman-Bucy filter; the use of this estimator requires a full description of the target dynamics and expected noise. For a Saturn V launch vehicle, the equations of motion are far too complex to allow a real-time estimator to be realized on a medium-scale computer. In addition, the straight

Kalman-Bucy filter has a rather long time constant (mainly because of the assumed completeness of the signal and noise dynamical models), which would not allow accurate enough tracking during a loss-of-engine incident. A short time constant, or fast responding, estimator must be designed if good tracking data are to be realized after the loss of one of the five first-stage engines occurs. Accordingly, a modified Kalman-Bucy filter was designed and implemented; the modification was achieved by periodically recycling the error covariance matrix to increase the apparent gain of the estimator, and thus allow any change in the data trend to influence the estimator output. Unfortunately, the discontinuity in the velocity signal at the instant of recycling resulted in too high a noise level to provide a useful velocity feedforward signal for the angular control system.

To achieve fast response and to reduce periodic transients in the estimator output, it was decided to perform a polynomial fit for each short data span (nominally, 90 data points with a 1/64 second spacing for a total period of 1.4 seconds) and to overlap these fitting polynomials. A cubic polynomial was used to make the acceleration estimate smooth and continuous.

The estimator performance has been simulated by processing measurements obtained from the nominal tracking data and simulated measurement noise. The results of the simulation runs are presented in Table I. The simulation process will be described first, followed by a discussion of the estimator performance.

Tracking data for range, hour angle, and declination were obtained by evaluating, at 1/64 intervals, six-degree polynomials developed from nominal tracking data. The simulation covered a total tracking interval of approximately 69 seconds. The estimation errors were obtained by forming the difference between the position, velocity, and acceleration estimates and the true position, velocity, and acceleration obtained by evaluating the nominal tracking data polynomials and their first and second derivatives. For comparison, the rms value of the measurement noise samples for each 30-sample interval was computed. The measurement noise is a stationary random process with a power spectral density that matches the 1/f trend observed in experimental determinations of angle fluctuation spectra. The estimation error curves were obtained for different total noise and noise correlation time

constant values. It is clear that decreasing the total noise and decreasing the noise correlation time constant will decrease the estimation errors.

The 147 sets of rms estimation errors on 30-sample intervals were also processed to yield rms estimation errors for the entire tracking interval. These total rms errors are arrayed in Table I as a function of total noise and time constant. From this table it is easy to see the extent to which the estimation errors are influenced by the measurement noise characteristics.

The values of total noise, equal to 3, and correlation time constant, equal to 1/14.76 second, correspond to the anticipated worst case conditions when the elevation angle of the laser beam is less than 10 degrees above the local horizon. The actual noise conditions may be less severe. In any event, as the launch vehicle rises, total noise will decrease significantly and the correlation time constant is expected to decrease. The reasons are that the encountered turbulence is less severe at moderate elevation angles and is less correlated as the target range increases. Hence, it is definitely expected that the estimation errors will decrease as time from lift-off increases.

## RANGE SERVO

A simplified block diagram of the range servo loop is shown in Figure 1. The input signal to the loop,  $f_{\text{IFR}}$ , is an IF signal, generated in the heterodyne receiver, with a phase shift proportional to the target range. A locally generated IF signal,  $f_{\text{IFfb}}$ , with a phase shift proportional to the computed range is multiplied with  $f_{\text{IFR}}$  in a phase detector circuit to provide an error signal with an amplitude proportional to the difference in the phase between  $f_{\text{IFR}}$  and  $f_{\text{IFfb}}$ . The detector output is filtered and converted to a binary signal for "sampled data" processing by the computer.

The computer process pertaining to the range loop can be separated into three parts for a simplified description. The first part is a computation which provides proportional plus integral compensation for the servo loop to effectively eliminate velocity errors, minimize acceleration errors, and assure good stability. The second part calculates the range rate and range output words. The third process provides



TABLE I. ESTIMATOR PERFORMANCE AS A FUNCTION OF MEASUREMENT  
AND NOISE PARAMETERS FOR FULL TRACKING PERIOD  
(0 to 68 seconds)

Data Quantity	Noise Correlation Time Constant (seconds)	Measured RMS Noise	Measured RMS Position Error	Measured RMS Velocity Error	Measured RMS Acceleration Error
Range (cm, cm/second, cm/second <sup>2</sup> )	1/14.76	1.04	1.05	8.87	39.0
		2.06	2.13	17.3	75.5
		2.96	2.94	24.2	104.0
	1/29.52	0.986	0.838	7.12	31.5
		1.95	1.59	13.6	60.0
		3.08	2.58	21.6	94.3
	1/44.28	1.0	0.764	6.48	28.7
		2.0	1.51	12.9	57.9
		3.0	2.17	18.1	80.1
Hour Angle (sec, sec/second, sec/second <sup>2</sup> )	1/14.76	1.0	0.985	8.03	35.0
		2.0	2.02	16.7	72.8
		3.0	2.89	23.3	102.0
	1/29.52	1.0	0.827	6.88	29.8
		2.0	1.61	13.7	60.2
		3.0	2.41	20.2	89.2
	1/44.28	1.0	0.736	6.04	26.5
		2.0	1.49	12.7	56.5
		3.0	2.14	18.5	82.9
Declination (sec, sec/second, sec/second <sup>2</sup> )	1/14.76	1.0	0.983	8.11	35.0
		2.0	2.08	17.6	76.6
		3.0	2.98	24.5	107.0
	1/29.52	1.0	0.852	7.19	31.7
		2.0	1.66	13.3	57.0
		3.0	2.42	20.6	91.4
	1/44.28	1.0	0.720	6.15	27.5
		2.0	1.49	12.8	56.6
		3.0	2.17	18.5	81.5

Note: Units of quantities in the table are arc seconds, centimeters, and seconds.

the feedback signal that enables a sufficiently accurate control of the phase shift of the locally generated IF signal. This is accomplished by controlling, with a digital word from the computer, the number of pulses that are to be added to a train of clock pulses. The resulting pulse train is then divided down to yield the local IF signal. This IF signal is a 3 to 4 bit binary signal which is used in a technique of gain switching to provide the desired multiplication for phase detection.

Two other channels of the range servo are indicated in Figure 1. Each channel has a separate phase control, IF generator, phase detector, filter, and sample-and-hold circuits. Switching between channels is accomplished by software programming.

The block diagram in Figure 2 shows the implementation of the range servo loop as simulated on the digital computer. The linearized and simplified representation of the hardware is simulated on the

computer for testing purposes only; the electronic controller represents a part of the software for the laser tracker.

To achieve the required accuracy of 0.5 cm in the output range word, a cycle time of 1/256 second for the electronic controller was found necessary, a 9 bit A/D converter was found adequate, and a bandwidth of 55 rad/second for the servo loop was selected. Depending on the magnitude of the error signal in the closed loop, the range servo will track in either the fine, medium, or coarse mode. As seen from Figure 2, these channels differ in gain values only. A digital signal from the peripheral A/D converter, proportional to the error in the loop, serves as the input to the controller. For a phase error of 0.5 rad, which corresponds approximately to an error in range of 40 cm, the fine-channel goes into saturation and the software switches the tracking operation from channel 3 to channel 2.

The range rate and the output range word are calculated numerically. Proportional plus integral compensation is included to eliminate velocity error, reduce acceleration errors, and assure good stability. The value of acceleration at each iteration is calculated by time differencing and averaging of available range rate words and past acceleration values. This

value of acceleration is then used to compensate for the acceleration error in the output range word.

The phase feedback in the loop is proportional to the range word calculated at the last iteration. This is updated by generating a digital word proportional to the change in range, which controls the number of pulses to be added to the train of clock pulses.

The range output, and hence the digital word proportional to the change in range, is calculated every 1/256 second, while the hardware and the converting equipment operates at 20 kHz. The synchronization between these two is maintained in the software.

Figure 3 shows the response of the servo during "worst case" tracking of the Saturn V launch where compensation has been made for an error caused by acceleration. It can be seen that an error in range at the output stays well within the allowable limits of 0.5 cm.

## ANGULAR CONTROL SYSTEM

The basic angular control system will function

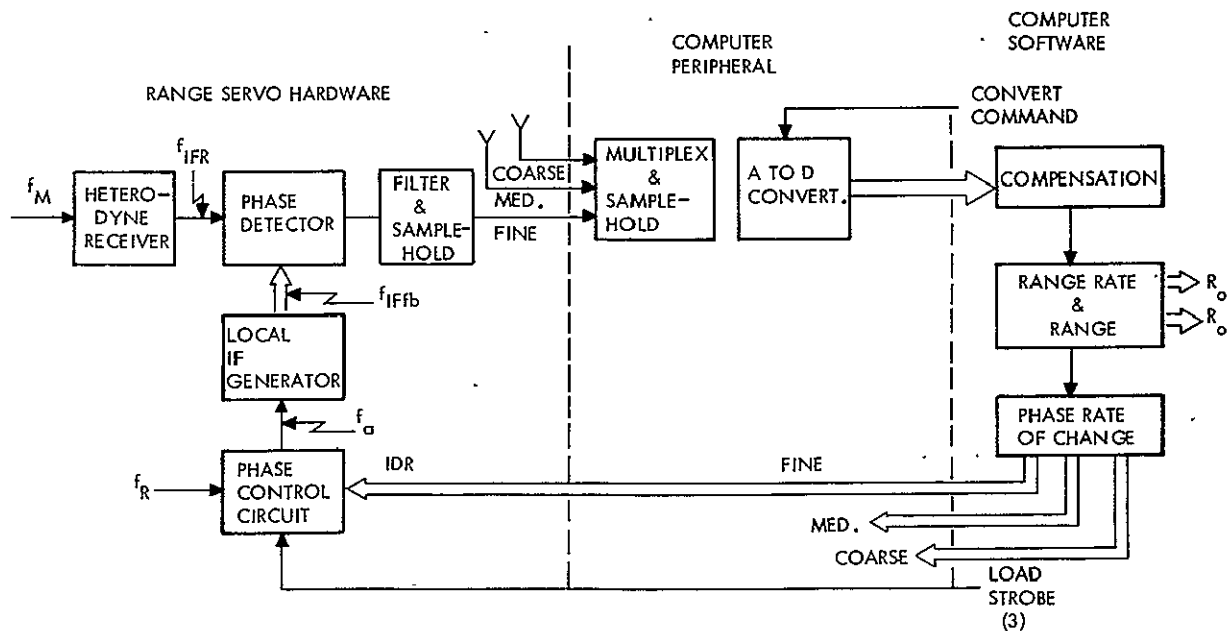


FIGURE 1. RANGE SERVO BLOCK DIAGRAM

in the three allowable system modes. These three modes relate to the acquisition functions of the over-all system. It is best to begin with a discussion of the track mode, which is the steady-state mode for the system program.

A functional block diagram is presented in Figure 4. The salient feature of this diagram is the way in which the error signals are obtained for the mount angle servo. Because of the presence of the target dynamics estimator, it might be desirable to interpose the estimator between the star tracker output and the position error input point of the angle servo; the purpose would be to smooth the noise on the star tracker output signal. However, the time constant of the estimator would introduce an undesirable lag. In the absence of any filtering by the estimator, the proportional plus integral compensation block in Figure 4 must include any noise filtering which must be done. This noise filtering decreases

the bandwidth of the position loop, usually below a value considered satisfactory. The classical trade-off between noise attenuation and a wide bandwidth tracking loop can be avoided by using the estimator to provide a velocity feedforward signal. By this means, good dynamic tracking performance can be obtained while position error measurement noise is substantially reduced.

When the return signal from the target is lost, a signal from the reacquisition hardware will cause the tracking system to enter the reacquire mode (Fig. 5). The basic feature of operation in this mode is that all command signals are provided to the angle servos by the target dynamics extrapolator. The philosophy here is that a loss of signal does not indicate a sudden change in target motion, causing a loss of track, but only an obstruction to transmission of the laser beam (typically a cloud or vapor). Hence while the re-

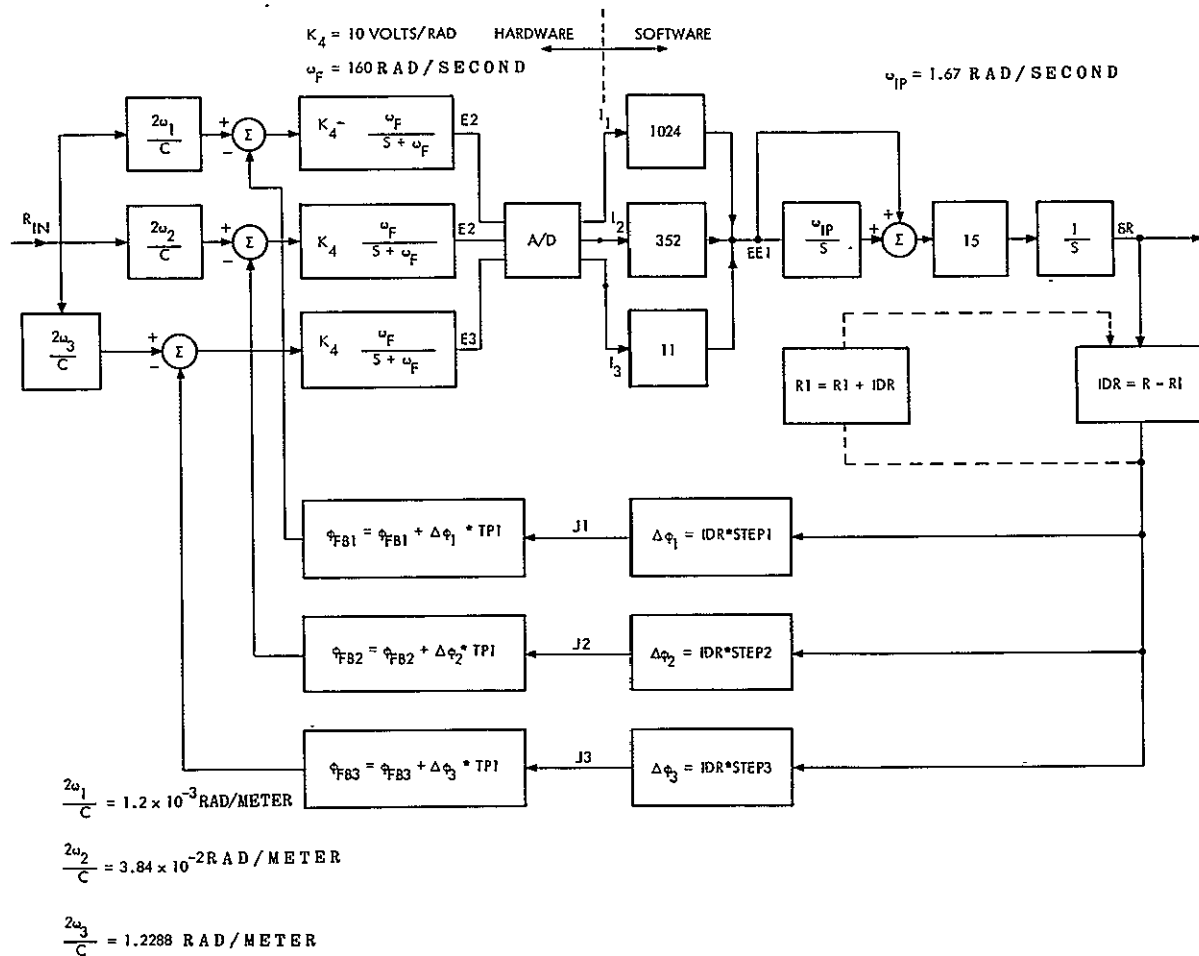


FIGURE 2. RANGE SERVO DETAILED DIAGRAM



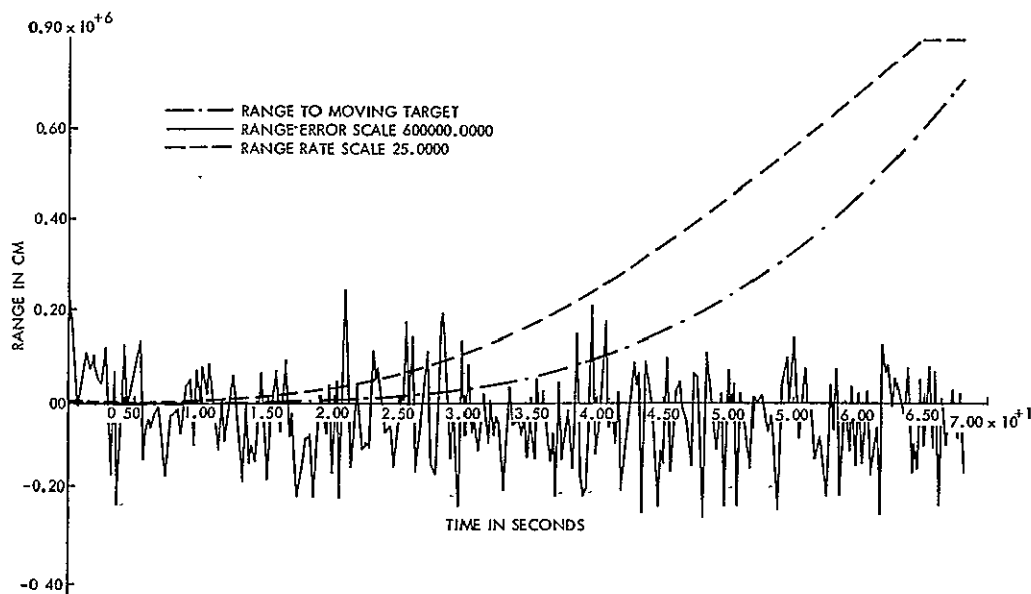


FIGURE 3. RANGE SERVO RESPONSE TO "WORST-CASE" TRACKING OF SATURN V LAUNCH  
(COMPENSATION FOR ACCELERATION ERROR INCLUDED)

acquisition system is searching for a return signal, the telescope will be kept pointed at the expected target position as provided by the extrapolator. Provided the loss of signal condition does not prevail for too long a time (less than 1.5 seconds), the angular tracking error may not be greater than 25 to 30 arc seconds, depending upon the target dynamics at the time of loss of signal.

Finally, it is necessary to mention system operation in the acquire mode. Figure 6 shows that basically the telescope mount is following a programmed target position, which could be a single position as in calibration tests and initial launch vehicle acquisition, or a sequence of positions as in acquiring a satellite. The reason for retaining the estimator is to minimize the velocity and acceleration estimation transient following switching to the track mode.

The hour angle and declination axes of the tracking telescope are individually controlled by identical servos. Because these high performance servos are implemented in a digital computer, much flexibility in design is available. In particular, it now becomes feasible to implement a procedure for compensating for servo saturation during large signal transients. The existence of the target dynamics estimator allows the use of velocity feedforward, permitting, in turn, the smoothing of position error signals without loss of dynamic performance. In other respects, the design is straightforward.

An axis drive of the type described above is generally limited by two types of saturations. The more important is the torque saturation characteristics of the electromagnetic torque motors. The inherent saturation of the torque motors is very gradual, but a very precise limit must be built into the motor drive circuits to prevent motor demagnetization. This gives an abrupt torque (or acceleration) limit which is very detrimental to servo stability and requires some form of compensation.

The rate of the servo drive is also limited either by the motor and the power amplifier or by the linear range of the angular velocity sensor. Therefore, a set of limits must be designed into the servo control circuits (or control program) to prevent the servos from exceeding these limits without affecting loop stability.

The design goals for the torque saturation compensation are not only to prevent a deterioration of servo stability when an abrupt torque limit is introduced, but also to minimize the time required to bring the servos out of the saturated condition. These goals are accomplished by modifying the control program so that the servos operate with full torque applied, first of one polarity and then switched to the opposite polarity until the servo error is brought to near zero. If the switching time is chosen properly, the servo will then enter the linear operating region at approximately the correct velocity.

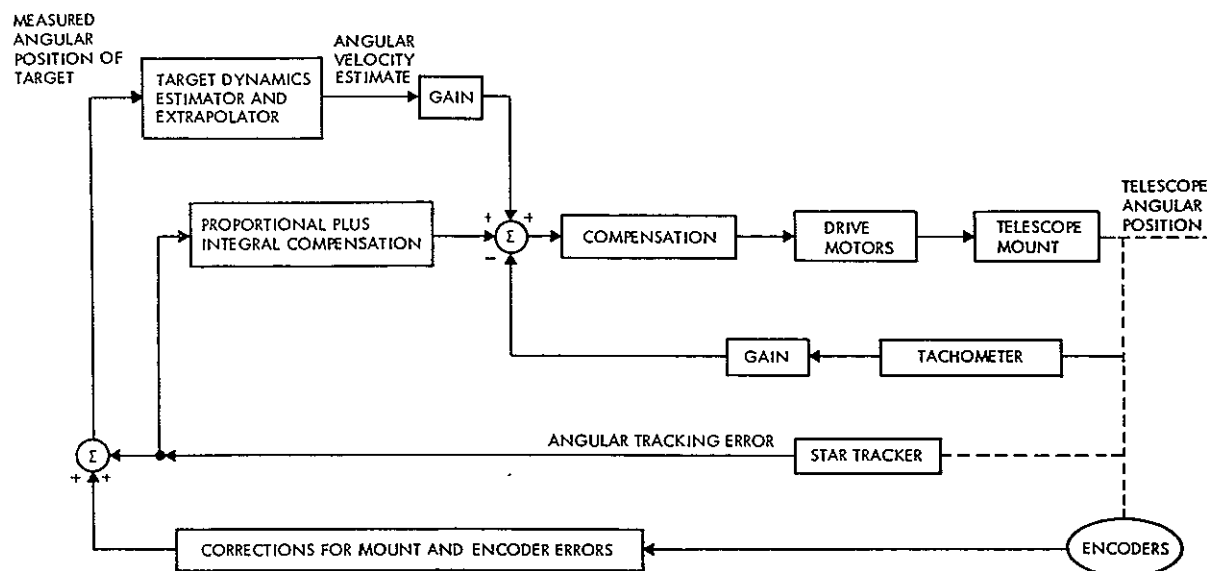


FIGURE 4. ANGULAR CONTROL SYSTEM CONFIGURATION IN TRACK MODE

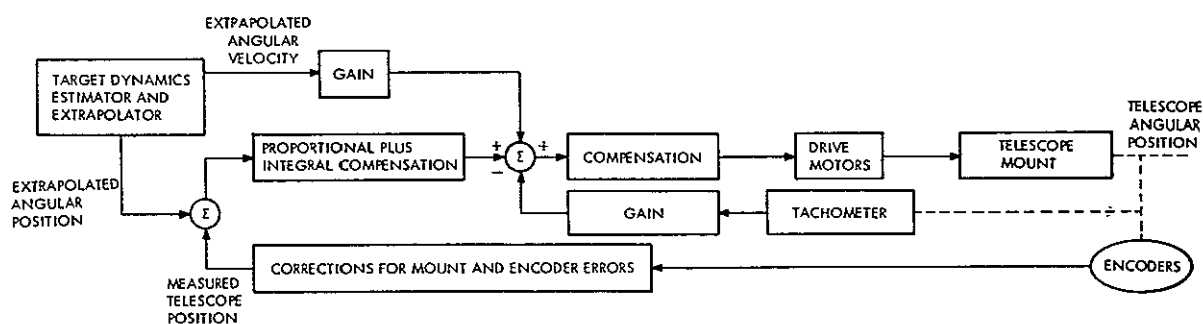


FIGURE 5. ANGULAR CONTROL SYSTEM CONFIGURATION IN REACQUIRE MODE

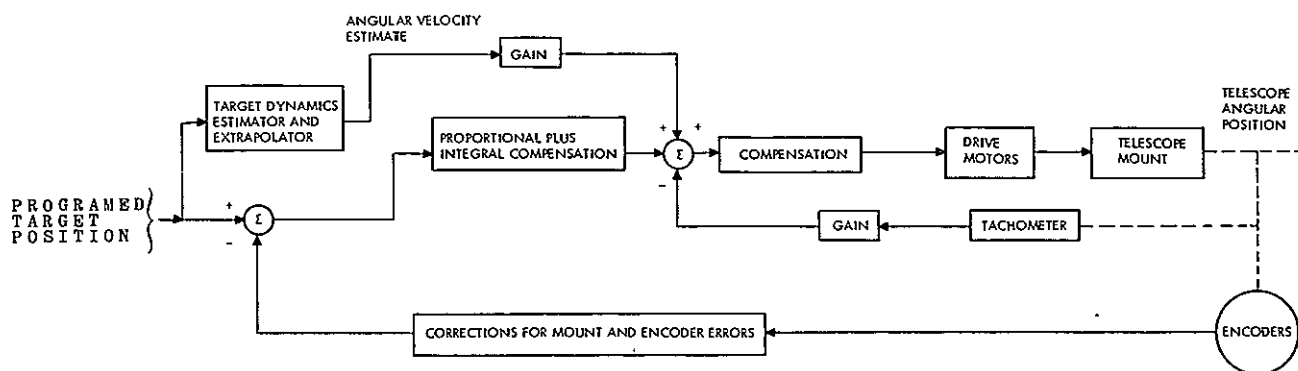


FIGURE 6. ANGULAR CONTROL SYSTEM CONFIGURATION IN ACQUIRE MODE

The pointing servos have integral compensation in both rate and position loops. These compensations are effective only during linear servo operation and must be removed from the control equations during the saturated mode of operation. The integral compensation equations are removed at the instant of time when the torque command has reached the + or - limit level. A simplified block diagram of the servo in this condition is shown in Figure 7.

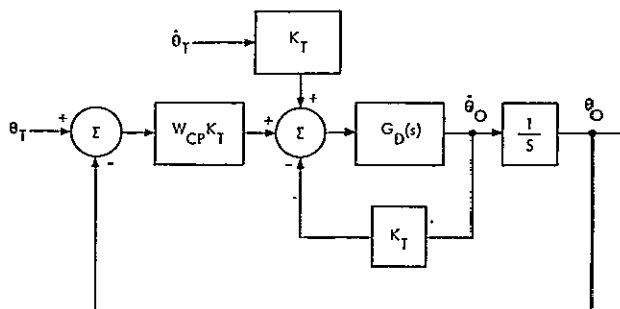


FIGURE 7. SIMPLIFIED BLOCK DIAGRAM OF THE ANGLE SERVO WITH INTEGRAL COMPENSATIONS REMOVED

To obtain a stable operation during the torque limited period of a transient, we may seek to adjust  $W_{CP}$  so that the velocity command to the rate loop does not exceed the velocity that can be obtained with the maximum torque command. For values of the drive torque below the limits, the system is linear and  $W_{CP}$  is determined from the linear analysis.

In the absence of rate feedforward, the velocity command to the rate loop is obtained from the position loop integral compensation. When rate feedforward is used, the compensation equations correct for the inaccuracies in the rate feedforward signal only. In either case, however, when the drive torque reaches the limit, this compensation must be removed from the control program to prevent a build-up of rate command during the saturated mode of operation. At the end of this period, the compensation should be reinstated with an initial condition equal to the condition at the time it was removed. The integral compensation in the rate loop provides a torque command during acceleration. This compensation must also be removed when the torque limit is reached and reinstated with the last computed integral value as the initial condition. During the saturation period, this value is used together with the proportional component to determine the torque requirement.

The servo rate may be limited by limiting the rate command to the servo rate loop. It is also

necessary under this condition to remove the position loop integral compensation to prevent a build-up of the rate command. The compensation in the rate loop could remain intact during this mode of operation. However, if the servo is in the saturated mode of operation when the rate limit is reached, the response of the rate loop is relatively slow and the velocity would overshoot significantly. This overshoot can be avoided by resetting (to a low level) the integral part of the torque command momentarily upon reaching the rate limit.

The angle servo control performance was studied in a digital simulation which included all linear characteristics of the model and the nonlinear parts of the control program. In addition to the nonlinearities built into the control program, the simulation also included the sampled data process, the conversion processes, and the axis friction-stiction characteristics. The purpose of the simulation study was to show that satisfactory performance can be achieved under the assumptions of low-noise star tracker output and under all possible transient conditions. Specifically, the following performance characteristics were studied:

1. Small and large signal step responses
2. Tracking of slowly moving targets
3. Tracking a Saturn V vehicle during launch (worst case)
4. Significance of rate feedforward

The response to a small step change in the angular command is shown in the plots of Figure 8. The 0.057 degree (1 mrad) step is too small to cause torque saturation, and the control program operates entirely in the linear range. The linear response is distorted, however, by the axis friction-stiction which was set at 6.78 and 10.8 N-m (5 and 8 ft-lb), respectively. Adequate stability and satisfactory speed of response are indicated. The response to a step angular command of 0.57 degree (10 mrad) is shown in Figure 9. This command is sufficient to cause torque command saturation which activates the part of the control program that compensates for this saturation. It is evident that the compensation yields a near optimum response for this input since the new commanded position is reached with practically no overshoot under the condition of maximum acceleration followed by near maximum deceleration.

When the step command is increased, the angular rate of change reaches the rate limit. Figure 10 shows a set of plots for a step input com-

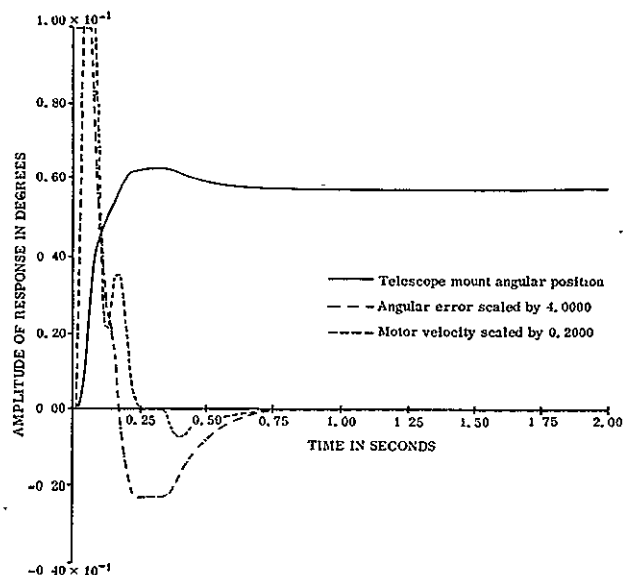


FIGURE 8. SMALL SIGNAL STEP RESPONSE

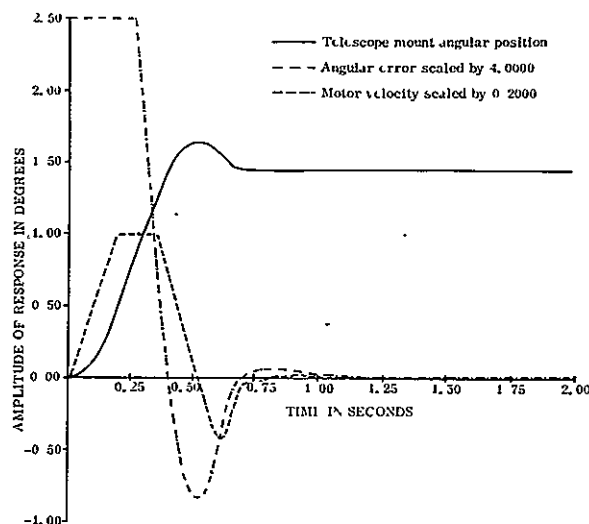


FIGURE 10. RESPONSE TO STEP CHANGE IN ANGULAR COMMAND, RESULTING IN BOTH TORQUE AND VELOCITY COMMAND SATURATIONS

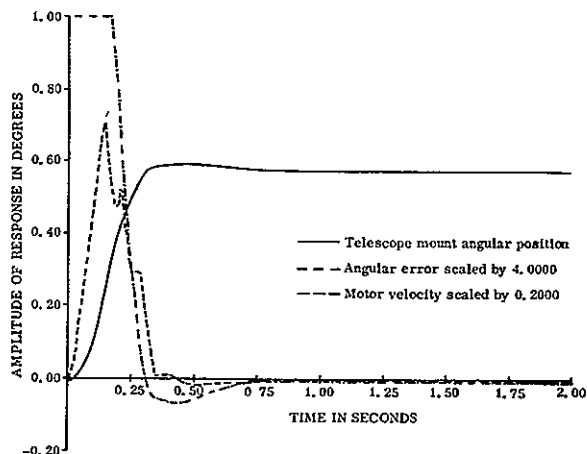


FIGURE 9. RESPONSE TO STEP CHANGE IN ANGULAR COMMAND, RESULTING IN TORQUE COMMAND SATURATIONS

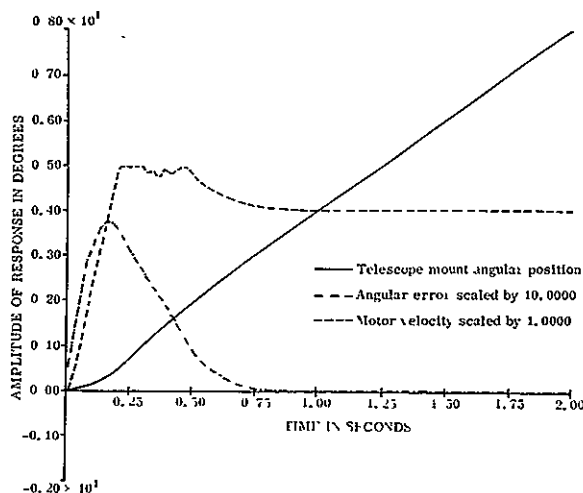


FIGURE 11. RESPONSE TO STEP CHANGE IN ANGULAR VELOCITY COMMAND, RESULTING IN SATURATIONS OF BOTH TORQUE AND VELOCITY COMMANDS

mand of 1.43 degrees (25 mrad). In this case, maximum acceleration takes place until the rate limit of 5 degrees/second is reached. The rate is limited to this level without overshoot and remains there until maximum deceleration is switched on. For this example, there is a relatively small overshoot at the end of the transient, but no instability is indicated. Both types of saturation also occur when a large step change of velocity command is applied. This type of response is shown in Figure 11, which again indicates fast recovery and good stability.

The performance of the servo during tracking of a slowly moving target is illustrated by the plots shown in Figure 12. In this run, the target velocity is varied according to the equation given below the plots. The dynamic errors in this example are negligible so that the tracking errors developed result from the combined effect of the discrete errors

in the conversion processes and the friction-striction load. The effect of the latter is quite evident in the stop-and-go characteristics at very low velocities in Figure 12. Peak errors are found at the point where the velocity changes sign; the value of the errors at this point is approaching  $\pm 1$  arc second.

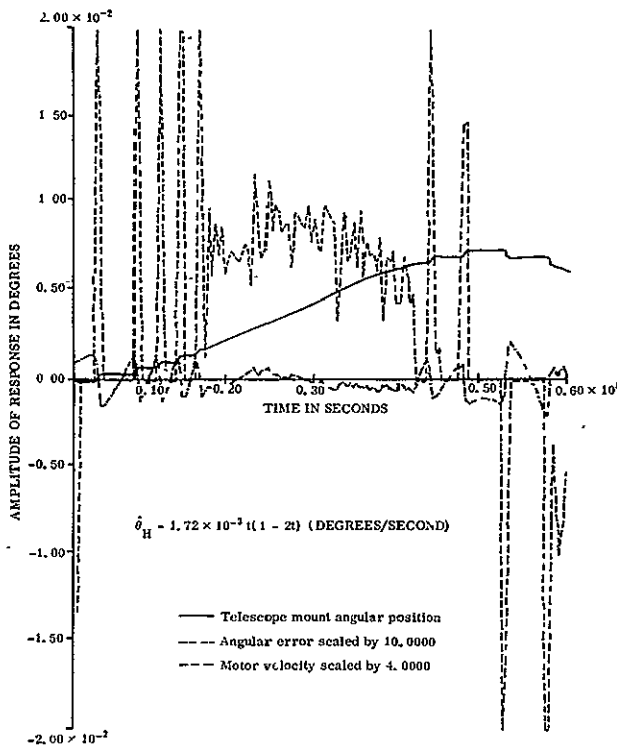


FIGURE 12. TRACKING A SLOWLY MOVING TARGET. VELOCITY RANGE OF 0.002 DEGREES/SECOND THROUGH ZERO

The tracking of a Saturn V launch has been simulated by approximating the expected launch trajectory with a 6-order polynomial with peak velocity of 3.25 cm/s and peak acceleration of 0.13 cm/s<sup>2</sup>.

These values of rate and acceleration, which are considered typical worst case, would result in a peak dynamic error of approximately 0.0013 degrees (4.17 arc seconds) without rate feedforward and less than 0.5 arc second when perfect rate feedforward is used. The plots of Figure 13 show the target angular trajectory, angular rate, and tracking errors when no rate feedforward is used. The peak error developed is close to the 4 arc

seconds expected. The simulation is repeated in Figure 14 but with 85 percent of the exact rate feedforward signal applied. In Figure 15 the exact rate feedforward is applied 100 percent. A perfect rate signal is not expected, but the plots indicate that slowly varying deviations of up to 15 percent of the true target angular rate would still yield a performance improvement of 5 to 1.

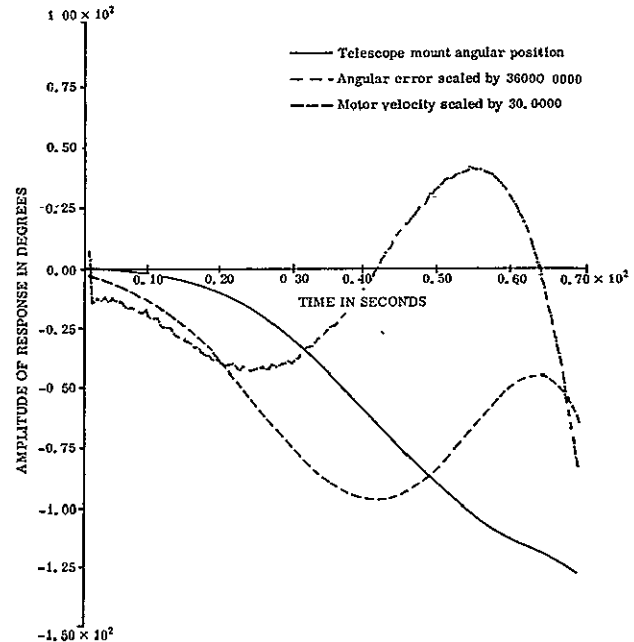


FIGURE 13. SIMULATION OF THE HOUR ANGLE SERVO DURING "WORST-CASE" TRACKING OF A SATURN V LAUNCH WITH NO RATE FEEDFORWARD USED

The linear control equations for the telescope angle servos were derived by means of conventional control theory. These equations involve linear integration, which could make the equations for numerical solutions lengthy and complex if many digits of accuracy are required. However, the control equations are part of a closed loop and compensation for inaccuracies is made automatically. It has been found sufficient, therefore, to use numerical integrating techniques which involve the previous and present sample (or calculated) values only.

The flexibility of programing has been used with advantage to implement torque and rate limits

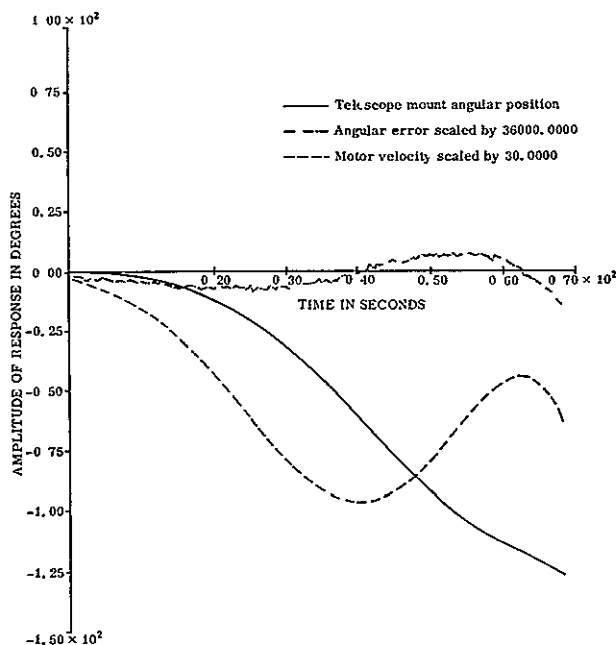


FIGURE 14. SIMULATION OF THE HOUR ANGLE SERVO DURING "WORST-CASE" TRACKING OF A SATURN V LAUNCH WITH 85 PERCENT OF RATE FEEDFORWARD APPLIED

and to solve the control equations for optimum performance during operations when these limits are applied. Simulations of the complete angle servo indicate unusually quick and stable responses in both linear and saturated conditions.

The accuracy of A/D and D/A conversion required to hold the discrete noise to a level which does not deteriorate the tracking accuracy was found to be well within the state-of-the-art. An A/D conversion of 13 bits total and a D/A of 9 bits was found adequate for an accuracy of 0.25 arc second in this application. The overall noise introduced by the conversion and computation processes was found by simulation to be approximately 0.5 arc second peak-to-peak.

When a good target angular rate signal is available, a very significant improvement may be realized by using rate feedforward. Simulations indicate that dynamic errors may be reduced by better than 10:1 if a true rate signal is available. Some indication of

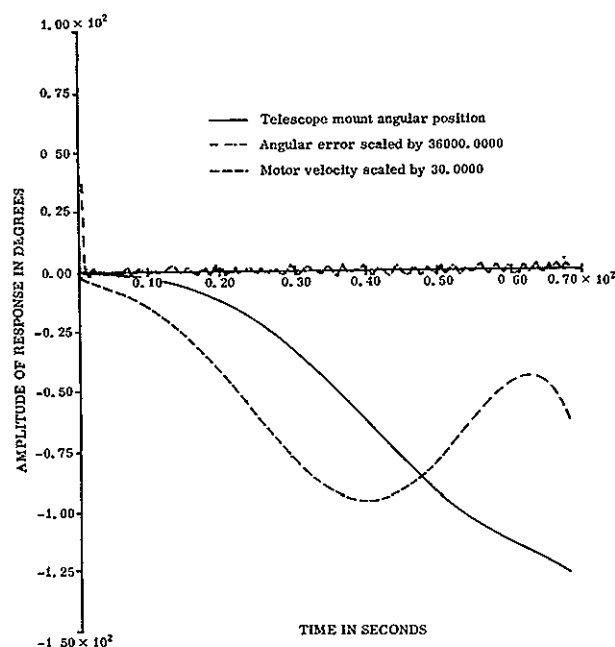


FIGURE 15. SIMULATION OF THE HOUR ANGLE SERVO DURING "WORST-CASE" TRACKING OF A SATURN V LAUNCH WITH 100 PERCENT RATE FEEDFORWARD APPLIED

how much the rate signal may deviate from the value was indicated by introducing a fixed 15 percent error in the signal used for feedforward. Under this condition, a 5:1 improvement of the dynamic errors was realized.

## CONCLUSIONS

It is apparent that the computational requirements of a laser pointing, tracking, and ranging system controller are complex and extensive. A change in mission, a change in mode of solution, a change in system hardware, a deterioration of saturation limits would all require significant reworking of the system controller. A programmable on-line digital computer represents the most powerful, most economical, and most maintainable as well as the fastest solution to the system controller requirements. A more detailed definition of computer requirements and programs can be found in Reference 1.

## REFERENCE

1. O'Donnell, J. J.; Glass, J.; Gajwani, S.; Knutrud, T.: Programed Computer Control for Laser Tracking. Final Report, Contract No. NAS8-21089, Sylvania Electric Products, Inc., May 1968.

PRECEDING PAGE BLANK NOT FILMED.

# LUNAR ROCKET RESCUE BEACON

By

Lee B. Malone, Jr.

N 69-36580

## SUMMARY

The results of a feasibility investigation for an emergency relay communications system between a lunar module (LM) and an extra vehicular astronaut (EVA) are presented. The proposed system uses a small, hand launched rocket containing a miniaturized transceiver. This communications relay is injected between existing Apollo communications equipment in the LM and the astronaut's back-pack. This paper shows that it is feasible to provide a short range, light weight, voice relay communications system between the LM and EVA for periods up to 200 seconds.

## DEFINITIONS

Beacon — A rocket launched transmitter which transmits a tone to indicate an emergency

Coded Beacon — A rocket launched transmitter which transmits a coded message to indicate one of several types of emergency situations

Transceiver — A rocket launched receiver and transmitter combination which permits voice communication between the lunar module and a remote astronaut in an emergency

PLSS — Portable life support system

AGC — Automatic gain control

## INTRODUCTION

With lunar exploration a near reality, it is highly desirable to provide the astronaut with an emergency communication device, i.e., some means of conveying information from the exploring astronaut to the lunar module (LM). The purpose of this study is to investigate the feasibility of an emergency communication system between the LM and extra vehicular

astronaut (EVA). To minimize the addition of hardware on the LM the existing receiving and transmitting equipment in the LM and the astronaut space suit is incorporated as a part of the communication system.

Since very little information exists on the propagation aspect of the lunar surface [1], low frequency communications will not be considered. Instead, maximum use of the existing LM and EVA communications system will be investigated. With the antenna heights of the LM and the EVA fixed, and assuming a smooth lunar surface, line-of-sight communications are limited to about 2.5 km (1.2 miles). For communications up to 50 km (30 miles), it was determined that a radio relay at an altitude high enough to be above the line-of-sight of the stations would be necessary. It was also determined that a miniature rocket package similar to the Thiokol M127A1 signal flare could be modified to propel a miniature communications relay to the required height (Fig. 1).

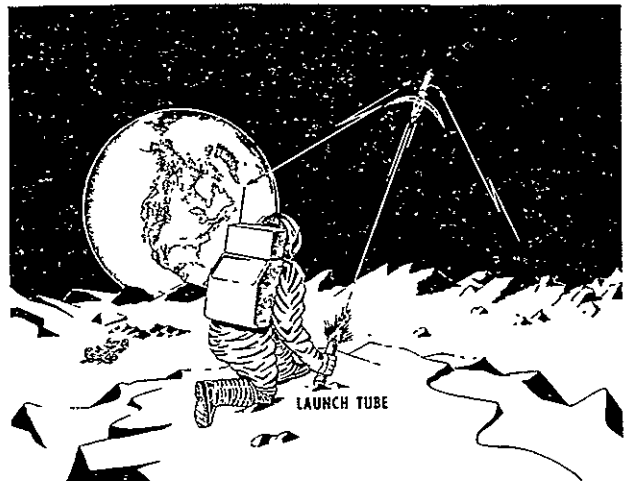


FIGURE 1. LAUNCH TUBE

The weak lunar gravitational field makes the rocket propelled relay method attractive since the altitudes and flight times attainable even by small rockets are amazingly high. A thermal battery

appears to be the most desirable power source for the communications relay. The thermal battery offers rugged construction, small package density and weight, and almost unlimited storage life.

To provide aid as rapidly as possible to an EVA in an emergency situation, it is desirable to incorporate a position-finding system in the LM. The position-finding equipment would detect the presence of the distress signal and give a visual indication of the azimuth and range to the relay. A portion of the position-finding circuitry will sample and store various readings of azimuth and range along the trajectory of the communications relay, allowing extrapolation of the trajectory and a minimization of error caused by the trajectory of the rocket. A continuous-wave, phase-comparison position-finding system was selected as a means of locating the EVA who had given the distress signal. Other techniques were considered and discounted for various reasons discussed. Expected accuracy of the selected position-finding system is given in the section on range and azimuth measuring system.

## INVESTIGATION OF METHODS OF COMMUNICATION

### GENERAL

Three possible methods for obtaining an emergency communication link between the EVA and LM were examined and compared. The three methods are (1) a transceiver which allows two-way communication and position finding, (2) a coded beacon which indicates the type of emergency, and (3) a

beacon which only indicates that an emergency has occurred. Amplitude modulation will be used with each method to be compatible with the LM and the astronaut communication system.

### TRANSCIVER SYSTEM

**Transceiver Description.** The transceiver-relay system is the most attractive of the three proposed systems because it provides much more information than either of the other two. It makes two-way communication possible in the simplex mode between the EVA and the LM in the event of an emergency. Also, the location of the EVA can be determined with this system.

The transceiver (Fig. 2) is comprised of a receiver and a transmitter. It relays voice and bio-medical data from the EVA to the LM and voice from the LM to the EVA. The detection and remodulation technique was used rather than straight frequency conversion because of the inherent higher efficiency of the class C power amplifier over the class A amplifier required with the frequency conversion technique.

The transmitter section consists of a crystal oscillator at 148.4 MHz, a doubler, a modulator, and a power amplifier. The receiver section consists of a low noise rf amplifier, a mixer, an IF section, a detector, and probably a video amplifier. The rf amplifier and the mixer should utilize field effect transistors for low noise and good isolation between the inputs and outputs of these stages. A portion of the output of the doubler will be used as the receiver local oscillator (L.O.). This will result in a rather high IF, but it will save at least one and possibly two

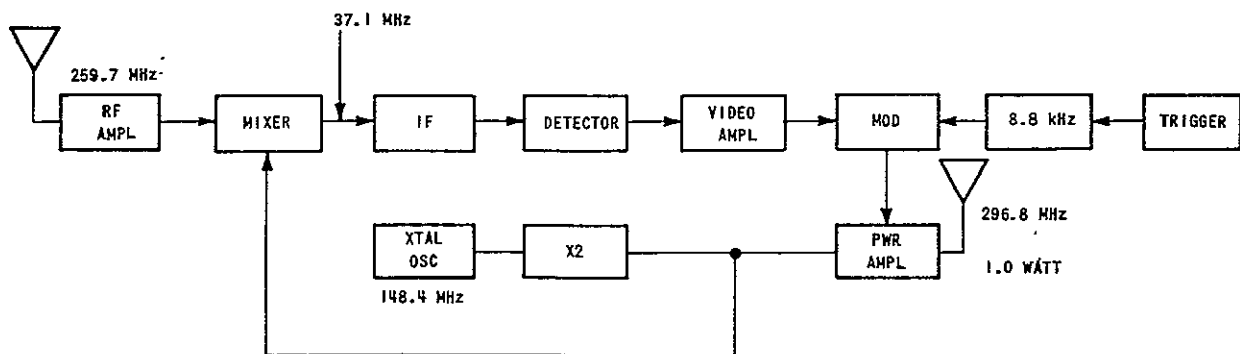


FIGURE 2. TRANSCIVER BLOCK DIAGRAM



stages. It may be possible to eliminate the video amplifier, and a decision on this will have to await a more extensive examination of the gain of the receiver front end. The 8.8-kHz oscillator provides a timing signal which is discussed later. The oscillator will be turned on at 20 seconds after launch for about 1 second and then automatically turned off. This time is used as a time-after-launch reference for azimuth and range determination. The transceiver parameters are given in Table I. Figure 3 shows the transceiver baseband response.

TABLE I. TRANSCEIVER PARAMETERS

Receiver frequency	259.7 MHz
Transmitter frequency	296.8 MHz
Power output (unmodulated)	1.0 W
Minimum expected input	-85 dBm
Receiver dynamic range	Greater than 80 dB
Receiver noise figure	6 dB

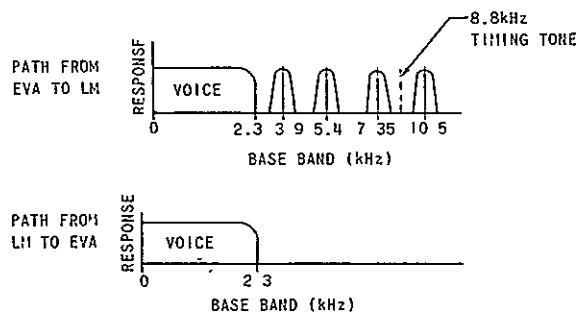


FIGURE 3. TRANSCEIVER BASEBAND RESPONSE

Signal-to-Noise Calculations for the Communications Loop. The signal-to-noise (S/N) calculations for the four paths in the communication loop are given in Table II. Refer to Figure 4 for a definition of the transmission paths. Antenna gain and cable losses for each system are assumed to be zero dB.

The S/N ratios throughout the loop are sufficiently high to provide reliable voice and data reception. Table II lists the tabulated transmission parameters.

#### CW BEACON SYSTEM

The simplest of the three emergency communication systems investigated is the one-way CW beacon

TABLE II. TRANSMISSION PARAMETERS

Path	$P_t$	P. L (Free Space)	S/N Out
1	27.42 dBm	104.75 dB	31.73 dB (voice + biomed + PLSS)
2	30.44 dBm	115.87 dB	22.39 dB (voice + biomed + PLSS)
3	37.27 dBm	114.71 dB	32.28 dB (voice)
4	30.28 dBm	106.90 dB	31.38 dB (voice)

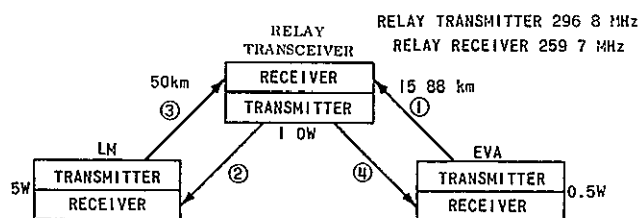


FIGURE 4. TRANSMISSION PATHS

system, but it provides less information than either of the other two proposed systems. It will indicate that an emergency has occurred but will not provide information about the type of emergency.

The rocket-boasted portion of the system contains a simple transmitter which is intermittently modulated by an audio tone. A block diagram of the rocket mounted equipment is shown in Figure 5.

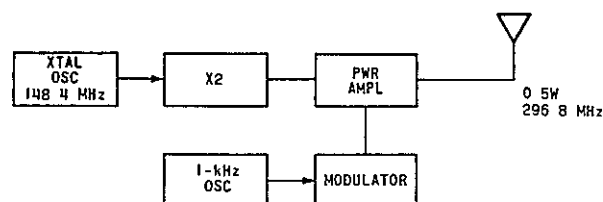


FIGURE 5. CW BEACON TRANSMITTER

The LM equipment could consist of the receiver already aboard the LM plus some shaping and trigger circuitry and a warning lamp. A block diagram of the LM based equipment is shown in Figure 6. The audio tone will be audible through the receiver speaker and will also be used to provide a visual indication of an emergency.

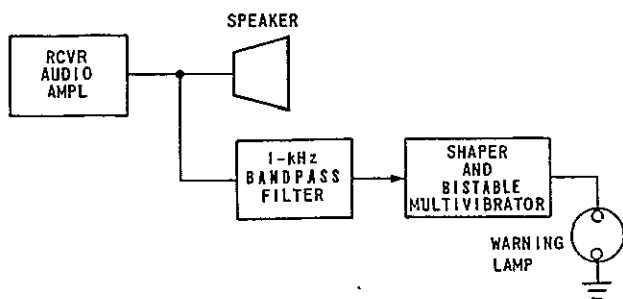


FIGURE 6. LM EQUIPMENT FOR CW BEACON SYSTEM

The transmitter will provide an unmodulated power of about 0.5 W with a modulation index of 50 percent. The actual modulation index can be anywhere between 0 to 100 percent; 50 percent was chosen for ease of calculation. The computed S/N ratio at the output of the 1 kHz filter is 32.52 dB. This S/N ratio is high enough to provide reliable information to the LM in an emergency.

#### CODED BEACON SYSTEM

Two types of coded beacon systems were examined. Both are fairly simple and provide the same information. They give an indication of the type of emergency that has occurred.

**Coded Beacon.** The first type of coded beacon investigated is the simplest and is the one recommended for use if the decision is made to use a coded beacon system. A block diagram of the coded beacon is shown in Figure 7. Five codes are possible with the system as shown but more can be added by increasing the number of resistors and lines to the subcarrier oscillator (SCO). The desired code is set into the transmitter by breaking all the lines except the one which represents the code. A dc voltage is then applied to the signal input of the SCO causing its frequency to shift by an amount which is proportional to the applied voltage.

The signal is received by the existing LM receiver. The video output of the receiver is passed through a bandpass filter to an FM discriminator. The output of the discriminator will be a dc voltage which is proportional to the frequency shift of the SCO. The level of the dc voltage causes one or more of a series of indicator lamps to be illuminated, giving a visual display of the received emergency code. A block diagram of the receiver system is shown in Figure 8. As an example of a code, suppose

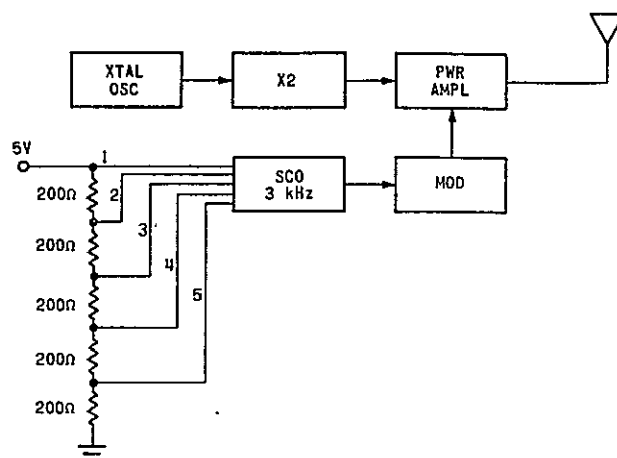


FIGURE 7. CODED BEACON

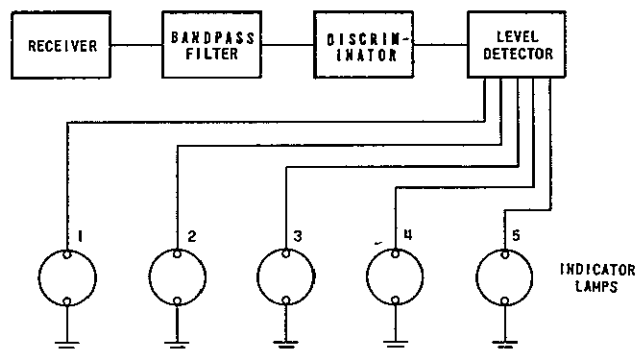


FIGURE 8. LM EQUIPMENT FOR CODED BEACON

that code No. 3 was sent. At the receiver, three of the indicator lamps will illuminate. It is also possible to use the SCO to give an audio indication of an emergency so that the LM astronaut will know to check the display to find out the type of emergency.

It should be mentioned that the SCO, the bandpass filter, and the discriminator are standard telemetry equipment and are therefore readily available [2].

The beacon transmitter power is 0.5 W unmodulated. The modulation index was chosen to be 50 percent. The computer S/N ratio at the output of the discriminator will be greater than 30 dB. With this S/N ratio the probability of noise triggering the indicator lamps will be much less than 1 percent.

**Alternate Coded Beacon.** The second coded beacon is somewhat more complicated than the first and is presented here only as a possible alternative. A block

diagram of the alternate coded beacon is shown in Figure 9. The outputs of the three SCO's are fed into the modulator. The desired code is set by breaking one or more of the lines from the SCO outputs to the modulator input. With three SCO's, seven codes are possible.

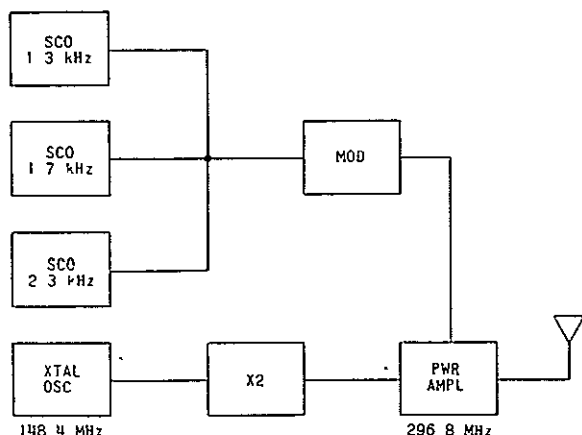


FIGURE 9. ALTERNATE CODED BEACON

The receiver system is shown in Figure 10. The video output of the receiver is applied to the inputs of three bandpass filters so that the composite signal is separated into its components. The outputs of the filters are rectified and the resulting voltage illuminates indicator lamps for a visual presentation of the code. An audio indication of the emergency will also be obtained through the receiver's speaker.

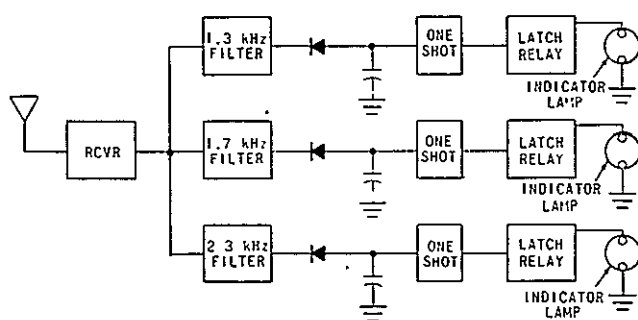


FIGURE 10. LM EQUIPMENT FOR ALTERNATE CODED BEACON

The S/N ratios for the three channels were computed. A modulation index of 30 percent was

assumed for each channel. The unmodulated transmitter power is 0.5 W. The S/N ratio at each filter output is 27 dB. This ratio will be high enough to ensure reliable reception of the transmitted code.

#### RELAY ANTENNA REQUIREMENTS

The antenna requirements for the beacon and coded beacon are fairly simple because the only pattern direction necessary is toward the LM. The requirements can be met by using a stub antenna mounted at the top or bottom of the relay package.

The requirement for the transceiver system is somewhat more complicated because there cannot be a null in the pattern in either the direction of the LM or the EVA. The pattern in the shape of a fat cardioid will be satisfactory if the null is at the top of the relay signal device. An acceptable pattern is shown in Figure 11.

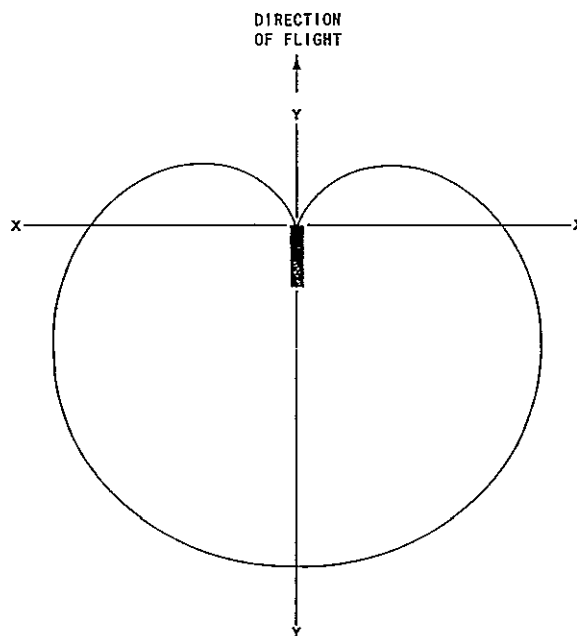


FIGURE 11. ANTENNA PATTERN FOR TRANSCEIVER

No decision has been made as to the method of obtaining the pattern since the time frame has not been sufficient for the antenna design. A suitable pattern to provide adequate coverage is believed to be achievable.

## RELAY TRAJECTORY INVESTIGATION

### TOTAL TRANSMISSION TIME

With the information that a modified rocket motor similar to the motor contained in the Thiokol signal flare could propel a 0.45-kg (1-lb) communications relay 8000 m (26 240 ft) into free space (Fig. 12), an investigation into the total time of flight of the relay was conducted. The following calculations show that the time of flight of the communication relay is approximately 200 seconds.

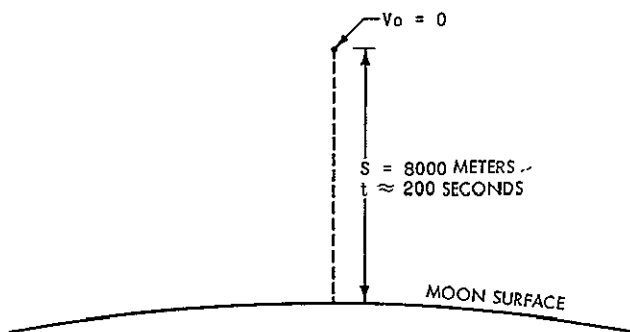


FIGURE 12. TIME OF FLIGHT OF COMMUNICATIONS RELAY

Given: Mean surface gravity of moon

$$= g_m \text{ (m/s}^2\text{)} = \frac{g_e \text{ (m/s}^2\text{)}}{6} = \frac{9.78}{6} = 1.64 \text{ m/s}^2$$

(or 5.37 ft/s<sup>2</sup>). Maximum altitude achieved by relay = S = 8000 m (26 240 ft).

Solution:

$$S_m = V_0 t + \frac{1}{2} g t^2$$

$$8000 = 0 + \frac{1}{2} (1.64) t^2$$

$$t^2 = \frac{8000}{0.82} = 9756 \text{ s}^2$$

$$t = \text{time to free fall 8000 meters on moon} = 98.77 \text{ seconds; therefore, time of flight} = 2(98.77) = 197.54 \text{ seconds}$$

$$\approx 3 \text{ min } 20 \text{ seconds}$$

$$\text{Average velocity} = \frac{S}{t} = \frac{8000}{98.77} = 80.5 \text{ m/s}$$

$$\text{(or 264 ft/s)}$$

Initial velocity = initial velocity of relay as it leaves the lunar surface

$$= 2(\text{ave. vel.}) = 2(80.5) = 161 \text{ m/s (or 528 ft/s)}$$

### ERRORS INTRODUCED BY THE TRAJECTORY OF RELAY

The position-determining equipment to be located in the LM measures the slant range to the communications relay. Figure 13 indicates that error which could be introduced into the position location because of various launch angles. It should also be observed that the launch angle also influences the time that the relay is in line-of-sight (above the horizon).

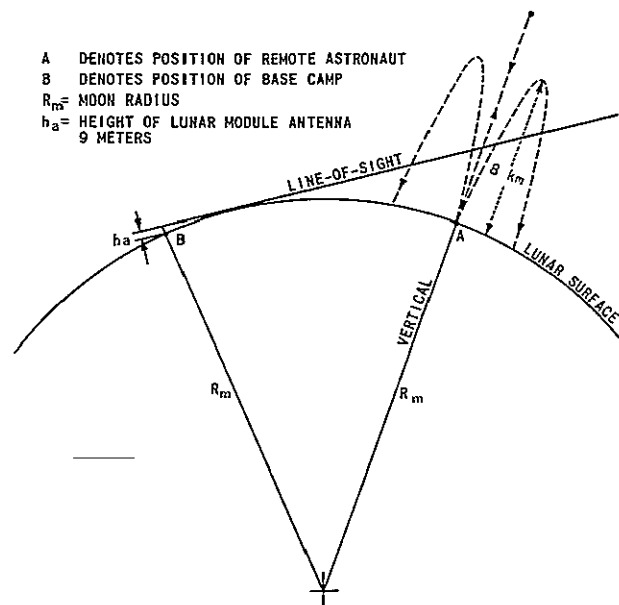


FIGURE 13. MASKING EFFECT OF LUNAR SURFACE

An investigation of the possible error caused by a launch angle of 45 degrees from the vertical was conducted. The following calculations indicate the trajectory of the communications relay caused by a 45-degree launch angle.

Given:

h = maximum height attained by the communications relay

R = distance from launch site upon impact on lunar surface

$\theta$  = launch angle from horizontal = 45 degrees

$V_0 = 161 \text{ m/s.}$

Solution:

$$R = \frac{2V_0^2 \sin \theta \cos \theta}{g_m} = \frac{2(161)^2 (0.707) (0.707)}{1.64}$$

$$= 15\,880 \text{ m (or } 52\,084 \text{ ft)}$$

$$h = \frac{V_0^2 \sin^2 \theta}{2g_m} = \frac{(161)^2 (0.707)^2}{3.28}$$

$$= 3956 \text{ m (or } 12\,975 \text{ ft)}$$

The above calculations were repeated for a launch angle of 5 degrees from the vertical and are as follows:

$$R = \frac{(2) (161)^2 (\sin 85 \text{ deg}) (\cos 85 \text{ deg})}{1.64}$$

$$= \frac{2(161)^2 (0.996) (0.087)}{1.64}$$

$$= 2740 \text{ m (or } 8988 \text{ ft)}$$

$$h = \frac{(161)^2 (0.996)^2}{3.28} = 7906 \text{ m (or } 25\,931 \text{ ft)}$$

The previous calculations indicate that the weak lunar gravitational field compounds the problem of position location by locating a communication relay launched by an astronaut removed from the base camp. It may be seen (Fig. 13) that the slant range and azimuth from the base camp to the relay at various points along the trajectory of the relay will not coincide with the azimuth and range to the astronaut. For this reason the position-finding circuitry will include the sample and hold logic previously mentioned that will allow extrapolation of the trajectory and minimization of the error in position location. It may also be seen from Figure 13 that the greatest "time-in-view" and smallest error in range and azimuth to the astronaut will occur when the relay is fired toward the line-of-sight. However, if the astronaut is lost, the line-of-sight will be unknown to him. It is recommended that the relay be launched as near vertical as is possible to provide a trajectory that will be best suited for most circumstances.

#### DETERMINATION OF MASK CAUSED BY CURVATURE OF MOON

To determine the usable portion of the trajectory of the communications relay, it is necessary to determine the blind spot in the trajectory caused by the curvature of the moon. See Figure 14 for a definition of the problem.

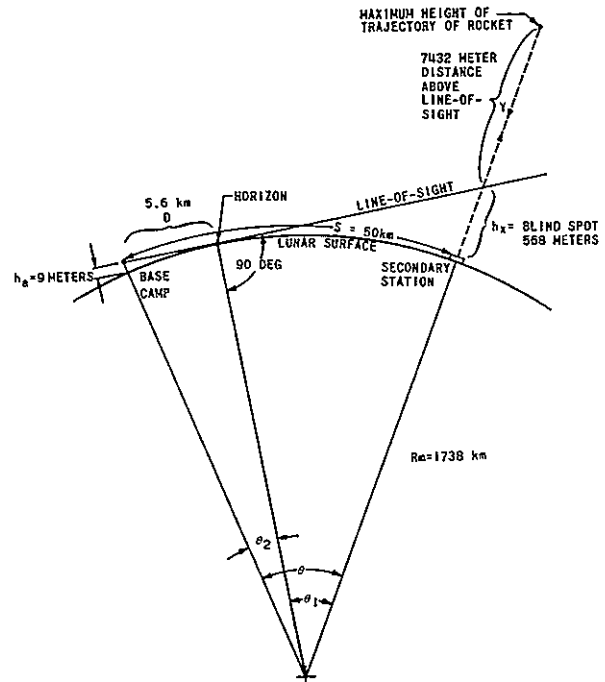


FIGURE 14. DETERMINATION OF BLIND SPOT IN TRAJECTORY

Given:

$R_m$  = radius of moon = 1738 km (or 1080 miles)

$S$  = distance from primary to secondary station = 50 km (or 30 miles)

$h_a$  = height of LM antenna = 9 m (or 29.5 ft)

$g_m$  = lunar gravitational attraction  
 $= 1.64 \text{ m/s}^2 \text{ (or } 5.37 \text{ ft/s}^2)$

Solution:

$$S = R_m \theta \text{ or } \theta = \frac{S}{R_m} = \frac{50 \text{ km}}{1738 \text{ km}}$$

$$= 0.02876 \text{ radians}$$

and

$$\theta = \frac{0.02876}{0.017453} = 1.648 \text{ deg}$$

$$\cos \theta_2 = \frac{1738}{1738 + 0.009} = \frac{1738}{1738.009} = 0.99999482$$

$$\theta_2 = 0 \text{ deg } 11 \text{ min } 4 \text{ sec} = 0.184 \text{ deg}$$

$$\theta_1 = 1.648 \text{ deg} - 0.184 \text{ deg} = 1.464 \text{ deg}$$

$$= 1 \text{ deg } 27 \text{ min } 50 \text{ seconds}$$

$$\cos \theta_1 = 0.99967362$$

$$\cos \theta_1 = \frac{R_m}{R_m + h_x} \text{ or } h_x = \frac{R_m}{\cos \theta_1} - R_m$$

$$- R_m = \frac{R_m - R_m \cos \theta_1}{\cos \theta_1} = \frac{R_m (1 - \cos \theta_1)}{\cos \theta_1}$$

$$h_x = 0.567433 \text{ km} = \frac{(1738)(0.00032638)}{0.99967362}$$

$$= 567.433 \text{ m (or } 1861.656 \text{ ft)}$$

Thus, the blind spot in the relay will consist of the first 567.433 m (1861.656 ft) in the trajectory and also the same distance when it returns by free falling to the lunar surface. It is necessary to determine the time within the flight of the relay at which the altitude  $h_x$  would be attained. The following calculations rounded off to the second decimal place reveal the following:

$$S = V_0 t - 1/2 g_m t^2$$

$$567.433 = 161 t - 1/2 (1.64) t^2$$

$$567.433 = 161 t - 0.82 t^2 \text{ or } 0.82 t^2 - 161 t$$

$$+ 567.433 = 0$$

$$t = \frac{-(-161) \pm \sqrt{(-161)^2 - 4(0.82)(567.433)}}{2(0.82)}$$

$$t = 3.66 \text{ and } 193.9 \text{ seconds}$$

Thus, the trajectory of the relay is in the blind spot for approximately  $2 \times 3.66$  or 7.32 seconds. The usable portion of the trajectory or the transmission time is the total time of flight minus the time within the blind spot.

Therefore,

$$\text{total transmission time} = 197.54 - 7.32 \text{ seconds}$$

$$= 190.22 \text{ seconds}$$

$$= 3 \text{ min } 10 \text{ seconds}$$

The calculations for the blind spot within the trajectory were repeated for a height of the lunar module antenna ( $h_a$ ) of 5 m. The results are:

$$h_x = 604.687 \text{ m (or } 1983.88 \text{ ft)}$$

$$t = 193.8 \text{ and } 3.80 \text{ seconds}$$

Thus, with  $h_a$  equal to 5 m (14.4 ft), the trajectory of the relay is in the blind spot for approximately  $2 \times 3.83$  or 7.66 seconds. The usable portion of the trajectory or the transmission time is the total time of flight minus the time within the blind spot, i.e.,

$$\text{total transmission time} = 197.54 - 7.60$$

$$= 189.94 \text{ seconds}$$

$$\approx 3 \text{ min } 10 \text{ seconds}$$

The previous calculations are based on a smooth lunar surface. Should the LM be located so that an object masks the line-of-sight between the LM antenna and the relay, the transmission path would be affected. Figure 15 provides an example of the effect of a mask on the transmission path. A mask would also affect the accuracy of the position location since detection of the relay could not be effected as early on the trajectory of the rocket. The more rapid rate of change in the trajectory at a later point in the trajectory would make extrapolation of the true position more difficult.

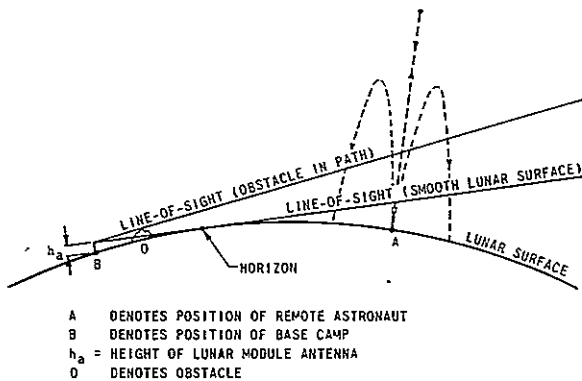


FIGURE 15. EFFECT OF MASK ON TRANSMISSION TIME

## RANGE AND AZIMUTH MEASURING SYSTEMS

### RANGING SYSTEM

The original requirement for the ranging system was to locate the position of the EVA within  $\pm 100$  m (328 ft). This requirement was later relaxed to an accuracy of  $\pm 500$  m (1640 ft). One method for measuring the range was considered and will now be discussed.

**Phase Comparison Technique.** The method for measuring range is to transmit a low frequency sine wave tone on a carrier and measure the phase shift between the transmitted and received tone. This method is especially attractive from the standpoint of bandwidth requirements.

To avoid ambiguous range measurements, the wavelength of the ranging tone must be at least twice the maximum expected range. For the required 50-km (30-mile) range, the wavelength must be at least 100 km (60 miles). The frequency of the ranging tone is

$$\begin{aligned}
 f &= \frac{c}{\lambda} \\
 &= \frac{3 \times 10^8 \text{ m/s}}{1 \times 10^5 \text{ m}} \\
 &= 3000 \text{ Hz.}
 \end{aligned}$$

The frequency chosen for the ranging tone was 2.1 kHz. This allows the astronaut to hear the ranging tone whenever it is transmitted by the transceiver and thus the astronaut can prevent voice from being imposed on the ranging tone. A block diagram of a suggested ranging system is shown in Figure 16.

The carrier signal from the relay transceiver causes the receiver AGC to operate, applying a voltage to AND gate number 1. This voltage, along with the outputs of the two transistor gates  $S_1$  and  $S_2$ , turns on the 2.1-kHz (range tone) oscillator. The output of the oscillator is applied to the modulator of the LM transmitter, thus sending the ranging tone to the transceiver.

A portion of the output of the oscillator is fed into a shaping circuit which squares the waveform and applies it to a  $\div 55$  counter and one shot circuit and to the input of a zero crossing detector. At the end of 55 cycles the one-shot output stage of the  $\div 55$  counter circuit is triggered, removing the output voltage of  $S_2$  and AND gate number 1, stopping the oscillator, and resetting the  $\div 55$  counter.

The ranging tone is received from the transceiver, detected, shaped, and applied to a second zero crossing detector. The outputs of both zero crossing detectors are applied to the trigger inputs of a bistable multivibrator. The shaped tone from the 2.1-kHz oscillator causes the multivibrator to go into the "1" state and the signal from the receiver causes it to return to the "0" state. The integrated output of the multivibrator is proportional to the range to the transceiver. The output of the multivibrator is averaged in the integrator and this average value is fed into the five AND gates. One of the AND gates is selected by the decode gates and its output is fed into a counter which measures the range. Five range measurements are made at selected intervals from an interval clock (probably 2 seconds apart). One measurement is held in each of the counters.

A time of flight measurement is made to give a reference for plotting the trajectory of the transceiver from the five range measurements. The transceiver will generate an 8.8-kHz tone 20 seconds after rocket propellant ignition. This tone turns off a counter at the LM which was started when the transceiver carrier was first received. The flight time in seconds to which the first range measurement was made can be found by taking the difference between 20 seconds and the time shown on the counter. The 20-second time interval was chosen so that the transceiver would

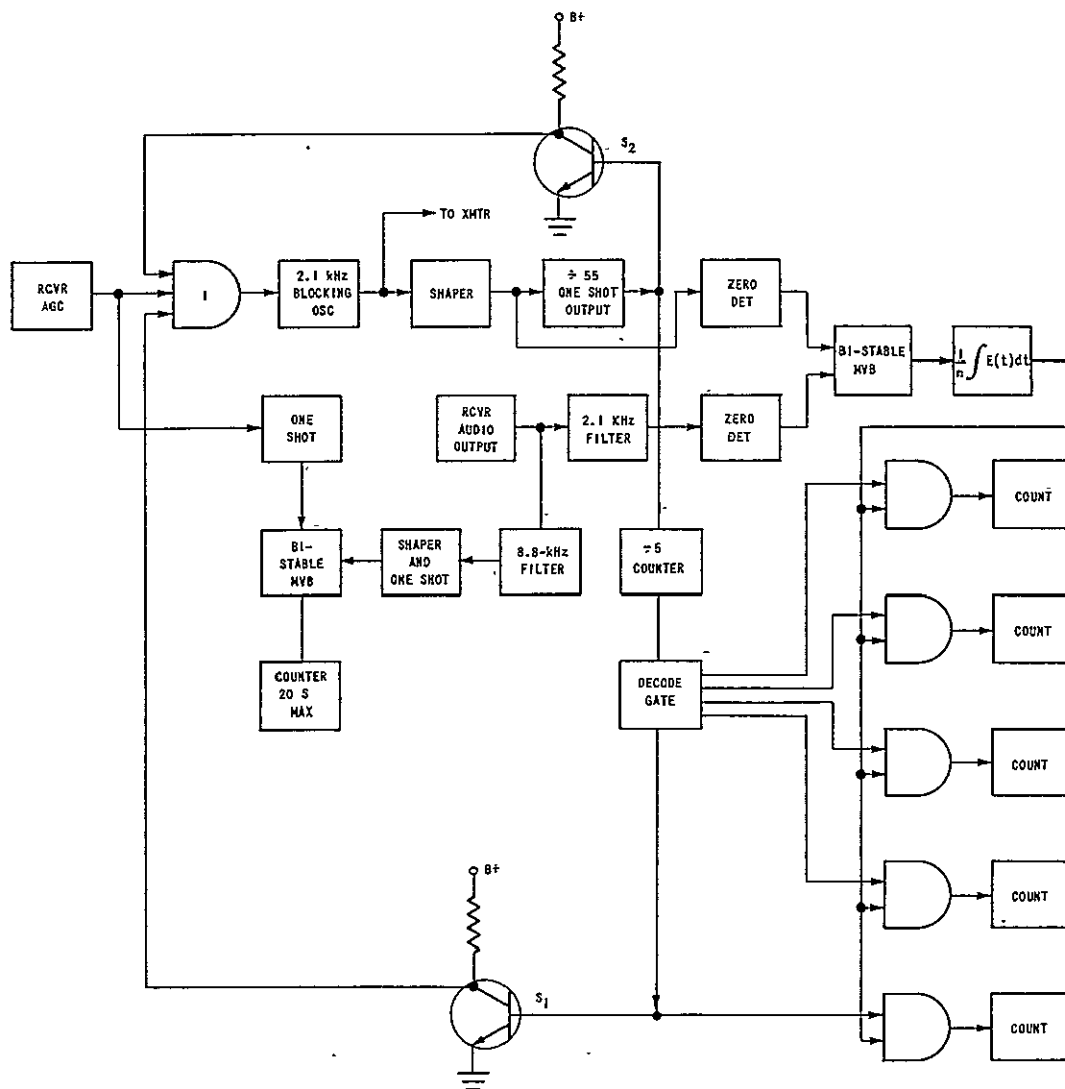


FIGURE 16. RANGE MEASURING SYSTEM

be above all lunar masking effects. The ranging signal (2.3 kHz) is turned off after the five counters are full and thus causes no interference with voice transmission.

Range Error Calculations. The modulation index of the ranging tone will be 0.459 so that it will be compatible with the present modulator. The total transmitted power will be

$$P_t = P_c + \frac{m^2 P_c}{2}$$

$$= 5.00 + \frac{(0.211)(5.00)}{2}$$

$$\begin{aligned} P_t &= 5.00 + 0.527 \\ &= 5.527 \text{ W or} \\ &= 37.42 \text{ dBm} \end{aligned}$$

P. L. = 114.71 dB (Free space attenuation)

$$\begin{aligned} P_R &= P_t - P.L. \\ &= 37.42 - 114.71 \\ &= -77.29 \text{ dBm.} \end{aligned}$$



The S/N ratio in dB at the input to the transceiver detector is

$$\begin{aligned}
 (S/N)_{IN} &= 10 \log_{10} P_t / P_N \\
 &= 10 \log_{10} P_t - 10 \log_{10} P_{IN} \\
 &= -77.29 \text{ dBm} - (-115.38) \text{ dBm} \\
 &= 38.09 \text{ dB.}
 \end{aligned}$$

The S/N ratio in dB at the output of the transceiver video filter is

$$\begin{aligned}
 (S/N)_O &= \left( \frac{m^2}{2 + m^2} \right) \left( \frac{B_N}{B_S} \right) (S/N)_{IN} \\
 &= \left( \frac{0.211}{2.211} \right) \left( \frac{54.4}{12.5} \right) (S/N)_{IN} \\
 &= (0.0954) (4.35) (S/N)_{IN} \\
 &= 0.415 (S/N)_{IN} \\
 &= (38.09 - 3.82) \text{ dB} \\
 &= 34.27 \text{ dB.}
 \end{aligned}$$

The range error for this portion of the path can now be calculated. The phase error caused by noise is given by

$$\begin{aligned}
 \phi_n &= 1/2 (S/N)^{-1/2} \\
 &= 1/2 \left( \frac{1}{\sqrt{2.675 \times 10^3}} \right) \\
 &= (1/2) \left( \frac{1}{51.7} \right) \\
 &= 9.66 \times 10^{-3} \text{ rad.} = 0.554 \text{ deg.}
 \end{aligned}$$

The range error is then given by

$$\begin{aligned}
 E_{R1} &= \frac{\phi_n}{360 \text{ deg}} \lambda_r \\
 &= \left( \frac{0.554}{3.6 \times 10^2} \right) \left( \frac{3 \times 10^8}{2.1 \times 10^3} \right) \\
 &= (1.538 \times 10^{-3}) (1.43 \times 10^5) \\
 &= 2.195 \times 10^2 \\
 &= 219.5 \\
 &\approx \pm 220 \text{ m (or 721 ft).}
 \end{aligned}$$

For the second portion of the loop the transmitted power is

$$\begin{aligned}
 P_t &= P_c + \frac{m^2 P_c}{2} \\
 &= 1.00 + \frac{0.211 (1.00)}{2} \\
 &= 1.1055 \text{ W or} \\
 &= 30.44 \text{ dBm.} \\
 P.L. &= 115.87 \text{ dB (Free space attenuation)} \\
 P_R &= P_t - P.L. \\
 &= 30.44 \text{ dBm} - 115.87 \text{ dB} \\
 &= -85.43 \text{ dBm.}
 \end{aligned}$$

The S/N ratio in dB at the input of the LM detector ( $S/N_{IN}$ ) is

$$\begin{aligned}
 (S/N)_{IN} &= 10 \log_{10} P_t / P_N \\
 &= 10 \log_{10} P_t - 10 \log_{10} P_N \\
 &= -85.43 - (-109.00) \\
 &= 23.57 \text{ dB.}
 \end{aligned}$$

The S/N ratio in dB at the point of the detector  $(S/N)_O$  is

$$\begin{aligned}
 (S/N)_O &= \left( \frac{m^2}{2 + m^2} \right) \left( \frac{B_N}{B_S} \right) (S/N)_{IN} \\
 &= \left( \frac{0.211}{2.211} \right) \left( \frac{41.6}{3.45} \right) (S/N)_{IN} \\
 &= (0.0954) (12.05) (S/N)_{IN} \\
 &= 1.15 (S/N)_{IN} \\
 &= 23.57 \text{ dB} + 0.61 \text{ dB} \\
 &= 24.18 \text{ dB.}
 \end{aligned}$$

The phase error is

$$\begin{aligned}
 \phi_n &= 1/2 (S/N)^{-1/2} \\
 &= (1/2) \frac{1}{\sqrt{262}} \\
 &= 1/2 \frac{1}{16.18}
 \end{aligned}$$

$$\phi_n = 3.1 \times 10^{-2} \text{ rad} = 1.78 \text{ deg.}$$

$$\begin{aligned}
 E_{R2} &= \frac{\phi_n}{360} (\lambda) \\
 &= \frac{1.78}{3.6 \times 10^2} (143 \times 10^5) \\
 &= (4.94 \times 10^{-3}) (1.43 \times 10^5) \\
 &= 7.06 \times 10^2 \\
 &= 706 \text{ m (or 2316 ft).}
 \end{aligned}$$

The total range error may now be calculated by

$$E_R = \sqrt{E_{R2}^2 + E_{R1}^2}$$

$$= \sqrt{(220)^2 + (706)^2}$$

$$= \sqrt{546.836}$$

$$= 739 \text{ m (or 2425 ft).}$$

The range error  $E_R$  can be reduced by averaging  $(E_{RA})$  over several measurements. The error averaged over N samples is [3]

$$\begin{aligned}
 E_{RA} &= \frac{\sqrt{NE^2}}{N} \\
 &= \frac{E}{\sqrt{N}}
 \end{aligned}$$

The number of samples (N) required to reduce the range error to 100 m (328 ft) is

$$100 = \frac{739}{\sqrt{N}}$$

$$\sqrt{N} = 7.39 \text{ samples}$$

$$N = 54.5 \approx 55 \text{ samples.}$$

The time  $\tau$  required to take 55 samples is given by

$$\begin{aligned}
 \tau &= NT \\
 &= (55) \left( \frac{1}{2.1 \times 10^3} \right) \\
 &= (5.5 \times 10) (4.76 \times 10^{-4}) \text{ s or} \\
 &= 26.2 \text{ ms.}
 \end{aligned}$$

The maximum distance that the transceiver can travel in this time is given by

$$\begin{aligned}
 S &= V_0 \tau \\
 &= (161 \text{ m/s}) (2.62 \times 10^{-2}) \text{ s} \\
 &= 4.21 \text{ m (or 13.8 ft).}
 \end{aligned}$$

The distance is insignificant when compared to the range error.

It is believed that it is worthwhile to use sampling to reduce the range error; to do so only requires the addition of an averaging circuit to the ranging system.

### AZIMUTH MEASURING SYSTEM

Several types of azimuth measuring systems have been investigated but only one appears to merit use with the emergency communication system. The azimuth measuring system uses three stub antennas arranged as shown in Figure 17. A block diagram of

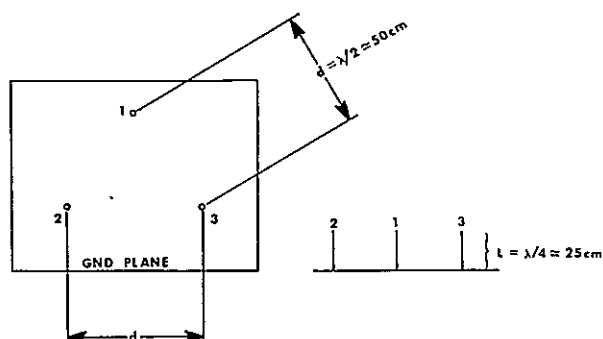


FIGURE 17. ANTENNA SYSTEM FOR AZIMUTH MEASUREMENT

the measurement system is shown in Figure 18. The signal from each antenna is applied to the input of one of the receivers. The receivers are actually RF amplifiers followed by limiters that remove the amplitude modulation from the signal. The outputs of the limiters are applied in pairs to the reference and signal ports of three phase detectors. The idealized outputs of the phase detectors are shown in Figure 19. The output of phase detector 1 shows the angle measurement for azimuth angles of 0 to 60 degrees. At 60 degrees the output of  $\phi_1$  reaches a level (0.65 V) and  $S_1$  and  $S_3$  are disabled; the output of  $\phi_2$  is connected to the integrator through  $S_2$ . At 120 degrees  $S_1$  and  $S_2$  are disabled by the level from  $\phi_2$ , and  $\phi_3$  is connected through  $S_3$  to the integrator. At 180 degrees  $S_2$  and  $S_3$  are disabled by the level from  $\phi_3$ , and  $\phi_1$  is reconnected through  $S_1$  to the integrator. At this point the output is negative, indicating an azimuth between 180 and 240 degrees. Negative outputs of  $\phi_2$  and  $\phi_3$  indicate azimuths between 240 and 300 degrees and 300 and 360 degrees, respectively. When the switch outputs are negative, 180 degrees must be added to obtain the correct azimuth.

The output of each phase detector is a voltage proportional to the phase difference between two input signals and is averaged by an integrator for 26.2 milliseconds to minimize error caused by noise.

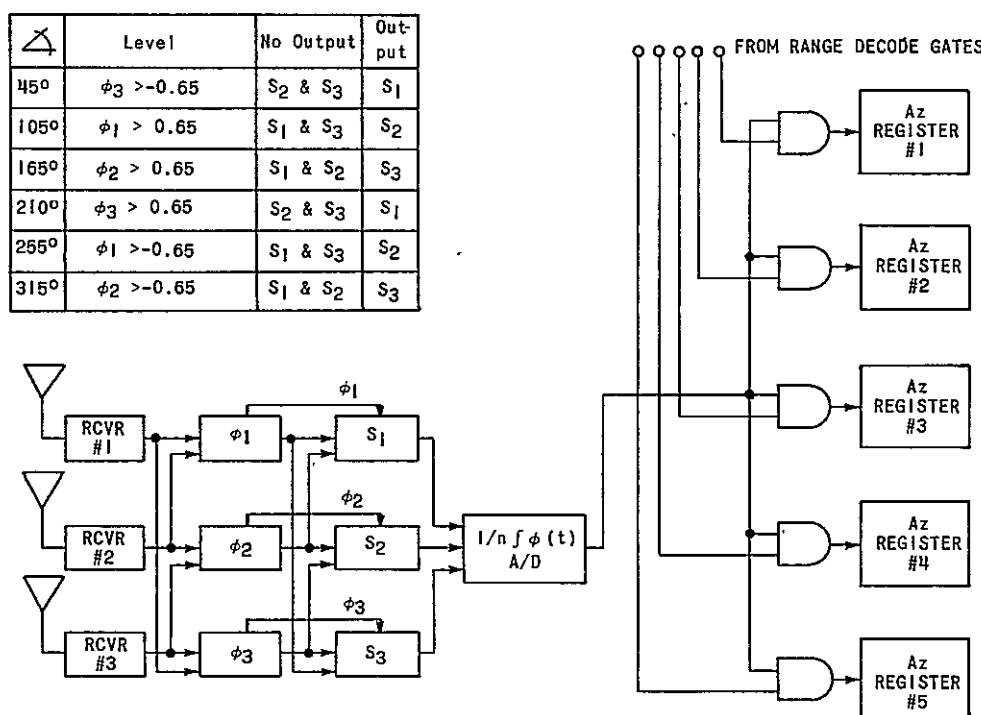


FIGURE 18. AZIMUTH MEASURING SYSTEM

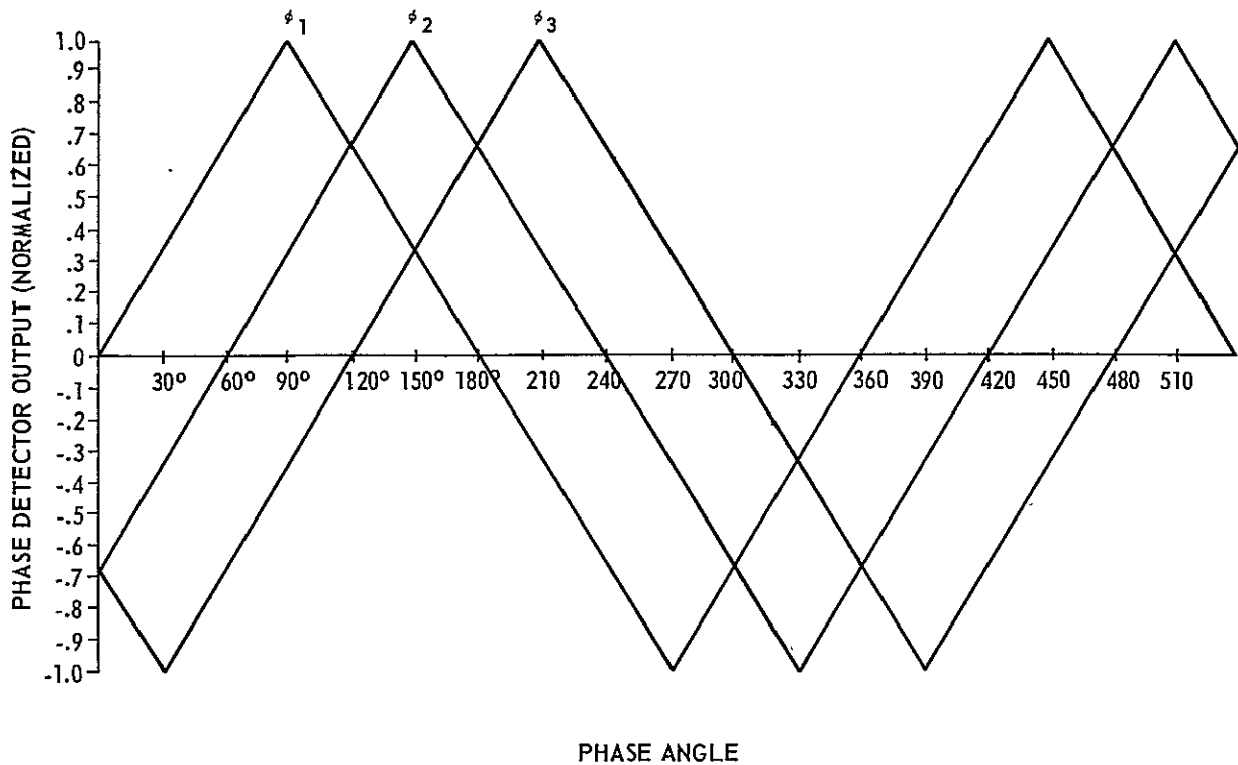


FIGURE 19. PHASE ANGLE OUTPUTS OF PHASE DETECTORS

Each integrator output is applied separately to an analog-to-digital (A/D) converter to obtain a suitable readout. Separate A/D converter inputs are required to identify the phase detector used. When the phase detector output is negative, the A/D converter performs the correction necessary to read out the proper azimuth. The A/D converter output is then applied to five AND gates. Each AND gate also receives a separate input from the range decode gates. When an input from the range decode gates is present, the azimuth measurement at that AND gate is read into its corresponding azimuth register. Five such azimuth measurements are made, each corresponding to a range measurement.

The accuracy of the measurements is a function of the S/N ratios of the signals and the linearity of the phase detector inputs. The signal power at the antenna (previously calculated) is -85.43 dBm. The noise power ( $P_n$ ) in the receiver is given by

$$P_n = 4KT BW$$

where K is the Boltzmann constant, and T is the

effective noise temperature of the receiver given by

$$\begin{aligned} T &= (F - 1) T \\ &= (4 - 1) (300^\circ \text{K}) \\ T_E &= 900^\circ \text{K}. \end{aligned}$$

The bandwidth of the azimuth receiver (B) is assumed to be 10 kHz. Then the noise power is

$$\begin{aligned} P_n &= 4(1.38 \times 10^{-23}) (9 \times 10^2) (10^4) \\ &= 4.968 \times 10^{-16} \text{ W or} \\ &= -123.04 \text{ dBm}. \end{aligned}$$

The S/N ratio in dB at the input to the phase detector is

$$\begin{aligned} (S/N) &= 10 \log_{10} P - 10 \log_{10} P_n \\ &= (-85.43) - (-123.04) \\ &= 47.61 \text{ dB}. \end{aligned}$$

This value will be the same for the output of all three receivers since they are identical. The phase error caused by noise is

$$\begin{aligned}\phi_n &= 1/2 (S/N)^{-1/2} \\ &= 1/2 \left( \frac{1}{\sqrt{5.76 \times 10^4}} \right) \\ &= \frac{1}{2 \times 2.4 \times 10^2} \\ &= 0.208 \times 10^{-2} \text{ rad or} \\ &= 0.119 \text{ deg.}\end{aligned}$$

The total phase error between the two signals being compared in any phase detector is approximately

$$\begin{aligned}\phi_{nr^2} &= \phi_{n1^2} + \phi_{n2^2} \\ &= 2(1.42 \times 10^{-2}) \\ &= 0.168 \text{ deg.}\end{aligned}$$

This is a calculated approximation of the error, which can be further reduced by integration. The azimuth measurements are sampled at the output of the phase detectors in the same manner as the ranging measurements.

The error at the output of the integrator is given by

$$\phi = \frac{\phi_{nr}}{\sqrt{n}} \quad (\text{deg})$$

where  $n$  is the number of samples, and

$$\phi = \frac{0.168}{\sqrt{55}} = \frac{168 \times 10^{-1}}{7.42} = 0.0226 \text{ deg.}$$

This value of  $\phi$  considers only the effect of thermal noise. If bias errors and thermal expansion and contraction of the antennas are considered, it is reasonable to expect  $\phi$  to approach 0.115 degree. This value will be used throughout the remainder of the paper.

## POSITION DETERMINATION

It should be noted (Fig. 20) that the calculated distance between the LM and the EVA is a chord length instead of the arc length or distance along the lunar surface actually required.

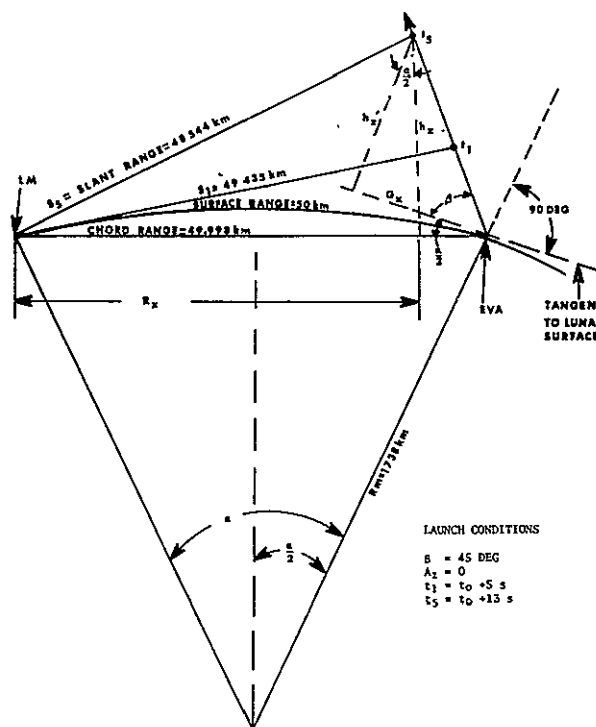


FIGURE 20. ERROR IN HORIZONTAL RANGE CAUSED BY LAUNCH ANGLE

The solution of the chord length, assuming a 50-km distance along a smooth lunar surface, is calculated from a Taylor series expansion.

Given:

$$R_m = \text{radius of moon} = 1738 \text{ km}$$

$$S_r = \text{surface distance} = 50 \text{ km}$$

Solution:

$$\begin{aligned}\text{Chord length} &= S_r - \frac{S_r^3}{24 R_m^2} \\ &= 50 - \frac{50^3}{24(1738)^2} = 49.99828 \text{ km} \\ &= 49.998 \text{ km.}\end{aligned}$$

Since the error between the calculated chord distance and the distance along the lunar surface is approximately 2 meters in 50 km, it is negligible. It is apparent that this error would decrease as the distance between the LM and the EVA decreases.

It should also be noted that the slant range determined by the ranging circuitry will not coincide with the chord range ( $R_x$ ) when the communications relay is launched at an angle other than one that provides a utopian solution. The error between slant range and range along the chord at various times along the trajectory of the communications relay for an azimuth of 0 degrees is determined as follows:

$$R_x = 49.998 - (G_x) (\cos \alpha/2) + (h_x') (\sin \alpha/2)$$

where

$$G_x = (V_0) (\cos \beta) (t), \quad h_x' = (V_0) (\sin \beta) - 1/2 gt^2$$

also

$$h_x = G_x \sin \alpha/2 + h_x' \cos \alpha/2$$

and

$$\text{Slant range} = S_x = \sqrt{h_x^2 + R_x^2}$$

The following results may be obtained for a sample taken at 13 seconds after the relay is launched at a reference azimuth of 0 degrees (toward the LM).

Given:

Distance along lunar surface = 50 km

$V_0 = 161 \text{ m/s}$

Launch angle =  $\beta = 45 \text{ degrees}$

$\alpha/2 = 1/2 (1.648 \text{ degrees}) = 0.824 \text{ degree}$   
(from relay trajectory investigation)

Results:

$h_x = 1361.7 \text{ m}$

$R_x = 48.537 \text{ km}$

$S_x = 48.556 \text{ km}$ .

Thus it may be seen that a difference of 19 meters exists between the slant range and the range along the chord for a sample taken at 13 seconds after launch. It is apparent that this difference will diminish with earlier detection of the relay.

More important is the difference in the slant range and the actual range to the EVA, which is 456 meters in this case. For this reason five samples are taken on slant ranges at 2-second intervals with the first sample being taken at the instant when the line-of-sight between the LM and the communications relay is obtained. With the range and azimuth information available from five points along the trajectory of the relay, it will be possible to extrapolate the trajectory of the relay to a point on the lunar surface. The extrapolation can be made manually with the aid of a set of grid maps or mathematically extrapolated from equations developed to provide the azimuth and range at the time of launching. It should also be possible to program the LM computer so that it may be used to calculate the position of the EVA.

Figure 21 is an example of the extrapolation of the position of the EVA from calculated points at various sampling times along the trajectory of the relay.

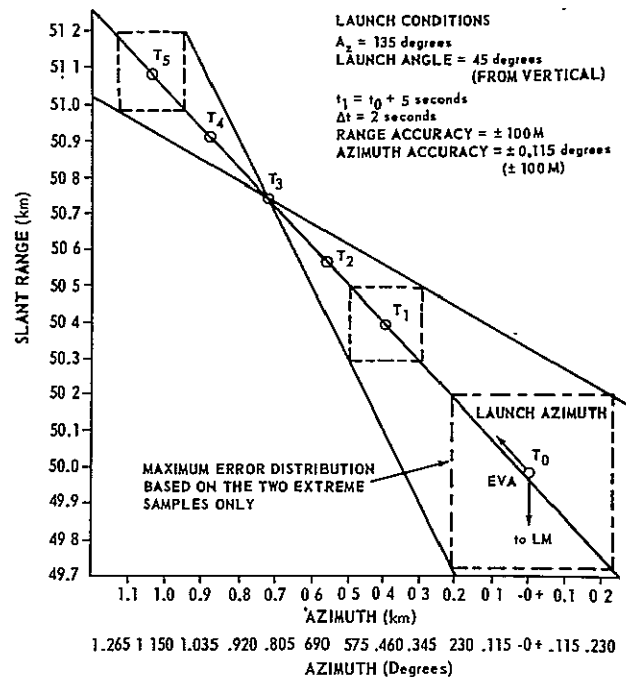


FIGURE 21. MAXIMUM ERROR IN EXTRAPOLATED POSITION OF EVA

Table III lists the calculated values of slant range and azimuth of various sampling times along the trajectory of the relay.

TABLE III. CALCULATED VALUES OF SLANT RANGE AND AZIMUTH

Time (s)	Slant Range, S(t) (km)	Azimuth, $A_z(t)$ (deg)	Azimuth, A(t) (meters)
0	49.998	0 (Reference)	0
5	50.404	0.4583	403.1
7	50.572	0.6394	564.5
9	50.741	0.8195	725.9
11	50.912	0.9986	887.3
13	51.083	1.1764	1048.8

By plotting the azimuth and range information available from five samples along the trajectory of the relay and with the time between samples and the time of the first sample known, an extrapolation back to the initial launching site ( $t_0$ ) can be made.

Another approach to finding the position of the EVA is a mathematical extrapolation of the initial launching site. The equations for mathematically extrapolating the position of the EVA are as follows:

$$S(0) = \frac{S_1 + S_2 + S_3 + S_4 + S_5}{5} + \frac{S_1 - S_5}{8} (T_1 + 4)$$

$$A_z(0) = \frac{A_1 + A_2 + A_3 + A_4 + A_5}{5} + \frac{A_1 - A_5}{8} (T_1 + 4)$$

where  $S(0)$  is the range to the EVA at the time of launching,  $t_0$ , and  $A_z(0)$  is the azimuth (from a reference azimuth) to the EVA at the time of launching.

If the first sample is taken prior to a minimum time, the range and azimuth to the EVA will coincide with the information obtained from the first sample. This time, of course, depends on the launch angle and the acceptable tolerance on error. Calculations of this time indicate that for a location within 500 meters and a launch angle of 45 degrees, the first sample would have to be obtained prior to 3 seconds

after launching the relay. This approximation was made considering a two-sigma range on the possible error in the information obtained from the first sample. It is remotely possible that the first reading may contain a large error so that it should not be utilized without comparison with the other readings. In any case, however, extrapolation of all five samples would increase the accuracy of the location.

## MULTIPATH CONSIDERATIONS

Previous discussions have not considered the effects of multipath and the attenuation caused by low grazing angles. Several things can be done to minimize these effects. Some of these are listed as follows:

1. Restrict the range of the system to a maximum surface distance of 25 km, or increase the height of the rocket trajectory by using a more powerful propellant. This will increase the time that the LM to rocket elevation angle will exceed five degrees (Fig. 22).

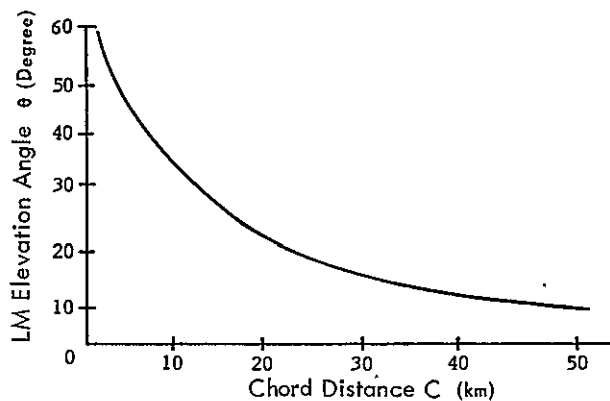


FIGURE 22. LM TO ROCKET ELEVATION ANGLE

2. Use antennas on the LM that will not detect signals whenever the LM to rocket elevation angle is less than five degrees.

3. Replace the hand-launcher part of the rocket with a tube launcher capable of being oriented to within four degrees from the EVA local vertical. Range and azimuth measurements can now be made at elevation angles of several degrees above this horizon.

4. Modify the timing circuitry within the rocket to provide a coded time burst spaced at 10-second intervals throughout the rocket flight. The effects of multipath on an amplitude modulated voice signal are easily recognized; therefore, the LM astronaut can reject position readings until the communications link is reasonably free from multipath. Since the rocket was launched within four degrees from the local vertical, the error introduced by making position measurements above an LM elevation angle of five degrees is greatly reduced. Extrapolation will further reduce this error to within the calculated values.

## ROCKET CONFIGURATION AND PERFORMANCE CHARACTERISTICS

### REQUIREMENTS

The following requirements (Table IV) have been established as feasible and may be used as a guide in any attempt to develop the transceiver.

TABLE IV. COMMUNICATIONS RELAY TRANSCEIVER REQUIREMENTS

Total device weight	0.9 kg (2 lb)
Payload weight	0.45 kg (1 lb)
Payload	radio transceiver
Payload altitude capability	8000 m (26 240 ft)
Transmission distance	50 km (30 miles)
Transceiver power output	1 W
Transmission time	3 min
Operational environment	lunar surface
System size	similar to the Thiokol M127A1 military hand signal

### PACKAGING

The Thiokol M127A1 signal flare is a signal device currently being manufactured and could be modified to

contain a transceiver for a payload. The M127A1 is a hand-held percussion initiated signal device. Figure 23 is an artist's concept of the rocket propelled communications relay in the M127A1 package. The M127A1, as it exists now, is capable of placing a 0.1 kg (0.22 lb) payload at an altitude of 8230 m (27 000 ft) on the moon. Of course, such items as the stabilizing fins would be useless on the moon and other methods of achieving flight stability would have to be substituted. The removal of the fins would allow a greater payload, but the replacement of the black powder as the propellant with an existing state-of-the-art propellant of high specific impulse would greatly increase payload capability of the device. Also, it was determined from Thiokol personnel that the weight of the rocket could be reduced, if necessary, by using different lightweight materials for the motor housing and payload storage container. Figure 23 provides a general description of the signal device (communications relay), which would be separable into three basic components: the cap containing the firing pin, the hand-held launcher, and the signal device itself consisting of the rocket motor, the thermal battery, and the communications relay electronics.

Considering cost, available space, and reliability, the most desirable method of packing the electronics appears to be a hybrid microcircuit system using a thick film discrete technique of packaging into a single package the stages of the system that lend themselves readily to integration. This method of packaging will allow customization of the circuit design at a price that will compare with discrete component packaging. Some discrete components will be required in any case as they do not lend themselves to integration. It is feasible that packaging of the electronics could be accomplished within the available space using this method. The stages of the system would then be interconnected on printed circuit boards stacked to conform to the configuration of the rocket canister.

It also appears that packaging of the electronics using discrete components could be accomplished with a minimum increase in size and weight of the package. Breadboarding of the system would be necessary to establish firm requirements on the number of discrete components to be certain that 100-percent discrete packaging could be contained in the available space.

Since a large number of discrete components for tuned circuits are required, the system is not



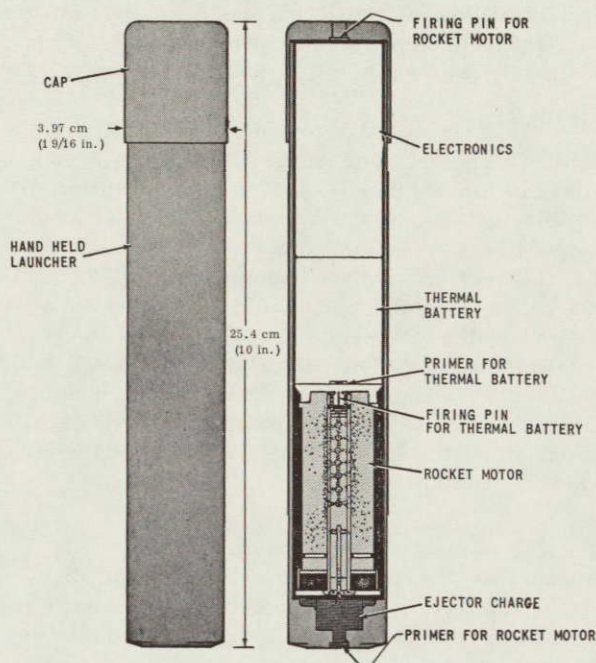


FIGURE 23. LUNAR ROCKET RESCUE BEACON

suited to thin-film large-scale integration. Also the cost factor for thin-film large-scale integration prohibits the use of this technique.

The thermal battery for the communications relay will require a volume 3.5 cm in diameter by 5 cm high (1.4 in. by 2 in.). It should be observed that the diameter conforms to the configuration of the rocket canister.

The transceiver could be constructed to allow checkout of the electronics without activation of the thermal battery.

#### ARMING OF THE COMMUNICATIONS RELAY

Because of the power drain on the thermal battery and operator safety, the signal device must remain unarmed until launch time of the rocket. The M127A1 method of arming appears applicable for use in the communications relay rocket. The device cannot be ignited until the cap is taken from the forward end and placed on the rearward end. This places a firing pin in the cap in contact with the primer for the rocket motor. Striking the device on the cap

ignites the ejector charge which propels the signal device a safe distance from the launcher tube prior to ignition of the primary propellant in the rocket. The chamber pressure generated upon ignition of the rocket motor drives the firing pin for the thermal battery. The primer in the thermal battery is struck by the firing pin, causing activation of the thermal battery which supplies power to the electronics of the relay. If necessary, the method of striking the device on the cap to cause activation of the device can be replaced by firing techniques more compatible with the dexterity of a suited astronaut. A spring-driven firing pin activated by a switch would be an acceptable substitute should the necessity arise. This type of activation would also allow easier vertical launching.

#### COST

Two costs should be considered. First is the cost associated with the transportation of additional weight to the lunar surface. As previously mentioned, thin-film large-scale integration will not buy an appreciable reduction in size or weight of the electronics over the hybrid microcircuit system using a thick film technique of packaging discrete chips into a single package. This technique will reduce size because of customization of the system stages.

The second cost to be considered is the total system price. Thin-film large-scale integration could not be justified on a cost per system basis because of the large initial cost of tooling. As a rule, large scale integration is not economically feasible unless a large number (approximately 15 000) of custom circuits are to be produced. The hybrid microcircuit technique for packaging discrete chips into a single package will compare in terms of cost per system with the price of a discrete-components-only system if as many as 10 systems are manufactured.

### INVESTIGATION OF PURCHASED FINISHED COMPONENTS

#### THERMAL BATTERY

The power source that appears most desirable for the communications relay transceiver is a thermal battery. The thermal battery offers rugged construction, small package density and weight, and almost unlimited storage life. If a mechanically initiated



primer is used, the thermal battery for this application will be approximately 3.6 cm in diameter by 5 cm high (1.4 by 2.0 in.). The primer for the battery will be activated by a firing pin contained in the rocket motor. The firing pin is operated by the motor chamber pressure (Fig. 23). The thermal battery selected would supply approximately 8 W at 28 V  $\pm 10$  percent within 1 second after activation of the primer. After 3 minutes of operation the battery would be capable of supplying 4 W at 28 V  $\pm 10$  percent. The operational temperature range of the thermal battery selected is  $-54^{\circ}$  to  $93^{\circ}$  C ( $-65^{\circ}$  to  $200^{\circ}$  F). The external surface of the battery will heat to approximately  $93^{\circ}$  C ( $200^{\circ}$  F) because of the electrochemical reaction within the battery. More thermal insulation could lower the external temperature of the thermal battery if it is deemed necessary, or thermal insulation between the battery and the electronics could be used.

#### COMMUNICATION SYSTEM

It was determined through discussion with various manufacturers of radio communication equipment that presently no equipment on the market will perform the desired task under the frequency, size, and weight limitations that are imposed.

#### POSITION-FINDING EQUIPMENT

It was determined through discussion with several manufacturers of ranging and direction-finding equipment that presently no equipment on the market will perform the desired task under the size, weight, and frequency limitations that are imposed.

#### PROPULSION SYSTEM

It was determined that the Thiokol M127A1 military hand signal is a device that could be modified to propel the communications relay to an altitude necessary to provide emergency communications.

### CONCLUSIONS

The investigation has shown that it is feasible to provide a short range, lightweight voice communications relay system between the LM and an EVA. Furthermore, the investigation has shown that three proposed emergency communications systems are

feasible from the standpoint of the electronics required: (1) The proposed systems do not depend upon surface conductivity and should not be seriously affected by surface anomalies if the elevation angles are not too low, (2) SNR margins are fully adequate with an ample safety factor, and (3) the system is compatible with existing LM/EVA hardware.

It is suggested that consideration not be given to the CW beacon system because the coded beacon supplies much more information with very little additional complexity. It is also suggested that some consideration be given to one other type of system which would utilize the transceiver but would not utilize the position-finding equipment. It would thus allow two-way communications between the LM and the EVA and transmission of the biomedical data, but would avoid the addition of any equipment to the LM. Since in most cases the EVA should be able to provide position information, the information obtained from the two systems would be the same.

The number of components required for the transceiver will be about three times the number required for the coded beacon. Either unit could be put into the rocket payload through use of thick-film integration techniques.

The major problem with the transceiver seems to be the requirement for the antenna pattern. Since the antenna pattern requirements could become a significant portion of the technical problem, more study of this problem is necessary before a decision can be made on which system should be used.

The range-and azimuth-finding systems are for the most part digital equipment and consequently will be easy to design. It should not be too difficult to keep the position-finding equipment well below the 9-kg (20-lb) weight limit. The antenna for the range-finding equipment could be the LM communication antenna, but the azimuth indicating system will require separate antennas. Some type of ground plane will be needed for the azimuth antennas. The choice of systems appears to be one of the following:

1. Transceiver with position-finding capability
2. Transceiver
3. Coded beacon

Table V lists the capabilities of each system. The transceiver with the position-finding capability



TABLE V. SYSTEM CAPABILITIES

Function	Transceiver with position	Transceiver	Coded Beacon
Automatic Position Finding	Yes	No	No
Two Way (Simplex) Communications	Yes	Yes	No
Voice Communication with MCC-H	Yes	Yes	No
Indicates Type of Emergency	Yes	Yes	Yes
Audio warning in LM	Yes	Yes	Yes
Visual warning in LM	Yes	Yes	Yes
Bio-med Data	Yes	Yes	No
Integration of relay package required	Yes	Yes	No
Additional weight	Highest	Intermediate	Lowest
Cost	Highest	Intermediate	Lowest

will be the most complex and expensive of the three systems. The coded beacon will be the least complex and expensive. The transceiver without position finding appears to be the most economical in terms of information furnished, especially since it is very likely that some position information can be supplied by the EVA.

The power source which appears most desirable for the communications transceiver is the thermal battery, and a modified Thiokol signal flare is a feasible means of providing a vehicle to propel the transceiver. A hybrid microcircuit system utilizing a thick film technique of packaging discrete chips into a single package is recommended as the best means of packaging the transceiver electronics. This technique will give customization of the circuitry at a price, including tooling, that will compare with a discrete component system.

## REFERENCES

1. Vogler, L. E.: A Study of Lunar Surface Radio Communication. National Bureau of Standards Monograph 85 issued Sept. 14, 1964.
2. Ehling, Ernest H.: Range Instrumentation. Prentice-Hall Inc., Englewood Cliffs, N. J., 1967.
3. Davenport, Wilbur B., and Root, William L.: An Introduction to the Principles of Communication Theory. McGraw-Hill Book Company, Inc., New York, N. Y., 1961.

## BIBLIOGRAPHY

Hancock, John C.: An Introduction to the Principles of Communication Theory. McGraw-Hill Book Company, Inc., New York, N. Y., 1961.

Lee, Y. W.: Statistical Theory of Communication. John Wiley & Sons, Inc., New York, N. Y., 1960.

Sears, F. W., and Zemansky, M. W.: College Physics. Addison-Wesley Publishing Co., Inc., Cambridge, Mass., 1956.

Skodnik, Merrill I.: Introduction to Radar Systems. McGraw-Hill Book Company, Inc., New York, N. Y., 1962.

Stiltz, Harry L.: Aerospace Telemetry. Prentice-Hall, Inc., Englewood Cliffs, N. J., 1961.

Tollison, James B.: Apollo Extra-Vehicular Communications System, Manned Spaceflight Center, Houston, Texas.



## BUFFER FULLNESS CONTROLS FOR A DATA COMPRESSOR USING SATURN VEHICLE DATA

By

N 69 - 36581

Gabriel R. Wallace

### SUMMARY

This paper presents results of experimental studies of buffer fullness in a zero order, fixed corridor, nonredundant sample transmitted (ZFN) data compressor. Although this study is continuing, some results are now evident. The buffer fullness is monitored while various methods of control are tried. The data fed into the data compressor were recovered from Saturn flights. Important factors of buffer fullness control are the input data, output rate, allowable data compressor time delay, and allowable information loss. For nonstationary ensembles (such as the Saturn data sources) with large variations in data compressibility, some method of rate control seems to be indicated. For an ensemble of data sources exhibiting relatively high compressibility and low variations, tolerance control of buffer fullness seems possible.

### INTRODUCTION

The results of a study on methods of control of buffer fullness of a zero order data compressor are presented. The experiments were performed with the predictor type of data compressor operating on real data recovered from Saturn PCM/FM telemetry links.

As of today, no major data compressor unit has been flown for use with the Saturn's telemetry system. It was desired to determine if the ZFN flight data compressor shown in Figure 1 could operate efficiently with ordinary Saturn PCM telemetry flight data. Experiments were conducted to determine if a common setting of the data compressor control parameters would suffice for reasonably similar flights. Maximum buffer input rates were monitored to determine data compression ratios during high activity periods. During the flights that were studied, the times of maximum activities (as expected) were

noted to be at lift-off, during calibrations, and at stagings.

The method of experimentation using real data was selected because many studies have revealed the importance of input data characterization (it can greatly affect the data compression ratio) without offering an easy method of accomplishing data characterization. The method used allows a realistic representation of the data compressor's behavior in actual Saturn flight situations without having to solve the data characterization problem. Obviously, many combinations of various sensor outputs can occur to comprise a data ensemble so that rather than trying to provide a detailed data characterization at this time, the basic assumption is made that future Saturn flights will not drastically change from those discussed in this paper. Consequently, the methods of buffer fullness control of this study will serve as a meaningful and useful intermediate step until more experimentation on data characterization is accomplished.

A brief description of the Saturn PCM/FM telemetry link and the zero order predictor data compressor is presented to allow the reader to note both the conceptual simplicity of the schemes and the potential difficulties of proper evaluation of such an integrated, modified PCM telemetry system; i. e., a system using a data compression device.

With the modified system (and thus the experimental parameters) explained, this paper discusses specifically three buffer fullness control elements of the data compressor: the output bit rate, the tolerance control, and selective data removal as shown in priority control.

The buffer fullness experimentation is rather straightforward as shown in Figure 2. The pre-detection tapes (in this case, recovered PCM data from the Saturn instrumentation units) are played into a PCM ground station where the airborne NRZ-L [1] wavetrain is recreated. The NRZ-L wavetrain



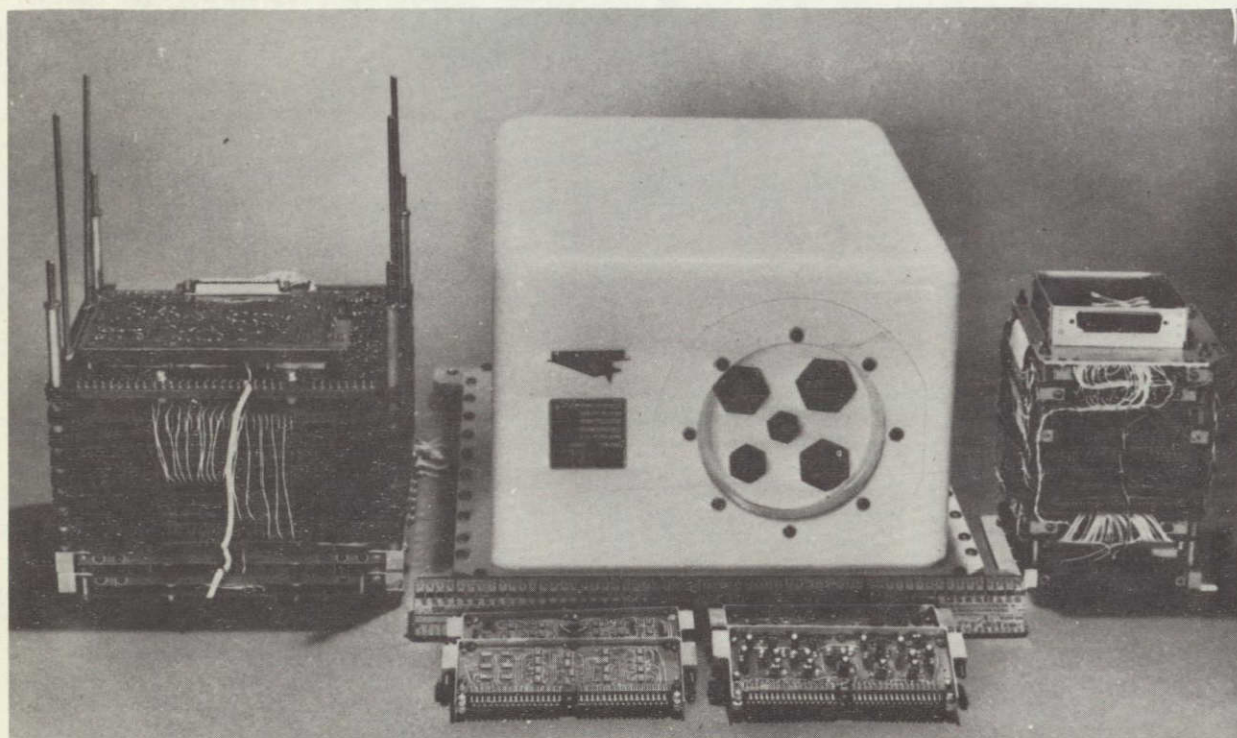


FIGURE 1. ZFN AIRBORNE DATA COMPRESSOR

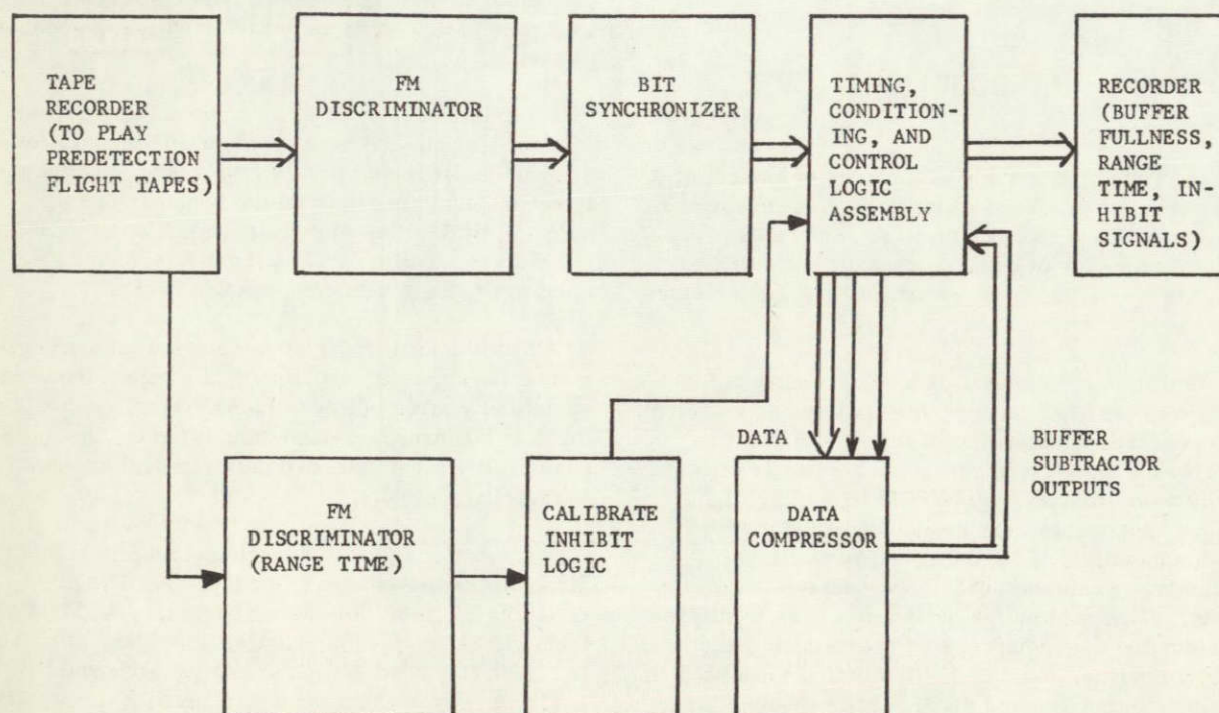


FIGURE 2. BLOCK DIAGRAM OF BUFFER FULLNESS EXPERIMENT

(exactly the same as the airborne transmitter assembly would sense) is then fed into the data compressor and its buffer memory fullness is monitored.

## SATURN PCM/FM TELEMETRY SYSTEM

For the most part, the Saturn PCM/FM telemetry system is an uncomplicated system with a large data capacity and a high degree of flexibility. Figure 3 outlines the block diagram of a PCM/FM system contained on each stage of the Saturn. The remote location submultiplexers afford complete physical coverage of the entire stage at a 4, 12, 40, or 120 samples per second (sps) rate. A PCM/FM system as used on the Saturn can control up to 1800 different analog or digital sources at a 4 sps rate, if so desired. Preflight programming determines the number of sources to be sampled at each rate.

Although each Saturn flight has its own peculiarities, there are many likenesses. The flight profiles showing the approximate times of high data activity are quite similar (Fig. 4). Even the Saturn V has a flight profile resembling those of the Saturn IB flights of this test. Of particular interest are common items in the flight profiles which would likely indicate the critical (to the data compressor) high activity periods: lift-off, staging, and calibration.

## ZFN DATA COMPRESSION UNIT

The inflight data compression will normally take place at point A as shown in Figure 3. If a data compressor is to be flown on the Saturn, it will become a series element at this point. Each channel of data will be monitored to determine redundancy. If data

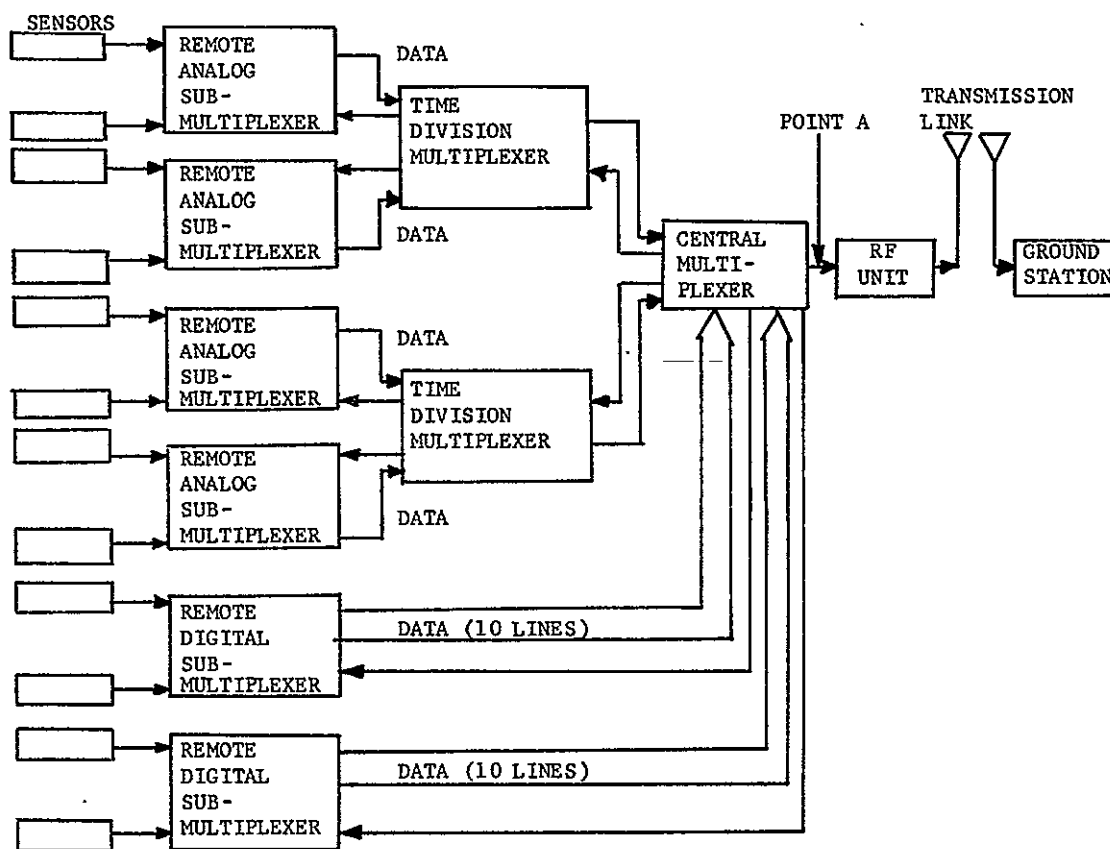


FIGURE 3. BLOCK DIAGRAM OF SATURN PCM/FM TELEMETRY

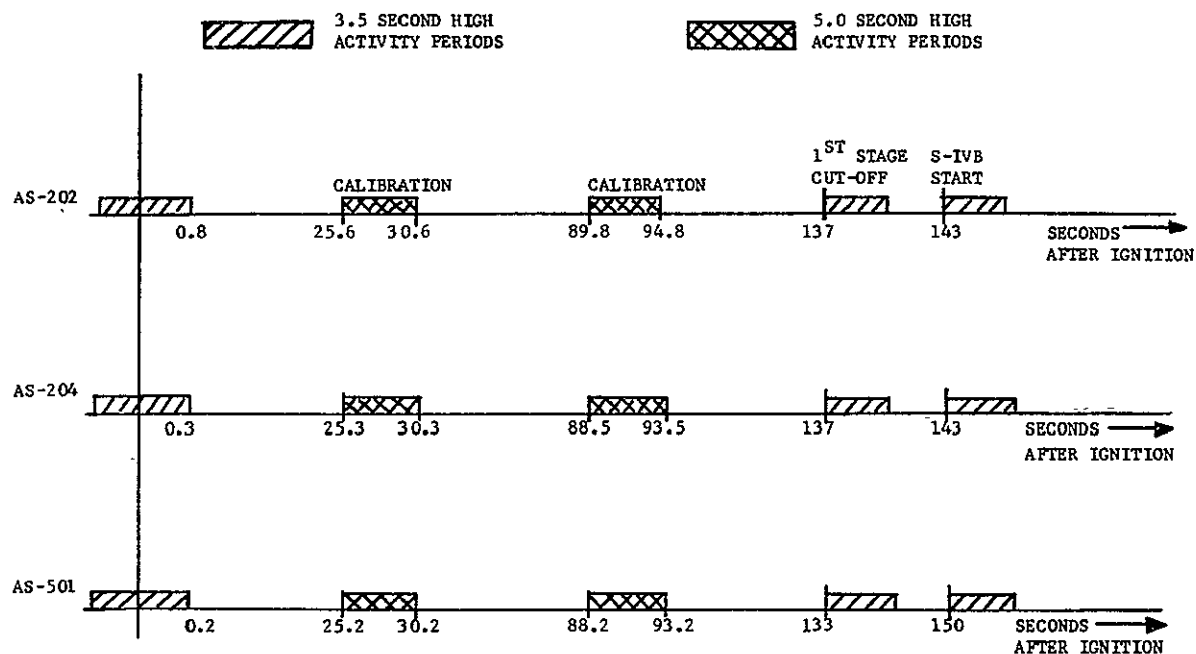


FIGURE 4. SATURN FLIGHT PROFILES (AS-202, AS-204, AND AS-501)

are redundant, the information will not be transmitted; if the data are not redundant, the channel will be assigned an identification and transmitted in the regular manner. Figure 5 outlines a block diagram of the data compressor used in this experiment.

The data compressor unit has a logic subsection containing over 460 integrated circuits [2]. The 480-word reference memory is a hybrid nondestructive readout (NDRO)-destructive readout (DRO) combination. Each word is 26 bits in length. The larger buffer memory (1024 words) stores non-redundant information and provides the necessary constant output rate. The data compressor is fairly flexible in operation. Five different functions of the data compressor may be programmed: (1) input data format and rates, (2) buffer fullness levels to be detected, (3) detail control logic functions, (4) tolerance limits and priority assignments, and (5) output rate. To insure true compatibility with existing Saturn flight hardware and to give some measure of both the electrical and mechanical integrity of the unit, a full qualification test to Saturn flight standards was conducted and successfully completed.

The "rules" of operation for the zero order predictor type of data compressor (Fig. 6) [3] for zero order, fixed corridor, nonredundant sample transmitted (ZFN) are as follows:

- (a) The occurrence of a nonredundant sample requires that a new corridor be established. This is accomplished by drawing lines of zero slope through the end points of the tolerance range placed around the nonredundant sample.
- (b) If a subsequent sample lies inside the corridor, it is a redundant sample and is discarded.
- (c) If a subsequent sample lies outside the corridor, it is a nonredundant sample and is transmitted.

Thus, one may easily see that the ZFN data compressor device is relatively simple in basic design. The rules of the algorithm are also straightforward and relatively easy to implement.

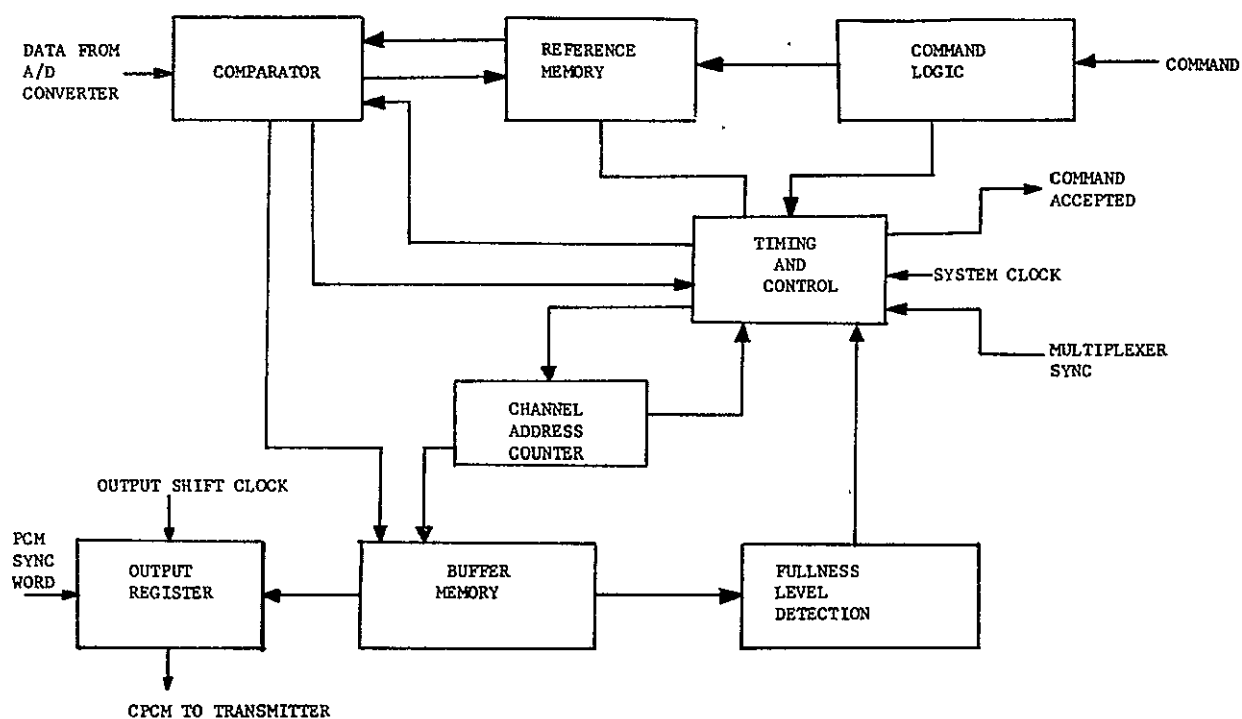


FIGURE 5. FUNCTIONAL BLOCK DIAGRAM OF THE TELEMETRY DATA COMPRESSOR

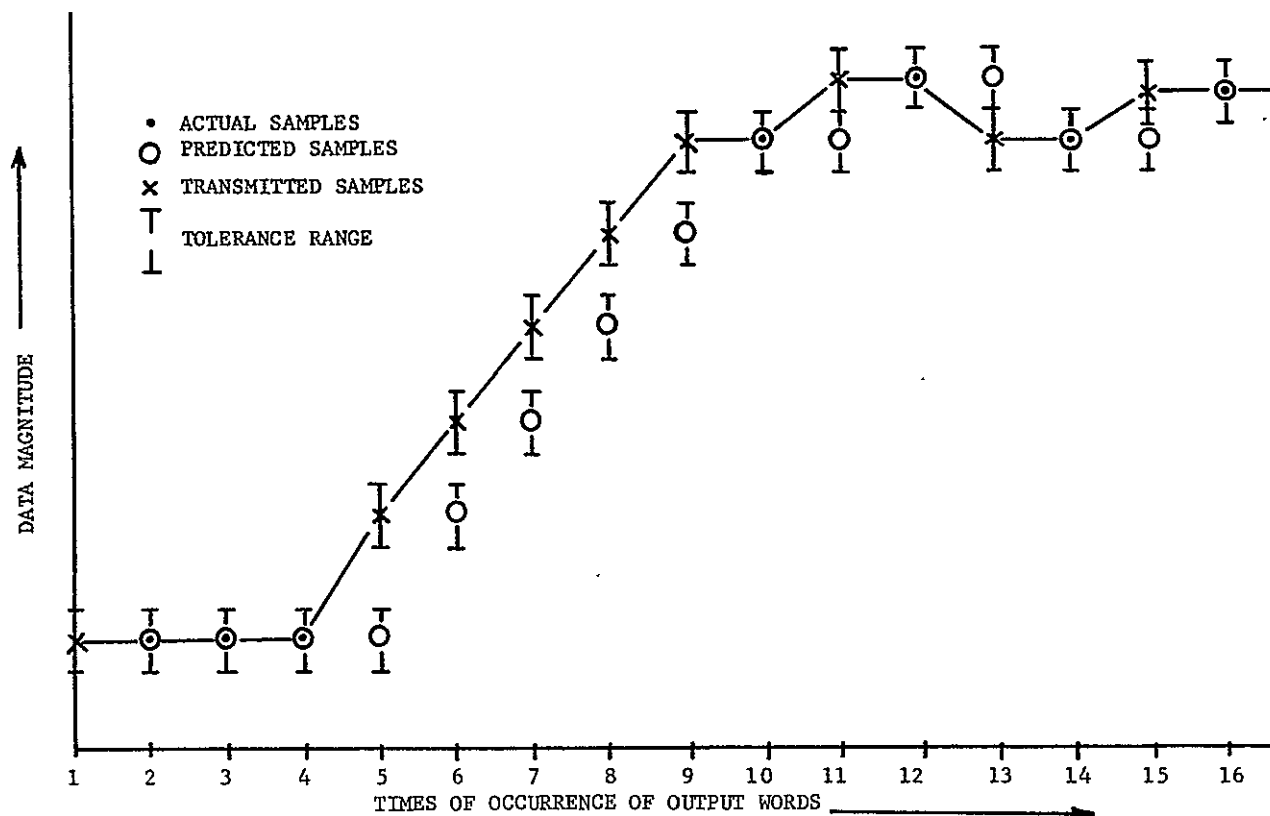


FIGURE 6. ZFN ALGORITHM (ZERO ORDER, FIXED CORRIDOR, NONREDUNDANT SAMPLE)



## NOTED INPUT DATA VARIATIONS OF SEVERAL SATURN FLIGHTS

The data used in this data compression buffer fullness study were taken from flights AS-202, AS-203, and AS-204. In all of these flights, the data channels were sampled and multiplexed through similar telemetry systems located on three Saturn Instrument Units. The sampling rates for these systems were primarily 12 and 120 sps with an output bit rate of 72 000 bits per second (72 kBps). The highest activity periods for each flight occurred during the same time intervals, as graphically illustrated by the flight profiles presented in the previous section (Fig. 4).

From flight to flight, variations existed in the data channel assignments of the PCM system and in the percentages of data types; the former is of little

consequence, while the latter is of concern if the variations are appreciable. Percentages of data types are a consideration because during high activity periods, certain types of parameters vary, while others remain relatively constant. To more readily determine optimum buffer control for more than one flight, similar data should be processed for each flight under reasonably similar conditions; this was attempted in the experimentation. Table I shows a list of the different parameters with their percentages of occurrence on each flight. A reasonable comparison of data types and percentages between the flights is shown as well as the percentage of priority assignments given to each type of measurement. The assignment of priorities will be discussed later. To easily prevent the buffer from saturating during the high activity periods, three program variations were fabricated. Program 4 is made by reducing all similar sensor type measurements proportionally

TABLE I. FLIGHT PARAMETER OCCURRENCES

Type of Measurement	Percentage of Measurement List			Percentage of Measurements List Given a Priority Assignment (%)
	AS-202 (%)	AS-203 (%)	AS-204 (%)	
Acceleration (A)	2	5		50
Acoustic (B)				0
Temperature (C)	31	30	22	10
Pressure (D)	7	9	29	75
Vibration (E)				0
Flow Rate (F)	5	5	2	100
Position (G)	5	5	4	80
Guidance and Control (H)	16	17	11	50
RF and Telemetry (J)	8	7	5	50
Signal (K)	5	8	13	100
Liquid Level (L)				0
Voltage-Current (M)	13	9	9	10
Angular Velocity (R)	8	5	5	100
Miscellaneous (N)			1	50

(about 30 percent); Program 2 is made by further deleting guidance and control (H type) and discrete (K type) measurements; and Program 3 is made by adding back the K type measurements. As a result, a different number of time slots are processed in each flight program. The results are outlined in Table II.

TABLE II. DATA INPUT RATES TO BUFFER

Flight	Program Variation	Time Slots/Second-Buffer Input Rates
AS-202	1	4424
	2	2304
	3	2664
AS-203	1	5436
	2	3468
	3	3972
AS-204	1	4116
	2	2016

Two broad areas of interest are high activity data periods (data changing at a rapid rate) and low activity periods. These periods can be recognized from looking at the flight profiles outlined earlier in Figure 4. While the occurrences and approximate durations of such high activity periods as lift-off and staging can be easily and accurately predicted, predicting the degree of activity is not so simple, except for calibration periods. Even by using the selections similar to those indicated by Table I, variations of significance in the high data activity periods among the flights were observed. These variations are outlined in Table III. Note that only a few noisy channels can significantly affect the degree of activity. For instance, if only five of the 120 Hz channels are noisy (and thus exhibit a low degree of compressibility), in Table III the figures in column A will become those outlined in column B. This noise problem was not conclusively checked in the study because of the time-consuming work involved. Each channel or source would have to be monitored individually to determine its noise level. However, it is doubtful that any significant noise problem existed, because all three flights behaved in much the same manner in both the active and inactive periods.

TABLE III. LIFT-OFF PERIOD DATA COMPRESSION RATIOS

Flight	A	B
	Data Compression	Data Compression With 5 Noisy 120 Hz Channels Added To Measurements
AS-202 Program 1	2. 62:1	1. 69:1
AS-203 Program 1	3. 42:1	2. 32:1
AS-204 Program 1	4. 0:1	2. 02:1

## BUFFER LENGTH CONTROL PARAMETER EXPERIMENTS

Before data compression algorithms can be applied to a particular data system, information such as tolerance values, output bit rate, priority, time slot position, and sampling rates must be programed into the reference memory of the data compressor. For simplicity, this experiment was not considered as a multifactor with possible parameter interactions. Of the various programable features of the compressor, output bit rate, priority assignments to certain channels, and tolerance control lend themselves to controlling the buffer queue length. Ideally, it is desirable to keep the output bit rate at a minimum to have the greatest compression ratio, but at the same time try to minimize the length of the buffer and thus minimize the real-time delay of the reception of sensor information.

The following sections discuss the effects of three control parameters on buffer queue length during open-loop (no adaptive feedback) operation of the ZFN data compressor. The parameters are output bit rate, tolerance control, and priority control; tests that determine the relative control afforded by these parameters, both singly and in combinations, are described.

## OPEN-LOOP OPERATION

Open-loop plots are merely used to show the basic behavior of the device being tested; in this case the plots are functions of buffer size, input rate, and output rate; input data in all cases are the recovered Saturn PCM data. With no adaptive feedback (i. e., open-loop operation), high activity data were fed into the data compressor and the buffer fullness was monitored. Table IV outlines the initial tolerances used for these open-loop tests. Figures 7, 8, 9, and 10 show the resulting buffer fullness plots. The first three plots (Figs. 7, 8, and 9) show the lift-off periods of buffer fullness plots of high activity data. Unfortunately, during these high activity periods, it appears to be very easy to allow buffer saturation to occur, even with a relatively high output bit rate (thus denoting poor or low rate compressibility). Figure 10 shows the other end of the possibility spectrum as the data for the open-loop plot are taken during a "low activity" period. Consequently, since more compressibility obviously exists, the "open-loop" operation of the unit seems to provide adequate buffer fullness control. The output bit rate obviously has a steady and significant effect on buffer fullness (i. e., the shape of the buffer fullness curve can be changed drastically). This fact is probably best illustrated by Figure 8, although plots 7, 9, and 10 also show this.

From the open-loop study, we can see that generally in the high activity periods (for the sources and initial tolerances programed) the ensemble of data compressibility may range from 5.35:1 to 2.62:1 for the different flights studied. Table V tabulates the results of the open-loop portion of the buffer fullness study.

## TOLERANCE CONTROL

The tolerance control parameter keeps a fixed output rate, but degrades the data by increasing the width of the tolerance corridor in which the data sample is considered redundant. With large tolerances, only large changes in each data channel will be treated as nonredundant information. Each channel of data is programed into the reference memory of the data compressor with an initial (called 1K) tolerance. As the buffer queue length increases, the tolerance corridor can be programed to switch to 2K and also to 4K values. Table VI shows a list of tolerance values assigned to each type of measurement for the three flights. The 1K values, being the

most narrow corridor, were selected so that they would be unaffected by the noise level of the Saturn telemetry system; therefore, noise would not create an excessive number of channels which exceeded the tolerance corridor. This noise level was established by stripping out a few "typical" data channels and observing the level of each. Going from one tolerance level to another (1K to 2K) should show a large decrease in buffer fullness or increase in redundant samples if noise has a large effect. Undersampled data would also exhibit this effect of rapid buffer fullness control by tolerance changes, but this idea was discarded because observations have shown that little undersampled data exist on Saturn PCM links. Another distinct possibility that would cause this same effect is a data distribution similar to that outlined in Figure 11; however, this deals in data characterization and will be covered in detail in future studies.

Figures 12, 13, and 14 show tolerance control plots of buffer fullness versus range time. Figure 12 shows a tolerance control plot of data taken from flight AS-202. Three data runs were made using tolerance controls of 1K, 2K, and 4K, while maintaining a fixed output bit rate of 12 kbps. In the high activity periods, very little control is afforded using tolerance control; this is verified by Figures 13 and 14 for flights AS-203 and AS-204, respectively. However, other experimentation revealed that tolerance control would probably be effective during periods of low data activity.

TABLE IV. MEASUREMENT TOLERANCE ASSIGNMENTS

Type of Measurement	Initial Tolerance- Called 1K Tolerance (%)	Widest Permissible Tolerance-Called 4K Tolerance (%)
Acceleration (A)		
Guidance and Control (H)	0.1	0.78
Acoustic (B)	1.56	6.4
Vibration (E)	1.56	6.4
Temperature (C)	1.56	6.4
Pressure (D)	0.78	3.2
Flow Rate (F)	0.2	0.78
Position (G)	0.78	3.2
RF and Telemetry (J)	0.2	0.78
Discretes (K)	Accept All Samples	0.1
Liquid Level (L)	1.56	6.4
Voltage, Current, and Frequency (M)	1.56	6.4

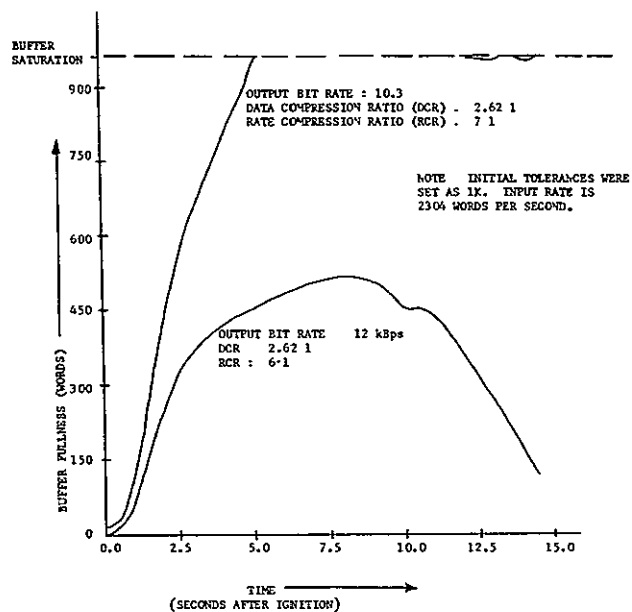


FIGURE 7. AS-202 OPEN-LOOP PLOT FOR LIFT-OFF PERIOD (#1)

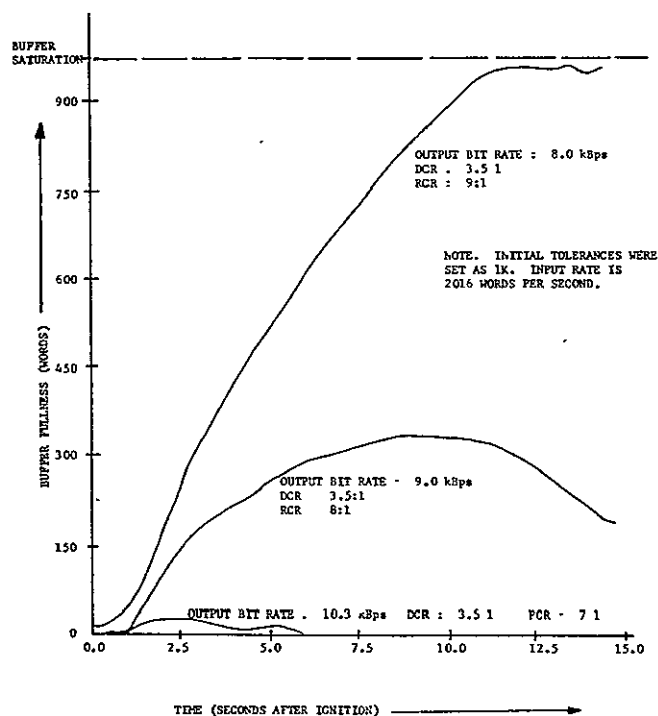


FIGURE 9. AS-204 OPEN-LOOP PLOT FOR LIFT-OFF PERIOD (#3)

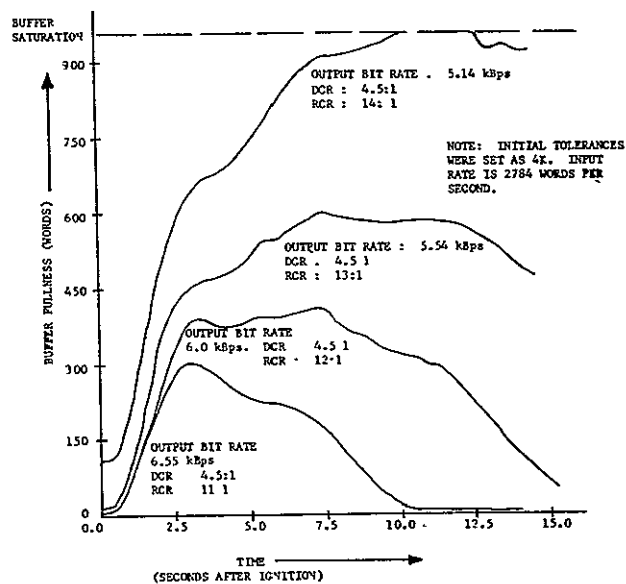


FIGURE 8. AS-202 OPEN-LOOP PLOT FOR LIFT-OFF PERIOD (#2)

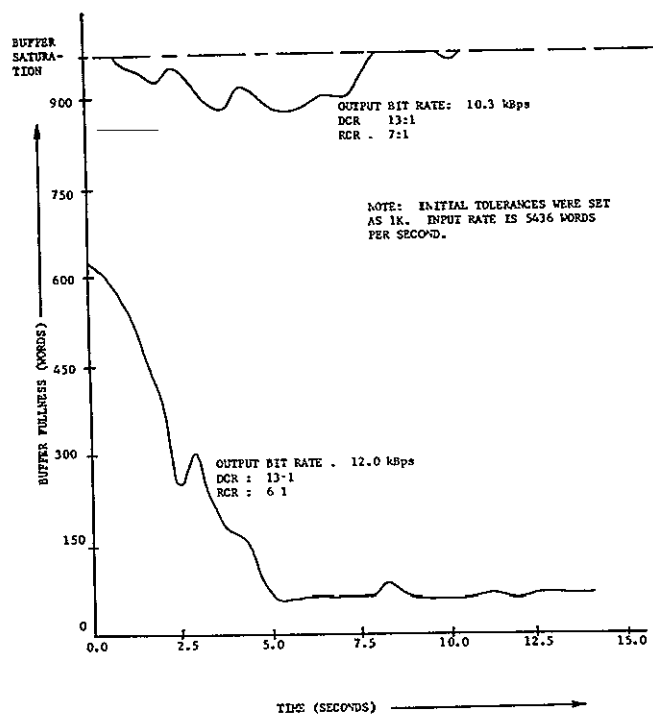


FIGURE 10. AS-203 OPEN-LOOP PLOT FOR LOW ACTIVITY PERIOD

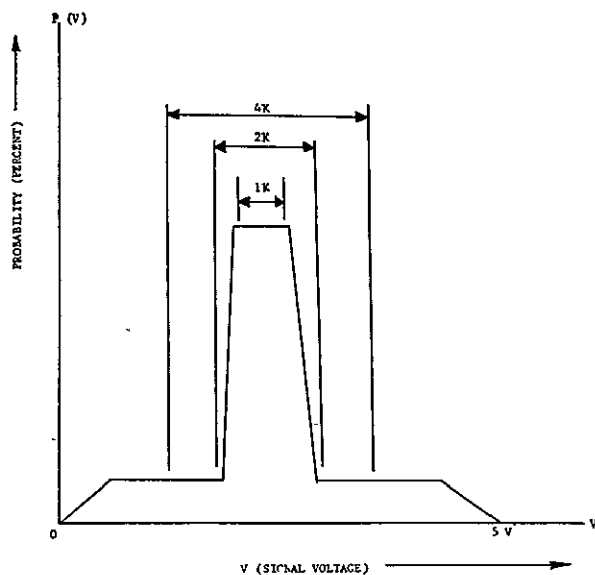


FIGURE 11. POSSIBLE DATA DISTRIBUTION OF SATURN PCM DATA

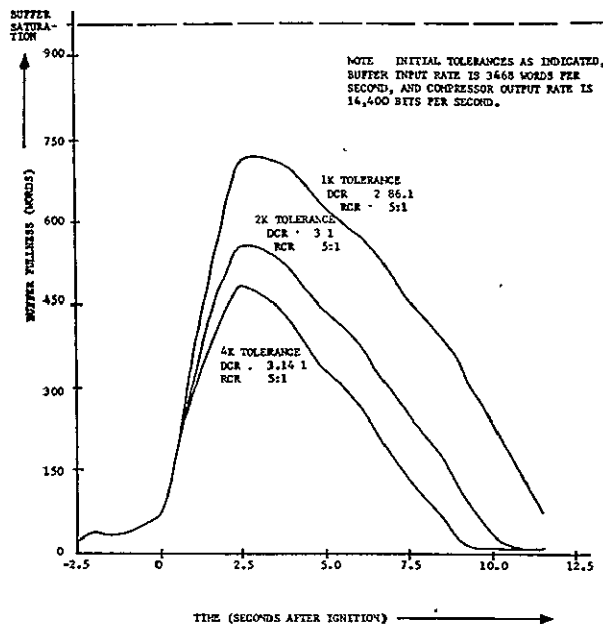


FIGURE 13. AS-203 TOLERANCE CONTROL PLOT (#2)

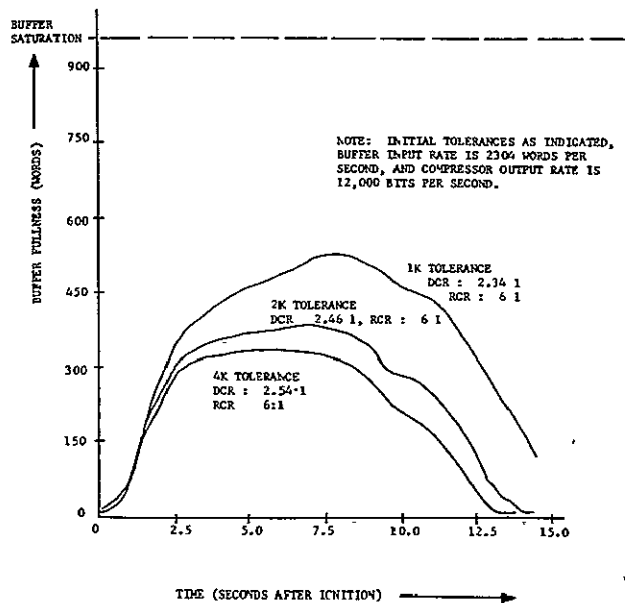


FIGURE 12. AS-202 TOLERANCE CONTROL PLOT (#1)

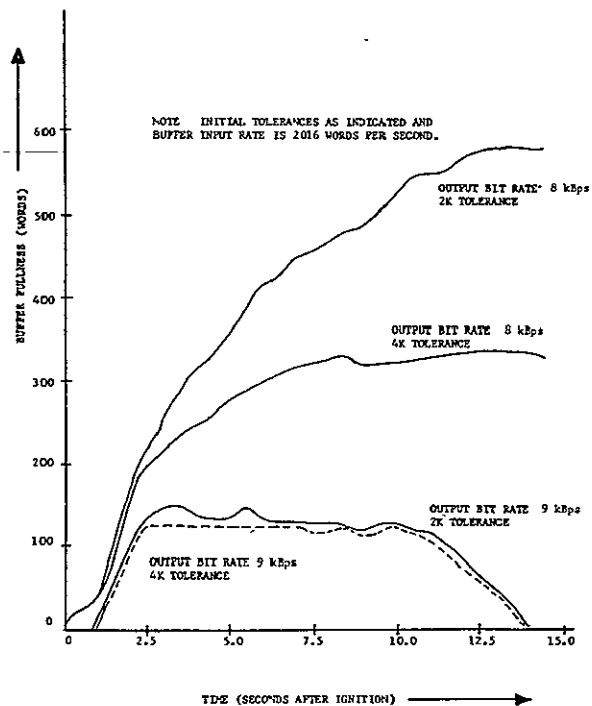


FIGURE 14. AS-204 TOLERANCE CONTROL PLOT (#3)

TABLE V. SUMMARY OF OPEN-LOOP PLOT CHARACTERISTICS

Open-Loop Plot (Figure)	Flight	Buffer Input Word Rate	Compressor Output Bit Rate	DCR	RCR	Required Buffer Length
7	AS-202	2304	10 300	2.6:1	7:1	Saturated
7	AS-202	2304	12 000	2.6:1	6:1	500 Words
8	AS-202	2784	5 140	5.3:1	14:1	Saturated
8	AS-202	2784	5 540	5.3:1	13:1	600 Words
8	AS-202	2784	6 000	5.3:1	12:1	100 Words
8	AS-202	2784	6 550	5.3:1	11:1	300 Words
9	AS-204	2016	8 000	3.5:1	9:1	1000 Words
9	AS-204	2016	9 000	3.5:1	8:1	325 Words
9	AS-204	2016	10 300	3.5:1	7:1	50 Words
10	AS-203	5436	10 300	13:1	7:1	Saturation
10	AS-203	5436	12 000	13:1	6:1	650 Words

TABLE VI. TOLERANCE ASSIGNMENTS

Type Of Measurement	Tolerance (%)					
	1K	2K	4K	*4K	*8K	*16K
Acceleration, Guidance, and Control	0.1	0.1	0.1	0.78	1.56	3.2
Acoustic and Vibration	1.56	3.2	6.4	6.4	12.8	12.8
Temperature	1.56	3.2	6.4	6.4	12.8	12.8
Pressure	0.78	1.56	3.2	3.2	6.4	12.8
Flow Rate	0.1	0.1	0.1	0.78	1.56	3.2
Position	0.78	1.56	3.2	3.2	6.4	12.8
RF and Telemetry	0.1	0.1	0.1	0.78	1.56	3.2
Signal	Accept	Accept	Accept	0.1	0.1	0.1
Liquid Level	1.56	3.2	6.4	6.4	12.8	12.8
Voltage and Current	1.56	3.2	6.4	6.4	12.8	12.8
Angular Velocity	0.1	0.1	0.1	0.78	1.56	3.2

NOTE. Measurement types indicated\* were given 0.78 tolerances (signal measurements were given 0.1 instead of forced accept).

## PRIORITY CONTROL

By using priority tags, certain preselected non-priority channels will be rejected when the buffer fullness exceeds a certain level. The percentages of measurements assigned a priority tag for these tests are called out in the priority plots. The entire priority control in this type of test was introduced at the 128-word buffer fullness level.

Figures 15 and 16 show plots of buffer fullness versus range time. A study of these figures shows a large capability to control buffer fullness through priority control. To demonstrate the power of this type control, a very low buffer fullness level of 128 words was selected to actuate the priority control. In reality, a higher buffer fullness level would be utilized.

However, another factor must be considered. Although priority control seems the most effective, it also loses the most information. Consequently, priority control should not be employed except as an emergency measure to prevent buffer overflow.

## CONCLUSIONS

By experimenting with buffer fullness controls when using recovered PCM data from AS-202, AS-203, and AS-204 flights, we determined the following.

1. Output bit rate was an excellent buffer fullness control parameter but was unsuitable for inflight changes (synchronization becomes a difficult problem with a changing bit rate).
2. Tolerance change is a poor method of buffer fullness control in high activity periods.
3. Priority assignment is an excellent method of buffer fullness control, but this method should be used carefully because it deletes information from the data compressor input.
4. High activity periods are predictable in times of occurrences and duration but not nearly so predictable concerning data compressibility (degree of redundancy).

If you ask, "Can you use this ZFN data compressor unit on the Saturn vehicle and insure that you will have 100 percent of the channels monitored, 100 percent of the time?", the answer is no. Basically, the problem resolves into two important factors: (1) the data compression during high activity periods and (2) the delay between the sensing of the transducers and the time of actual transmission. Note that even though the average data compression for a flight seems to be around 15:1 (denoting a high degree of redundancy), during the high activity periods (the pacing items) the data compressibility can be as low as 2:1.

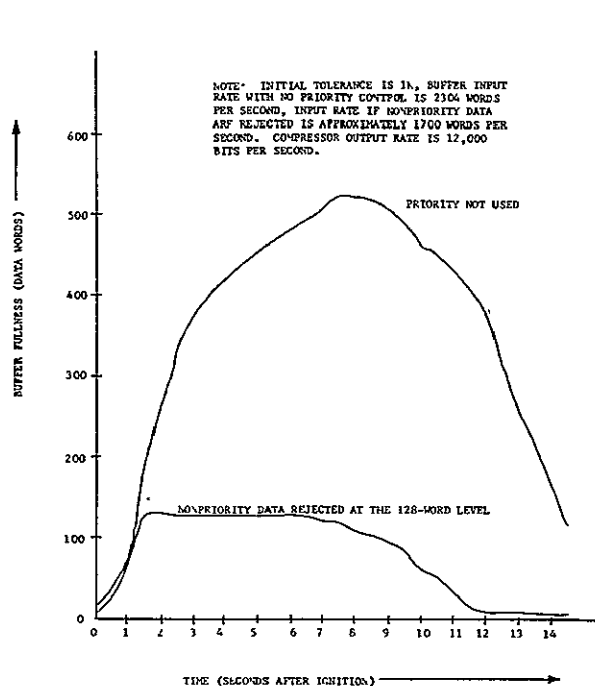


FIGURE 15. AS-202 PRIORITY CONTROL PLOT (#1)

Now imagine a condition where this same ZFN data compressor unit can be used on a Saturn vehicle. If a user of telemetry data can allow a one-second maximum time delay between sensor sensing and transmission, and could settle with 35 percent of the present total information channels during a high activity period, then this unit could give a probable 4:1 reduction in output bit rate over that now afforded.

The preceding paragraphs indicate that under certain conditions, the ZFN data compressor unit used on a Saturn type launch vehicle can yield a 4:1 advantage over a system with no compression. These

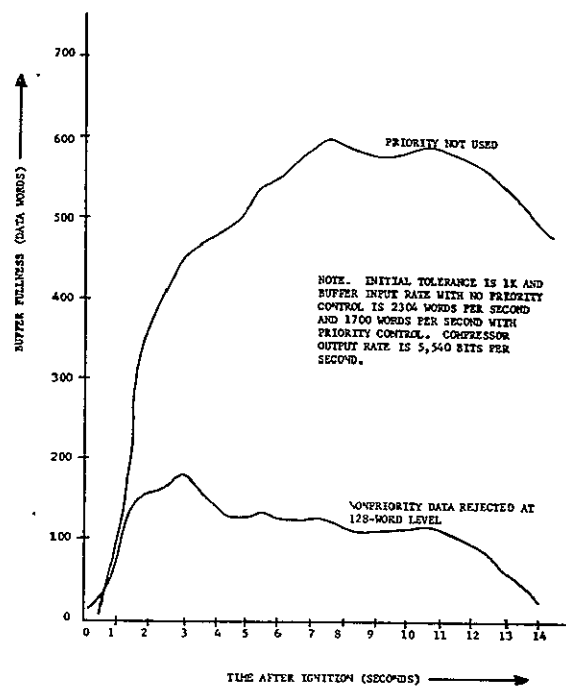


FIGURE 16. AS-202 PRIORITY CONTROL PLOT (#2)

paragraphs also show that although there are small gains in using the ZFN compressor, it would probably not be suited for a nonorbital propulsion stage. However, it would be well suited on vehicles where data do not change so rapidly (i. e., the data possess high redundancy content). Such a situation would probably occur on orbital vehicles or perhaps on deep space probes. If the data had a higher degree of redundancy most of the time, then the ZFN data compressor unit would afford a proportionally higher degree of output bit rate reduction. Or, in a situation where a longer delay can be tolerated, more variation in ensemble data compressibility can be allowed by adding a larger buffer.

## REFERENCES

1. Telemetry Standards Prepared by Telemetry Working Group of Inter-Range Instrumentation Group of Range Commander's Conference. IRIG Document No. 106-60, Revised, June 1962.
2. Massey, H.: An Experimental Telemetry Data Compressor. 1965 National Telemetry Conference, Houston, Texas, April 1965.
3. Wallace, Gabriel R.: Redundancy Removal Techniques for Compression of Telemetry Data. Research Achievements Review, Volume III, Report No. 1, NASA TM X-53760, 1968.

# RADIATION EFFECTS TESTING OF SATURN TELEMETRY HARDWARE

By

T. C. Lawson

N 69 - 36582

## INTRODUCTION

An engineer designing semiconductor circuits for operation in a nuclear radiation environment has much detailed information to enable him to design reliable equipment. However, the effects of radiation on a design employing semiconductor devices can be quite complex because of the various combinations of the types of devices used and the different types of radiation encountered. Maximum confidence that the equipment will perform its intended functions in its expected radiation environment, such as a nuclear powered space vehicle, is achieved by the design engineer only after the equipment has been tested in such an environment. Also, existing designs not originally expected to operate in a nuclear environment are finding application where their performance could possibly be reduced or rendered completely unsatisfactory. For these reasons, system or subsystem testing to the expected radiation environment is necessary. Only after such testing can the confidence mandatory in critical applications be established.

## TEST METHODS

Various methods may be used in testing an electronic assembly in a nuclear radiation environment. Testing in this type of environment is considerably different from most other environmental testing because of the distance required between the test item and auxiliary equipment. An even greater distance is required between the environment and the test personnel. Also, equipment that has been bombarded with neutrons will be radioactive and unsafe to handle for a long period after exposure. These factors must be considered when determining the method of testing.

Table I lists three possible approaches to testing. A simple test program would be to irradiate the test item while applying typical input signals and monitoring the output. The test item would be subjected to the radiation until a malfunction occurred, at which

TABLE I. METHODS OF IRRADIATION TESTING

- |  |
|--|
| 1. Irradiate Test Item to Required Level While Monitoring Output         |
| 2. Irradiate Test Item to Required Level While Monitoring Every Function |
| 3. Irradiate Test Item to Required Level and Then Check Performance      |

time the test is considered to be completed. The only information obtained from such a test would be that above a given level of absorbed radiation, the test item would no longer function. No information would be available to indicate what portion of the circuitry failed, what portions were marginal, or what portions would have continued to operate to the desired total absorbed dose. A post analysis of the test item would yield some of the information, but only after a long "cooling off" period and even then at the risk of the health of the technician doing the analysis. Standards have established "safe radiation levels" but nuclear radiation, no matter how reduced in intensity, has damaging effects and should be avoided whenever possible. As in any occupation, the information or results obtained by self-exposure to hazards must outweigh the disadvantage of the damaging effects. Naturally, if another test method will yield the same results with less exposure to the test personnel, it should be used.

At the other extreme, every component in a test item could be monitored during the test, and provisions could be made to replace the components suspected of having lower radiation tolerance. When a malfunction occurs, a new component can replace the faulty one, and the test can continue until the desired dosage is reached or until enough components have failed to warrant ending the test. One disadvantage of this method is that the lengths of cable required for monitoring and substituting components will load the circuits and provide noise pickup loops that render the operation of the test item marginal and, in many cases, inoperative.



Perhaps the most simple test would be to place the test item in the radiation environment, irradiate it to a predetermined dosage, remove it from the environment, and then test it. This cycle would be repeated until the desired total dosage was reached or until the test item failed. Although it is simple, this method exposes the test personnel to a greater dose of radiation and should be used only when other methods will not suffice.

Each of the three methods discussed may be the optimum for a certain situation; however, a compromise of the first two methods in Table I usually provides the most useful data.

Typical input conditions are applied to the test item, and the output is monitored along with a reasonable number of intermediate points. Provisions are also made to substitute parts of the circuitry suspected of having low radiation resistance. The degree of compromise will depend upon the item being tested and the test facilities.

## TEST CONFIGURATIONS

The Atomic Energy Commission has imposed certain requirements on test facilities to protect the personnel; yet, in planning a test program, emphasis should be placed on maximum safety. Figure 1 is a representation of a typical test site. The reactor that will provide the source of radiation energy is housed in a building in an isolated area surrounded by a rodent-proof fence. Water storage and cooling towers are located nearby. The 0.915m-thick floor of the reactor building is of concrete construction under which is a basement or equipment pit. The attenuation provided by the concrete reduces the intensity of the radiation energy in the basement to a value suitable for the use of auxiliary equipment. Approximately 15 m of cable is required between the test item and the equipment in the basement. When testing Saturn telemetry hardware, a complete telemetry system is used (Fig. 2). Since each assembly in the system is a complicated entity, and to irradiate the entire system during one test would exceed the capabilities of the monitoring facilities, each assembly is irradiated individually while connected in a complete system. All subsystems are located in the equipment pit except for the item being tested. The test data are transmitted approximately 5 km to a ground station for recording and analysis. Control and monitoring of the reactor and monitoring of the

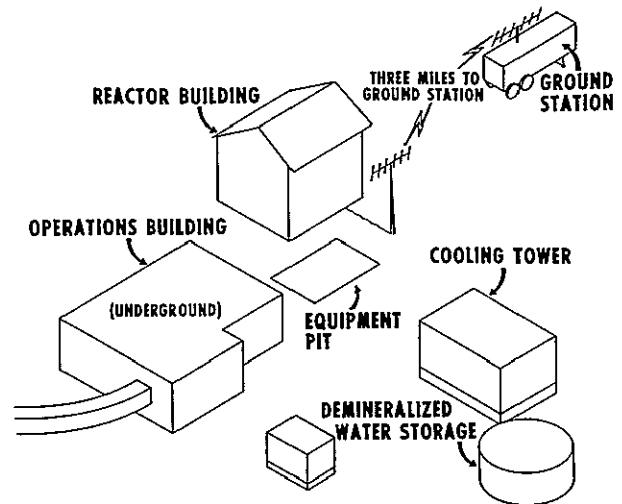


FIGURE 1. TEST FACILITIES

intermediate test points are performed in the operations building, which is located underground. Thus, the radiation energy is attenuated to a negligible intensity so that the test personnel are safe. Cable ducts are provided between the equipment pit and the underground operations building.

Figure 3 is a block diagram of a typical test. The high radiation intensity area is in the immediate vicinity of the reactor, the low radiation intensity area is in the equipment pit, and the safe areas are underground in the operations building and the ground station. The block diagram shows three telemetry assemblies under test: a single sideband assembly, an analog multiplexer, and a PCM assembly. Typical analog voltage sources located in the low radiation intensity area are applied simultaneously to the PCM assembly under test and to a comparison assembly. The digitized output of each assembly modulates an rf transmitter for transmission through a multi-coupler to the ground station where the two signals are compared to determine when a malfunction occurs. Analog signals are also applied to the multiplexer in the test environment and to a like assembly in the low intensity area. Data from both of these assemblies are processed by the PCM system and transmitted to the ground station for comparison. A vibration simulator provides signals to the two single sideband assemblies. Their outputs modulate rf transmitters and the data are compared at the ground station. Portions of the circuitry suspected of having low resistance to radiation are duplicated in the low intensity area and are switched into the test item

### INSTRUMENT UNIT TELEMETRY SYSTEM DATA FLOW DIAGRAM (TYPICAL FOR OPERATIONAL VEHICLES)

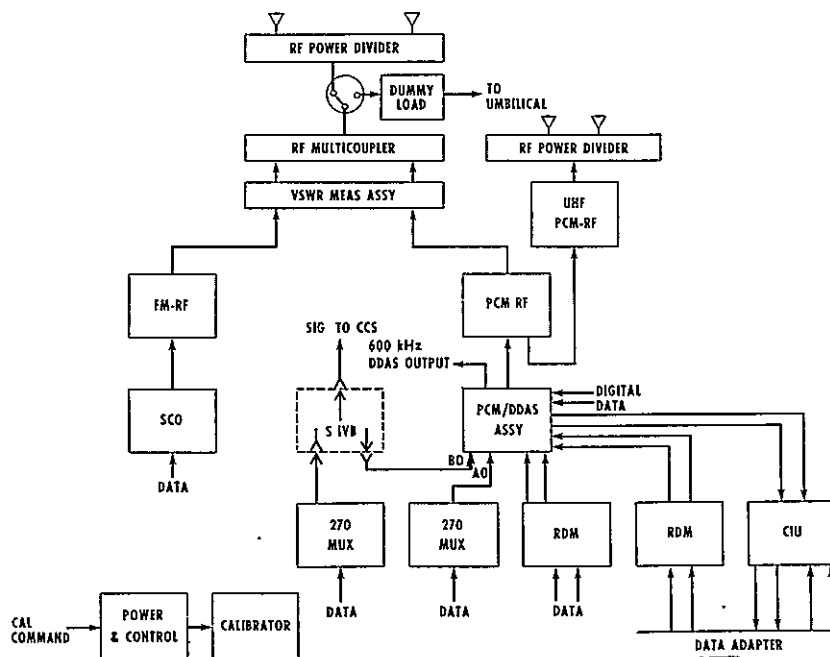


FIGURE 2. TYPICAL SATURN TELEMETRY SYSTEM

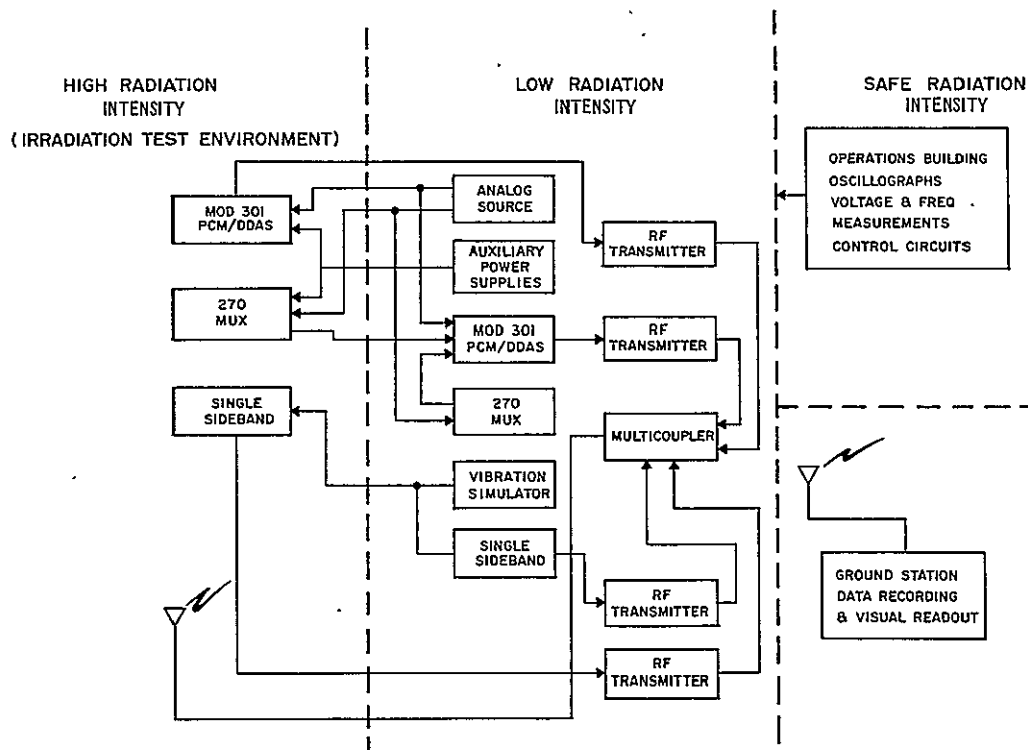
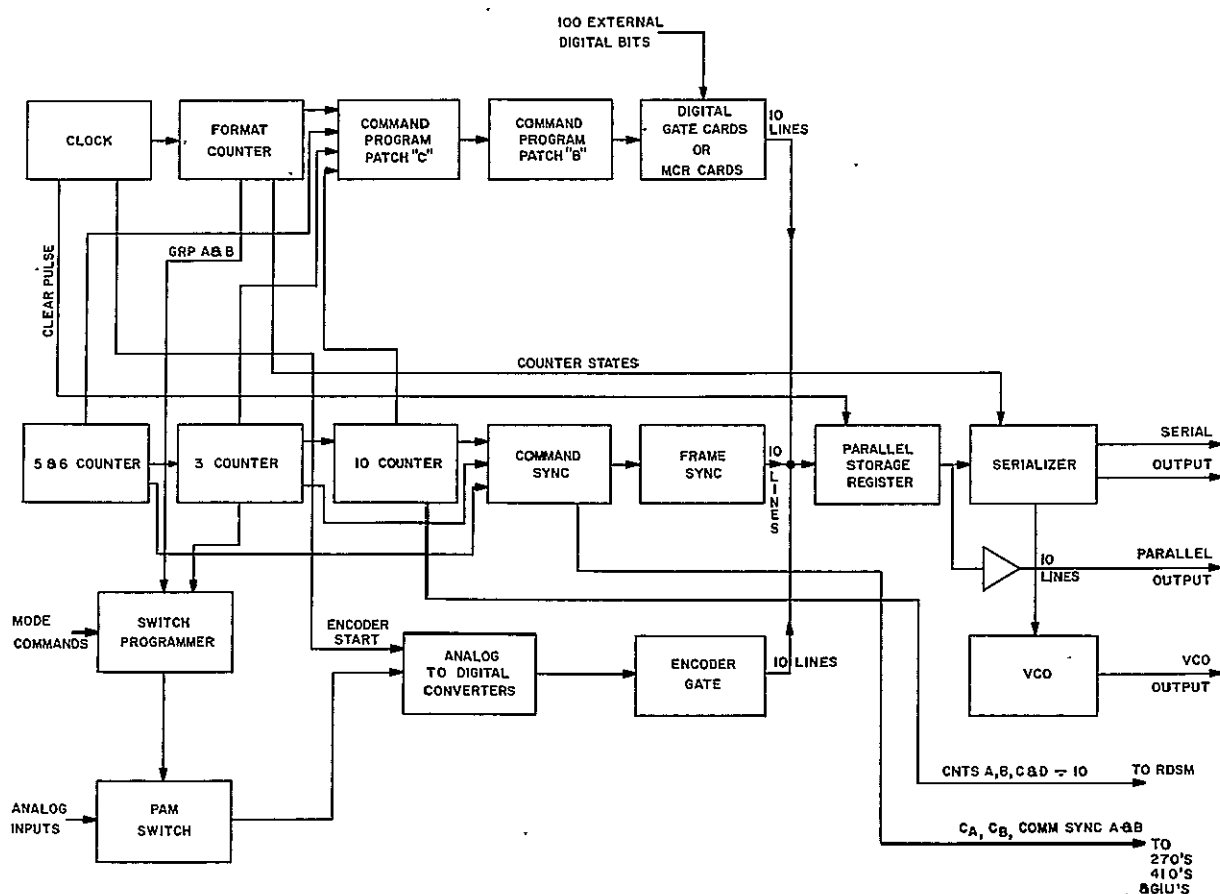


FIGURE 3. TYPICAL TEST

from the operations building. Oscillographs and dc voltage measurements are also recorded in the operations building. Figure 4 is a block diagram of a test item showing the various circuits that can be monitored. By observing the waveforms at the output of counters, sync generators, and switches, the circuits having the lower tolerance to radiation can be easily spotted. The test points, however, can be quite numerous when the test items are complex and several are included in one test. Therefore, a 30-channel multiplexer switch is used to simultaneously display four waveforms on an oscilloscope, thus providing a total of 120 oscilloscope monitor points.

The problems encountered in the monitor points are manifold. Isolation amplifiers are inserted in the monitor lines after the multiplexer switch, but the cables between the test points and the amplifiers often cause erratic operation because of added

capacity or noise pickup. Shielded cables are required to reduce the noise pickup from the reactor; and after a short time, the radiation attacks the dielectric in the cable and causes short circuits. Figure 5 is a photograph of a test setup showing the maze of cables. The multiplexer switch used for oscilloscope monitor points is housed in the concrete enclosure behind the test racks, and cables for dc voltage measurements and circuit substitution are connected directly to equipment in the operations building and the equipment pit. For safety, the entire test configuration is mounted on a flat railroad car, checked out, and then moved to the reactor. This movement flexes the cables and often the dielectric in the cables, made brittle by previous exposure to radiation, crumbles and short circuits result, thus adding to the problems encountered by having too many monitor points. The circuit monitor points together with the dosage monitoring devices result in the configuration shown in Figure 6.



PCM DDAS MOD 302

FIGURE 4. BLOCK DIAGRAM OF TEST ITEM

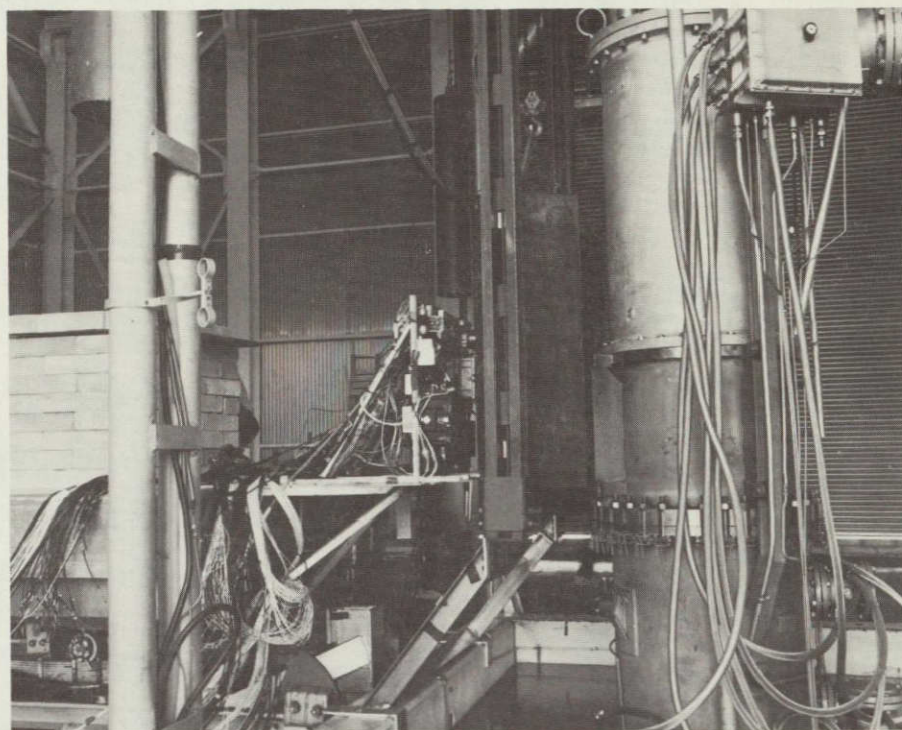


FIGURE 5. SIDEVIEW OF TEST CONFIGURATION

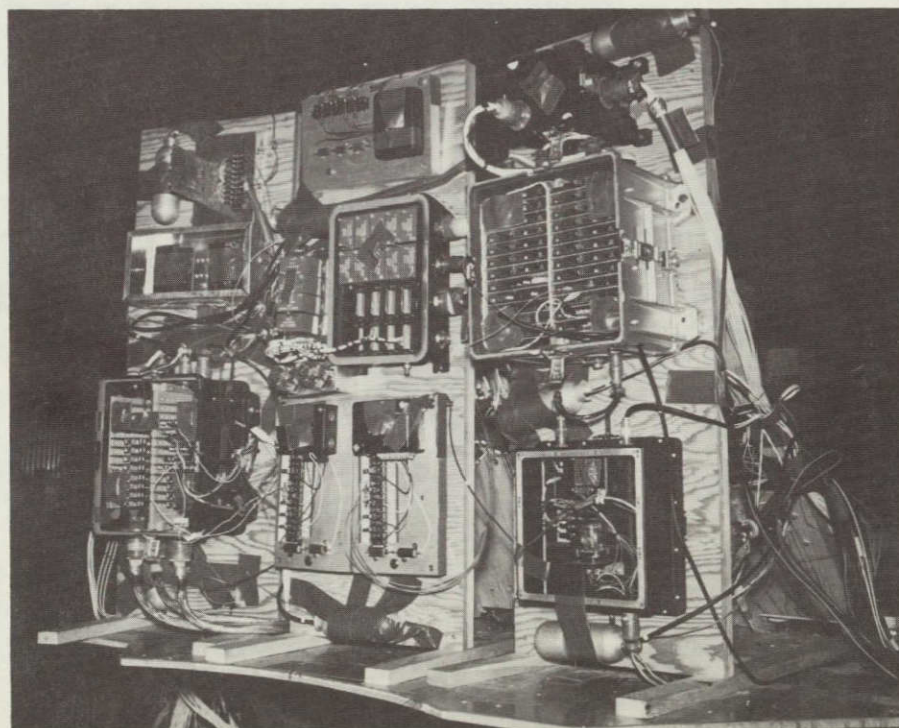


FIGURE 6. TEST PANEL

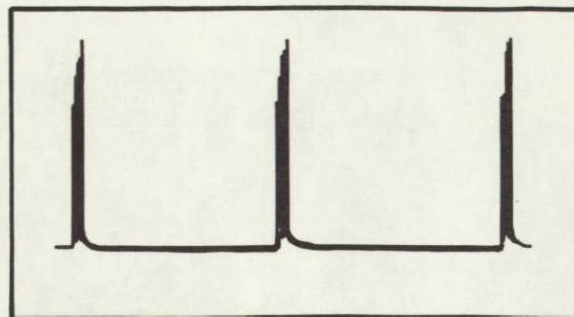


## TEST RESULTS

Much useful information has been obtained on existing Saturn telemetry hardware. Gamma rays produced little or no effect on the performance of the equipment tested; however, certain materials such as teflon insulation were deteriorated sufficiently to cause malfunctions when other environments like vibration or moisture are encountered.

Neutron bombardment is the damaging agent; however, most digital circuits performed satisfactorily to a level of  $1.0 \times 10^{13}$  n/cm<sup>2</sup>. (Only energy levels greater than 0.5 MeV were considered.) The analog circuits degraded to an unacceptable level at approximately  $1.0 \times 10^{12}$  n/cm<sup>2</sup>. The monitor points chosen provided the necessary information to complete an analysis of the failures. As an example, the output of channel 14 of the single sideband assembly decreased 7.9 dB at a radiation level of  $1.5 \times 10^{12}$  n/cm<sup>2</sup>. Other channels were affected to a lesser degree. This was attributed to the deterioration of the spectrum received from the second carrier supply board. Figure 7 shows the output of this carrier before radiation and shortly after failure. The output is normally 8  $\mu$ s bursts of a 491 kHz signal at a repetition rate of 4.74 kHz. The figure shows that the amplitude of the 491 kHz signal decreased considerably and the dc level increased. The circuit for the carrier is shown in Figure 8. It consists of a monostable multivibrator (Q1 and Q2) with a buffered output (Q3). Q5 and its associated components operate as a free running 491 kHz oscillator whose output is buffered by Q6 and Q7. Q4 is normally biased ON, causing the coil in the tuned circuit of the 491 kHz oscillator to saturate and this will stop the oscillation. When the monostable multivibrator is triggered, an 8  $\mu$ s negative pulse is applied to the base of Q4, turning it OFF. The coil in the oscillator is no longer saturated and 491 kHz oscillations occur for 8  $\mu$ s. The analysis of the circuit indicated that the gain of Q4 deteriorated to a value to permit Q6 and Q7 to partially turn ON. This accounted for the decrease in the 491 kHz output and the increase in dc level. In post radiation analysis, which took place after several months of "cooling off," replacement of Q4 returned the system to its normal operation.

Power supplies and voltage regulators performed satisfactorily to a level of approximately  $1.0 \times 10^{12}$  n/cm<sup>2</sup>. Figure 9 is a comparison of two



PRE-IRRADIATION

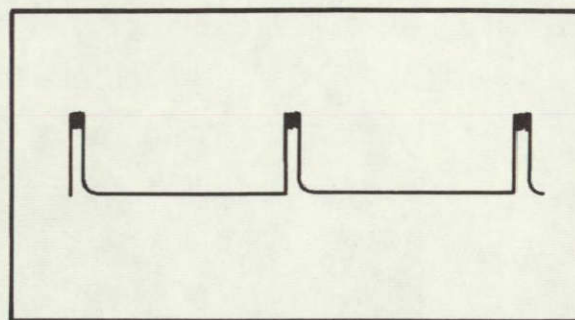
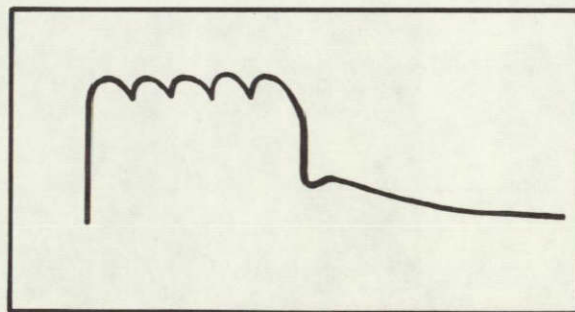
 $1.56 \times 10^{12}$  n/cm<sup>2</sup> $1.56 \times 10^{12}$  n/cm<sup>2</sup>

FIGURE 7. CARRIER SUPPLY OUTPUT

different supplies that meet the same specifications, but were designed by different companies. Power supply 2 remained well within specification to a level of  $2.2 \times 10^{13}$  n/cm<sup>2</sup>, and power supply 1 failed at  $1.0 \times 10^{12}$  n/cm<sup>2</sup>.

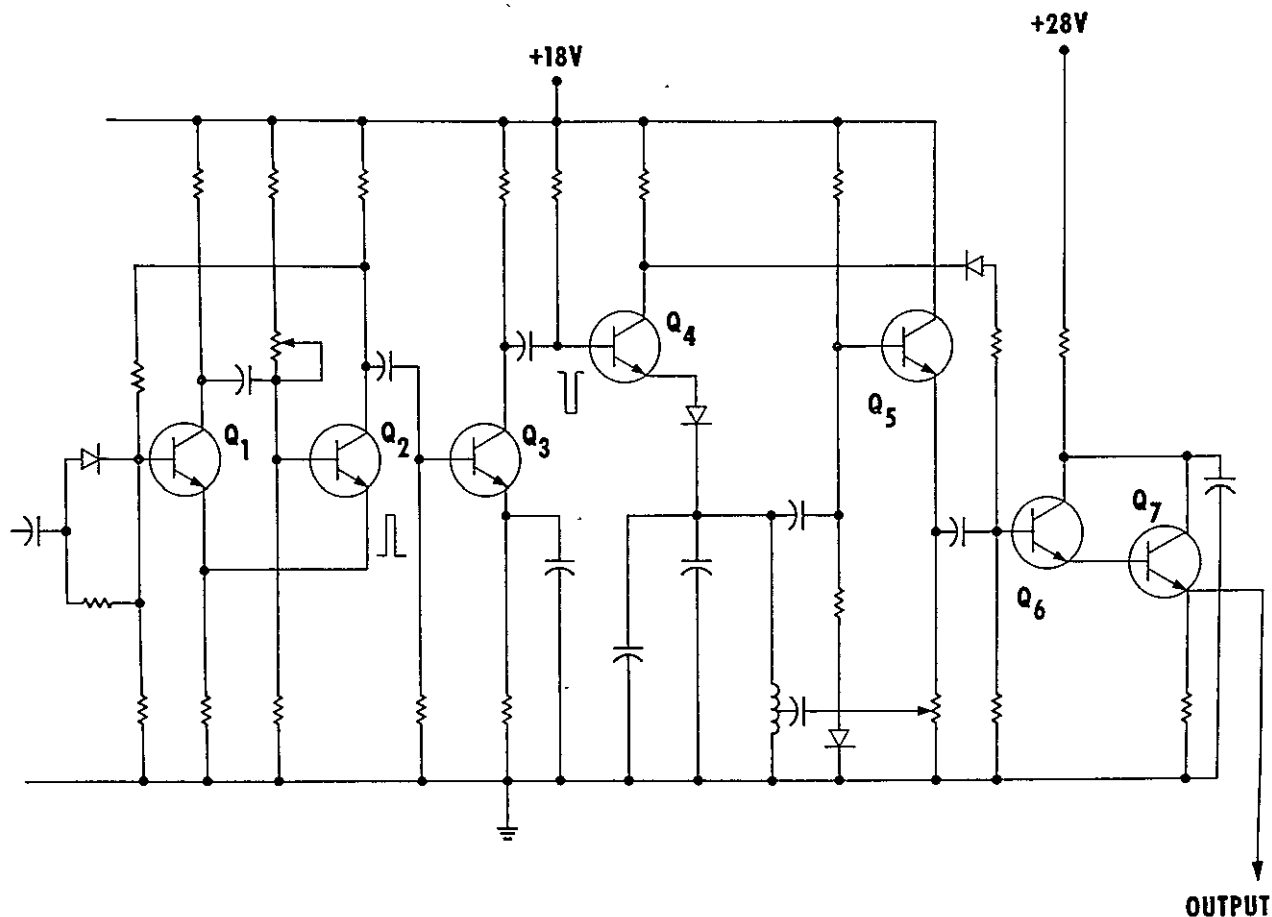


FIGURE 8. CARRIER CIRCUIT

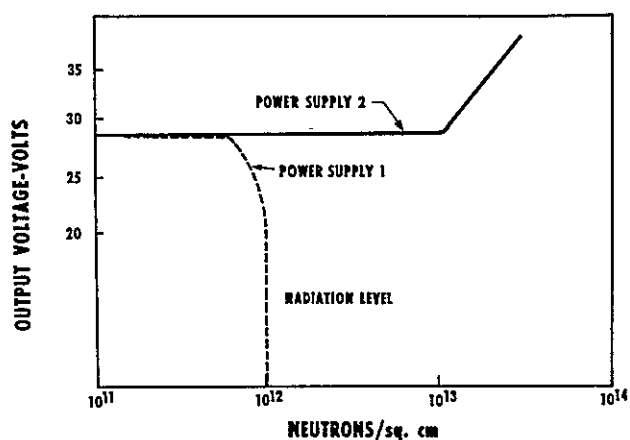


FIGURE 9. POWER SUPPLY PERFORMANCE

## CONCLUSIONS

Although the present Saturn telemetry hardware was not originally intended to operate in a nuclear radiation environment, very little redesign will be necessary to qualify both digital and analog systems to operate at expected radiation intensities on a nuclear powered space vehicle. Additional testing will be conducted to expose all weak points and to prove new designs.

PRECEDING PAGE BLANK NOT FILMED.

1968

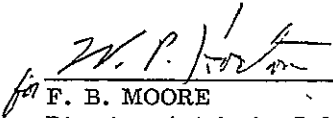
APPROVAL

NASA TM X-53810

RESEARCH ACHIEVEMENTS REVIEW  
VOLUME III REPORT NO. 5

The information in these reports has been reviewed for security classification. Review of any information concerning Department of Defense or Atomic Energy Commission programs has been made by the MSFC Security Classification Officer. These reports, in their entirety, have been determined to be unclassified.

These reports have also been reviewed and approved for technical accuracy.

  
F. B. MOORE  
Director, Astrionics Laboratory

## UNITS OF MEASURE

In a prepared statement presented on August 5, 1965, to the U. S. House of Representatives Science and Astronautics Committee (chaired by George P. Miller of California), the position of the National Aeronautics and Space Administration on Units of Measure was stated by Dr. Alfred J. Eggers, Deputy Associate Administrator, Office of Advanced Research and Technology:

"In January of this year NASA directed that the international system of units should be considered the preferred system of units, and should be employed by the research centers as the primary system in all reports and publications of a technical nature, except where such use would reduce the usefulness of the report to the primary recipients. During the conversion period the use of customary units in parentheses following the SI units is permissible, but the parenthetical usage of conventional units will be discontinued as soon as it is judged that the normal users of the reports would not be particularly inconvenienced by the exclusive use of SI units."

The International System of Units (SI Units) has been adopted by the U. S. National Bureau of Standards (see NBS Technical News Bulletin, Vol. 48, No. 4, April 1964).

The International System of Units is defined in NASA SP-7012, "The International System of Units, Physical Constants, and Conversion Factors," which is available from the U. S. Government Printing Office, Washington, D. C. 20402.

SI Units are used preferentially in this series of research reports in accordance with NASA policy and following the practice of the National Bureau of Standards.



## CALENDAR OF REVIEWS

### FIRST SERIES (VOLUME I)

REVIEW	DATE	RESEARCH AREA	REVIEW	DATE	RESEARCH AREA
1	2/25/65	RADIATION PHYSICS	12	9/16/65	AERODYNAMICS
2	2/25/65	THERMOPHYSICS	13	9/30/65	INSTRUMENTATION
3	3/25/65	CRYOGENIC TECHNOLOGY	14	9/30/65	POWER SYSTEMS
4 *	3/25/65	CHEMICAL PROPULSION	15	10/28/65	GUIDANCE CONCEPTS
5	4/29/65	ELECTRONICS	16	10/28/65	ASTRODYNAMICS
6	4/29/65	CONTROL SYSTEMS	17	1/27/66	ADVANCED TRACKING SYSTEMS
7	5/27/65	MATERIALS	18	1/27/66	COMMUNICATIONS SYSTEMS
8	5/27/65	MANUFACTURING	19	1/8/66	STRUCTURES
9	6/24/65	GROUND TESTING	20	1/6/66	MATHEMATICS AND COMPUTATION
10	6/24/65	QUALITY ASSURANCE AND CHECKOUT	21	2/24/66	ADVANCED PROPULSION
11	9/16/65	TERRESTRIAL AND SPACE ENVIRONMENT	22	2/24/66	LUNAR AND METEOROID PHYSICS

### SECOND SERIES (VOLUME II)

REVIEW	DATE	RESEARCH AREA	REVIEW	DATE	RESEARCH AREA
1	3/31/66	RADIATION PHYSICS	7	3/30/67	CRYOGENIC TECHNOLOGY
2	3/31/66	THERMOPHYSICS	8 **	5/25/67	COMPUTATION
3	5/26/66	ELECTRONICS	9	7/27/67	POWER SYSTEMS
4	7/28/66	MATERIALS	10	9/28/67	TERRESTRIAL AND SPACE ENVIRONMENT
5	9/29/66	QUALITY AND RELIABILITY ASSURANCE	11	11/30/67	MANUFACTURING
6	1/26/67	CHEMICAL PROPULSION	12	1/25/68	INSTRUMENTATION RESEARCH FOR GROUND TESTING

### THIRD SERIES (VOLUME III)

REVIEW	DATE	RESEARCH AREA	REVIEW	DATE	RESEARCH AREA
1	3/28/68	AIRBORNE INSTRUMENTATION AND DATA TRANSMISSION	5	11/21/68	COMMUNICATION AND TRACKING
2	5/22/68	ASTRODYNAMICS, GUIDANCE AND OPTIMIZATION	6	1/30/69	THERMOPHYSICS
3	7/25/68	CONTROL SYSTEMS	7	3/27/69	RADIATION PHYSICS
4	9/26/68	AEROPHYSICS			

\* Classified. Proceedings not published.

\*\* Proceedings summarized only.

Correspondence concerning the Research Achievements Review Series should be addressed to Chief, Research Program Office, S & E- R-R, Marshall Space Flight Center, Alabama 35812